On the role of stem cell regulators in shaping barley spike architecture

Inaugural dissertation

for the attainment of the title of doctor
in the Faculty of Mathematics and Natural Sciences
at the Heinrich Heine University Düsseldorf

presented by

Isaia Vardanega
from Possagno, Italy

Düsseldorf, June 2024

from the Institute for Plant Developmental Genetics
at the Heinrich Heine University Düsseldorf

Published by permission of the
Faculty of Mathematics and Natural Sciences at
Heinrich Heine University Düsseldorf

Supervisor: Prof. Dr. Rüdiger Simon
Co-supervisor: Prof. Dr. Maria von Korff Schmising

Date of the oral examination: 11.07.2024

Affidavit for the dissertation entitled:

On the role of stem cell regulators in shaping barley spike architecture

I declare under oath that I have produced my thesis independently and without any undue assistance by third parties under consideration of the 'Principles for the Safeguarding of Good Scientific Practice at Heinrich Heine University Düsseldorf'.

Düsseldorf, 21.08.2024

Place, date

Signature

Chapter 1 of this thesis is published in the following article:

CLAVATA signalling shapes barley inflorescence architecture by controlling activity and determinacy of shoot apical and rachilla meristems

Isaia Vardanega, Jan Eric Maika, Edgar Demesa-Arevalo, Tianyu Lan, Gwendolyn K. Kirschner, Jafargholi Imani, Ivan F. Acosta, Katarzyna Makowska, Götz Hensel, Thilanka Ranaweera, Shin-Han Shiu, Thorsten Schnurbusch, Maria von Korff Schmising, Rüdiger Simon

bioRxiv, https://doi.org/10.1101/2024.05.28.595952

Preprint published on: 31 May 2024

In addition, I was involved in the following research article:

The transcriptome landscape of developing barley seeds

Martin Kovacik, Anna Nowicka, Jana Zwyrtková, Beáta Strejčková, Isaia Vardanega, Eddi Esteban, Asher Pasha, Kateřina Kaduchová, Maryna Krautsova, Marie Červenková, Jan Šafář, Nicholas J Provart, Rüdiger Simon, Ales Pecinka

The Plant Cell, koae095, https://doi.org/10.1093/plcell/koae095

Article Published on: 18 April 2024

Table of contents

Summary **1**

Chapter 1 ***5***

1. Abstract **6**

2. Main **7**

3. Results **9**

3.1 HvCLV1 controls the activity of inflorescence and rachilla meristems to promote spikelet formation and repress multi-floret spikelets in barley spikes 9

3.2 The CLE peptide HvFCP1 acts with HvCLV1 to limit meristem activities 11

3.3 HvFCP1 and HvCLV1 control meristematic proliferation through coordination of cell division, auxin signalling and trehalose-6-phosphate 12

4. Discussion **14**

5. Materials and methods **15**

5.1 Phylogenetic analysis 15

5.2 Plant material and growth conditions 16

5.3 Plasmids construction and plant transformation 16

5.4 smRNAfish 17

5.5 Plant phenotyping 17

5.6 Sample preparation, microscopy and image processing 18

5.7 Peptide treatment 18

5.8 IM 3D reconstruction and Rachilla vibratome sections 19

5.9 RNA sequencing 19

5.10 Quantification and statistical analysis 20

6. Author contributions **21**

7. Acknowledgements **21**

8. References **22**

9. Figures **27**

10. Extended Data Figures 33

11. Supplementary information 39

Chapter 2 *45*

1. Abstract 46

2. Main 47

3. Results 51

3.1 Identification of the barley BAM gene family and complementary expression of HvBAM1 and HvCLV1 in vegetative and inflorescence meristems 51

3.2 HvBAM1 and HvBAM2 regulate IM size and plant height 52

3.3 HvCLV1, HvBAM1, and HvBAM2 act through independent pathways to shape spike architecture by regulating IM and RM activity, and SM identity 53

3.4 Transcriptome analysis revealed synergic and antagonistic regulation of genes involved in cell division, auxin signalling, inflorescence development, trehalose-6-phosphate metabolism, and sucrose synthesis 54

3.5 Phenotyping *Tc1b1b2* inflorescences at a cellular resolution by single-cell RNA sequencing 57

3.6 ScRNA-seq results provided an insight into the spatial expression of differentially regulated genes in *Tc1b1b2* in comparison to WT 59

4. Discussion 61

5 Materials and methods 65

5.1 Plant material and growth conditions 65

5.2 Plasmids construction and plant transformation 65

5.3 smRNAfish 66

5.4 Sample preparation, microscopy, and image processing 66

5.5 Bulk RNA sequencing 66

5.6 Single-cell RNA-sequencing and integration 67

6. Author contributions 69

7. Acknowledgements 69

8. References 70

9. Figures 77

10. Extended Data Figures 84

11. Supplementary information 87

List of abbreviations *92*

Final acknowledgements *93*

Summary

The grass family exhibits a wide range of inflorescence architectures, from the branched inflorescences of the *Oryzeae* tribe (rice), where grains develop on primary and secondary branches, to the simple spike-type inflorescences evolved in the *Triticeae* tribe (e.g. barley and wheat), where grains develop on vestigial axes called rachillae. Inflorescence shape and organisation are determined by activity and determinacy of the inflorescence meristem (IM) and by the position and identity of spikelet meristems developing on its flanks. In barley, the spikelet meristem (SM) is composed of an adaxial axis called rachilla meristem (RM), the subtending floret meristem (FM), which originates the reproductive organs, and the additional leaf-like lemma, palea, and glume primordia. The activity of the RM determines the number of florets produced by a spikelet, for instance, the indeterminate RM of wheat can form up to 12 florets, while the determinate barley rachilla arrests after the formation of a single floret.

In Arabidopsis, the activity of shoot and floral meristems depends on the transcription factor WUSCHEL, which promotes stem cell maintenance. WUSCHEL activates the expression of the CLAVATA3/ENDOSPERM SURROUNDING REGION (CLE) peptide CLV3, which is secreted by stem cells. CLV3 interacts with leucine-rich-repeat receptor kinases (LRR-RLKs) of the CLAVATA1 (CLV1) family to inhibit WUSCHEL, generating a negative feedback loop. An antagonistic pathway involves CLE40, another CLE peptide, that acts from the meristem's periphery via the CLV1-related receptor kinase BARELY ANY MERISTEM 1 (BAM1) to influence meristem shape. Additionally to BAM1, the closely related BAM2 and BAM3 also play a role in meristem function in Arabidopsis. Similar signalling mechanisms are conserved in grass species like rice and maize, where parallel CLAVATA-related pathways, involving the highly conserved CLE peptide FON2-LIKE CLE PROTEIN1 (FCP1), the CLV1 orthologs FLORAL ORGAN NUMBER1 (FON1) and THICK TASSEL DWARF1 (TD1), regulate the size and activity of the rice vegetative, inflorescence and floral meristems and the maize ears and tassel IMs.

In this study, we investigated the function of *Hordeum Vulgare* CLAVATA 1 (HvCLV1), the barley ortholog of CLV1, and discovered its role in coordinating the activity of different meristem types composing the barley spike. An extensive phylogenetic analysis allowed the identification of HvCLV1 and five closely related HvBAM genes in barley. A detailed characterization of the HvCLV1 expression pattern

and protein localisation throughout barley inflorescence development showed that HvCLV1 proteins mostly localise in the three outer cell layers of different meristem types composing the inflorescence. The identification of enhanced HvCLV1 internalisation in the RM, which indicates protein turnover after signalling, suggested a yet undescribed function of HvCLV1 in the regulation of RM activity. We generated three *Hvclv1* loss of function mutant alleles by CRISPR-Cas9 genome editing. *Hvclv1* mutants were semi-dwarf and formed shorter inflorescences in comparison to WT. Interestingly, their inflorescences occasionally formed an additional row of spikelets and multi-floret spikelets, bearing supernumerary grains. Detailed microscopy analysis of *Hvclv1* inflorescences at different developmental stages, revealed that *Hvclv1* developed an enlarged IM, which caused the formation of an additional row of spikelts, but also repressed spikelet formation in the main inflorescence axis. The RM was also enlarged in *Hvclv1*, and the enhanced RM activity allowed the formation of additional florets per spikelet.

Wild-type seedlings grown in medium with the barley CLE peptide HvFCP1 showed a reduction in their SAM height, while *Hvclv1* seedlings treated in the same way didn't show any difference in SAM size, suggesting that HvFCP1 and HvCLV1 act in the same pathway. To further investigate this, we generated an HvFCP1 transcriptional reporter line and showed that the HvFCP1 promoter is specifically active in the IM and RM, where it overlaps with HvCLV1. The *Hvfcp1* mutant displayed a similar inflorescence phenotype as *Hvclv1* and formed multi-floret spikelets, but didn't form additional rows of spikelets. This aspect, together with the *Hvclv1;Hvfcp1* double mutant phenotype, that resembled the phenotype of *Hvclv1,* and the identification of HvCLV1 internalisation in *Hvfcp1* background, indicated that additional peptides could interact with HvCLV1, suggesting that the broadly expressed HvCLV1 receptor can mediate signals from locally expressed CLE peptides to shape the barley inflorescence architecture, coordinating of the proliferation of different meristem types. Transcriptome analysis by RNA sequencing of *Hvclv1* and *Hvfcp1* inflorescences in comparison to WT revealed a common gene regulatory network influenced by the HvFCP1/HvCLV1 signalling pathway that involved differential expression of genes with a putative role in the regulation of cell division, auxin signalling, and Trehalose-6-Phosphate (T6P) homeostasis.

The overall mild phenotype of *Hvclv1* and the compensatory effect demonstrated for BAM1 in the Arabidopsis *clv1* mutant suggested that additional CLV-related pathways

could partially rescue the inflorescence phenotype of *Hvclv1*. We therefore generated transgenic plants carrying a CRISPR-Cas9 construct simultaneously targeting HvCLV1 and the two closely related barley receptors HvBAM1 and HvBAM2, and obtained different mutant combinations by segregation after back-crossing to WT.

The single mutants *Hvbam1* and *Hvbam2* showed only minor differences compared to WT, but higher-order mutants in combination with *Hvclv1* developed shorter plants with increasingly branched inflorescences. The enlarged RM of *Hvclv1* was enhanced in size in the double mutant *Hvclv1;Hvbam1* (*Dc1b1*) and allowed the formation of floret triplets. Interestingly the double mutant *Hvclv1;Hvbam2* (*Dc1b2*) and the triple mutant *Hvclv1;Hvbam1;Hvbam2* (*Tc1b1b2*), not only developed and enlarged RM, but the SMs on the upper part of their inflorescence changed identity and became actual branch meristems, bearing either disorganised or spirally distributed SMs of their flanks.

Transcriptional analysis of inflorescences from all the mutant combinations, in comparison to WT, highlighted the presence of additional RLKs and CLE peptides possibly involved in the regulation of barley meristem activity. It also revealed differences in the expression of genes involved in cell division, auxin signalling, T6P homeostasis, and sucrose synthesis. The results suggested similar functions of HvCLV1 and HvBAM2, even though through regulation of mostly different genes, and an opposite function of HvBAM1 compared to HvCLV1, consistent with previous results from Arabidopsis. Additionally, single-cell RNA sequencing of *Tc1b1b2* inflorescences confirmed the findings from bulk RNA sequencing. This technique enabled detailed phenotyping of the inflorescence at the cellular level, providing spatial insights into the expression patterns of the analysed genes.

Taken together, our results illustrate that specific regulation of meristems in grass inflorescences can facilitate future modifications of spike structure. Additionally, they imply that variations in the regulation of CLAVATA-related pathways may have significantly influenced the development of the diverse inflorescence architectures that evolved in grasses.

Chapter 1

CLAVATA signalling shapes barley inflorescence architecture by controlling activity and determinacy of shoot apical and rachilla meristems

Isaia Vardanega[1], Jan Eric Maika[1], Edgar Demesa-Arevalo[1,11], Tianyu Lan[2], Gwendolyn K. Kirschner[1,11], Jafargholi Imani[3], Ivan F. Acosta[4], Katarzyna Makowska[5], Götz Hensel[5], Thilanka Ranaweera[6,7], Shin-Han Shiu[6,7,8], Thorsten Schnurbusch[9,10], Maria von Korff Schmising[2,11], Rüdiger Simon[1,11,*]

[1] Institute of Developmental Genetics, Heinrich-Heine University, Düsseldorf, Germany

[2] Institute of Plant Genetics, Heinrich-Heine University, Düsseldorf, Germany

[3] Institute of Phytopathology, Justus Liebig University, Giessen, Germany

[4] Max Planck Institute for Plant Breeding Research, Cologne, Germany

[5] Centre for Plant Genome Engineering, Institute of Plant Biochemistry, Heinrich-Heine University, Düsseldorf, Germany

[6] Department of Plant Biology, Michigan State University, East Lansing, Michigan, USA

[7] DOE-Great Lake Bioenergy Research Center, Michigan State University, East Lansing, Michigan, USA

[8] Department of Computational Mathematics, Science, and Engineering, Michigan State University, East Lansing, Michigan, USA

[9] Leibniz Institute of Plant Genetics and Crop Plant Research (IPK), Gatersleben, Germany

[10] Institute of Agricultural and Nutritional Sciences, Martin Luther University Halle-Wittenberg, Halle, Germany

[11] CEPLAS, Center of Excellence in Plant Sciences, Heinrich-Heine University, Düsseldorf, Germany

*corresponding author, ruediger.simon@hhu.de

1. Abstract

Grasses exhibit a large variety of diverse inflorescence architectures, from complex branched inflorescences in *Oryzeae* (rice) to simple spike-type inflorescences in *Triticeae* (e.g. barley, wheat). Inflorescence architecture depends on shape, longevity, and determinacy of meristems that direct growth of the main rachis and lateral branches, but how individual meristem activities are determined and integrated within complex inflorescences is not yet understood. We found that activity of distinct meristems in the barley inflorescence is coordinated by a signalling pathway comprising the receptor like kinase *Hordeum vulgare* CLAVATA1 (HvCLV1) and the secreted CLAVATA3/ENDOSPERM SURROUNDING REGION (CLE)-family peptide FON2-LIKE CLE PROTEIN1 (HvFCP1). HvFCP1 interacts with HvCLV1 to promote spikelet formation but restricts inflorescence meristem and rachilla meristem proliferation. *Hvfcp1* or *Hvclv1* mutants generate branched inflorescences with additional rows of spikelets and supernumerary florets. Transcriptome analysis reveals that *HvFCP1/HvCLV1* signalling controls inflorescence branching through the regulation of trehalose-6-phosphate synthesis and sugar transport. Our discoveries reveal the potential to engineer barley inflorescence architecture by manipulating the regulation of distinct meristem activities.

2. Main

The *Poaceae* family (*Gramineae* or grasses) displays a large variety of inflorescence architectures that evolved from an ancestral compound spike with panicle-like branches on a main inflorescence axis (rachis)[1]. The multiple branching orders characteristic of panicles gradually simplified during evolution and domestication, generating the variety of current grass inflorescences[2]. The morphology of distinct grass inflorescence architectures depends on the initiation and placement of new meristems on the flanks of the shoot apical meristem (SAM), and on meristem size, longevity, identity, and determinacy[3]. During the vegetative phase, the cereal SAM generates only leaf primordia in a distichous pattern. In response to both external and internal signals, the SAM converts into an inflorescence meristem (IM), which can initiate spikelets directly on the rachis in *Triticeae*[2], including barley (*Hordeum vulgare* L.) and wheat (*Triticum* ssp.), or form primary and secondary branches[4] in *Oryzeae* (rice) and *Andropogoneae* (maize and sorghum).

Spikelet meristems (SM) first give rise to two small modified bracts (the glumes), and later to a variable number of floret(s) that develop from floret meristems (FMs) on a short axis called rachilla, which is sustained by a rachilla meristem (RM). Florets carry the leaf-like lemma and palea, which enclose modified petals called lodicules, and the sex organs, the stamen and carpel[5].

In barley, the IM remains indeterminate and generates triple spikelet meristems (TSM) on its flanks until developmentally programmed pre-anthesis tip degeneration causes IM senescence and death[5,6]. TSM splits into a central spikelet meristem (CSM), flanked by two lateral spikelet meristems (LSM). In two-rowed cultivars, lateral spikelets remain sterile and arrest before floret organs are fully developed[7]. Each SM further divides into the vestigial rachilla meristem (RM), an abaxial floret meristem (FM), and a subtending lemma primordium (LEP).

Inflorescence branching in barley is suppressed by the transcription factors COMPOSITUM1 (COM1), COM2[8,9], and HvMADS1, while INTERMEDIUM-m restricts floret number per spikelet and maintains indeterminacy of the IM[10,11]. In maize, inflorescence branching is controlled by the RAMOSA pathway, comprising RAMOSA3 (RA3), a trehalose-6-phosphate phosphatase that putatively regulates branching by a sugar signal that moves into axillary meristems[12]. Importantly, even

closely related grasses, such as the temperate cereals wheat and barley, differ in their inflorescence architecture because of differences in meristem behaviour. In wheat (*Triticum aestivum* L.), inflorescence growth arrests with differentiation of the IM into an SM, but the RM remains indeterminate, enabling the formation of up to 12 florets[2,5]. These examples illustrate how differential regulation of meristem activities finally impacts inflorescence architecture. However, the regulatory networks, feedback regulations, and external inputs that coordinate the size, longevity, and determinacy of different meristem types in the inflorescence are still unknown.

In Arabidopsis, the activity of shoot and floral meristems depends on the WUSCHEL transcription factor, which moves from a deeper meristem region to the stem cell zone to promote stem cell maintenance by suppressing auxin response factors. WUSCHEL promotes expression of the CLAVATA3/ENDOSPERM SURROUNDING REGION (CLE) family peptide CLV3, which is secreted from stem cells and interacts with leucine-rich-repeat receptor kinases (LRR-RLKs) of the CLAVATA1 (CLV1) family to repress WUSCHEL, thereby providing a negative feedback signal. CLE40 acts from the meristem periphery through the CLV1-related RLK BARELY ANY MERISTEM 1 (BAM1) to impact meristem shape[13]. CLV-related signalling pathways regulate diverse meristem activities, including root and cambial meristems[14], and CLE / CLV1-family signalling has also been described for rice and maize. In rice, the LRR-RLK FLORAL ORGAN NUMBER1 (FON1) and the CLE peptide FLORAL ORGAN NUMBER2 (FON2) restrict the sizes of FMs, IM, and the number of primary branches[15,16], while FON2-LIKE CLE PROTEIN1 (FCP1), which is highly conserved between cereal grasses, likely plays an antagonistic role and promotes maintenance of the vegetative SAM and root apical meristem[17,18]. The maize LRR-RLK THICK TASSEL DWARF1 (TD1) and CLE7 confine the diameter of both tassel and ear meristems. In *td1* mutants, an enlarged IM initiates disorganised supernumerary rows of spikelet pair meristems, which sometimes develop additional SMs[19,20]. In parallel, ZmFCP1 signalling suppresses stem cell proliferation in the ear meristem, which is enlarged in *Zmfcp1* mutants[18,20].

The development of cereal inflorescence architectures requires a close coordination of meristem ontogenies. Here, we investigated how CLV-related signalling pathways may contribute to this process in barley. We identify the barley HvCLV1 and HvFCP1 and show that they act in joint, but also separate, signalling pathways to impact multiple aspects of meristem development. Our findings extend the roles of CLV

signalling, from feedback signalling in stem cell homeostasis to coordination of meristem shape, organ formation, and determinacy in cereal inflorescences.

3. Results

3.1 HvCLV1 controls the activity of inflorescence and rachilla meristems to promote spikelet formation and repress multi-floret spikelets in barley spikes

To identify CLV1-related RLKs from barley, we analysed the phylogeny for all protein kinase sequences from two dicotyledons (*Arabidopsis thaliana*, *Solanum lycopersicum*) and four gramineous species belonging to the *Poaceae* family (*Zea mays*, *Oryza sativa japonica*, *Triticum turgidum* and *Hordeum vulgare*). Within the clade comprising AtCLV1, we identified six closely related genes from barley. HORVU.MOREX.r3.7HG0747230 represented the closest ortholog of *AtCLV1* in *Hordeum vulgare* and was named *HvCLV1*. *HvCLV1* grouped with the maize and rice orthologs *ZmTD1* and *OsFON1*, the other five genes in the clade were more closely related to *AtBAM1 to 3* and we designated them *HvBAM1* to *5* (ExtDataFig.1A). *HvCLV1* encodes an LRR-RLK protein of 1,015 amino acids, comprising an intracellular kinase domain and 20 extracellular Leucin Rich Repeats (LRRs), similar to the closely related ZmTD1 and OsFON1, and AtCLV1 with 21 LRRs (Fig.1A). *HvCLV1* expression was analysed using single-molecule RNA fluorescent *in situ* hybridisation (smRNA-FISH, Molecular Cartography™, Resolve Biosciences) on sectioned developing barley apices during vegetative (Fig.1B-D) and reproductive stages (Fig.1E-M, ExtDataFig.1B), and HvCLV1 protein localisation was analysed using the translational reporter line *pHvCLV1:HvCLV1-mVenus*, which expresses the HvCLV1 protein with the fluorophore mVenus fused C-terminally to the cytoplasmic kinase domain and functionally complements a *Hvclv1* mutant (see below, ExtDataFig.2N). We used the Waddington scale (Waddington stage, W) to define stages of barley development[21]. During vegetative (W1) and reproductive development (W3.5) (Fig.1B,E), *HvCLV1* is expressed mostly in the three outer cell layers in the apical meristem (Fig.1C,F), and throughout spikelet development in RM, FM, lemma primordium and flower organs (Fig.1H,L). *HvCLV1* mRNA and HvCLV1 protein were detected in similar patterns (Fig.1D,G,I,M). Longitudinal sectioning of the developing spikelet showed HvCLV1 internalization in the RM (Fig.1J,K, ExtDataFig.1D). HvCLV1 localised to the plasma membrane and to cytoplasmic

structures, which could reflect either *de novo* synthesis and intracellular trafficking, or turnover after signalling[22].

For a better understanding of the function of barley HvCLV1, we generated *Hvclv1* mutants by CRISPR-Cas9. Three independent alleles, *Hvclv1-1* to *-3*, which likely represent loss-of-function mutants, showed closely related phenotypes (ExtDataFig.2A, Suppl.info1). All *Hvclv1* mutants were semi-dwarfs (Fig.2A), with shorter stems, spikes and fewer internodes and tillers than WT (ExtDataFig.2B-E). *Hvclv1* mutants also developed fewer and smaller grains than WT (ExtDataFig.2F-K). Furthermore, a variable proportion of the *Hvclv1-1* spikes formed additional, ectopic rows of spikelets in a non-distichous phyllotaxis (crowned spikes) (Fig.2B-D), or carried multi-floret spikelets with two or three florets, separate embryos, and endosperms enclosed by partially fused lemmas (Fig.2E-G). These phenotypes were also observed in *Hvclv1* mutants grown in semi-field-like conditions in Germany between March to the end of July 2023, but not in WT (Suppl.info2). Detailed microscopic analysis of early development showed that *Hvclv1-1* and WT meristems developed similarly along vegetative stages (Fig.2H,I), although *Hvclv1* SAMs were slightly enlarged (see below). At W1.5 (between 10 and 13 DAS), meristems started to produce spikelet primordia while cells continued to accumulate in the IM until W2.5. IM size was then reduced during rapid spikelet initiation (W2.5 to W4.5). After termination of spikelet formation at W5 to W5.5, the width of the IM remained unaltered, and cells started to accumulate along the vertical axis (Fig.2J,K). *Hvclv1* mutant had larger IMs than WT at W1.5 (Fig.2K), and developed faster than WT, reaching each stage earlier (Fig.2I). IMs of *Hvclv1* always appeared more elongated than WT IMs (Fig.2K) but also arrested spikelet initiation earlier (Fig.2J). The length of the entire inflorescences was briefly reduced at early stages when *Hvclv1* mutants progressed rapidly through developmental stages but did not differ significantly from W4 onwards (ExtDataFig.2M). We conclude that *HvCLV1* first acts to restrict meristem growth and developmental progression of spikelet primordia, and promotes spikelet initiation at later stages.

To track the origin of the multi-floret spikelets and ectopic spikelet rows in *Hvclv1* plants, we imaged developing inflorescences by scanning electron microscopy (SEM). Bases of *Hvclv1* IMs were enlarged at the initiation of spikelet formation (W1.5) (Fig.2K), which correlated with the formation of an additional row of SMs in later stages. IMs then shifted from a distichous to a spiral phyllotaxis (Fig.3A,B). In WT, the barley

SM gives rise to the rachilla meristem (RM), which arrests development after initiation of a single floret (Fig.3C-E). SEM analysis showed that the RM continues to grow wider and for an extended time in *Hvclv1* (Fig.3F), forming either larger or additional florets, or even secondary RMs (Fig.3G-J). We conclude that *HvCLV1* is required to restrict RM activities to the formation of a single floret.

3.2 The CLE peptide HvFCP1 acts with HvCLV1 to limit meristem activities

In many plant species, CLV1-family receptors were found to interact with CLE peptides closely related to Arabidopsis CLV3 and CLE40, such as OsFCP1 from rice. We found that the barley gene HORVU.MOREX.r3.2HG0174890 encodes an evolutionarily conserved FCP1-like peptide, which we named HvFCP1 (Suppl.info3). Incubation of WT barley seedlings with growth medium containing 30 µM of synthetic HvFCP1 peptide caused a reduction in meristem height of the WT SAM, while SAM width was not affected. *Hvclv1-1* mutant seedlings were insensitive to HvFCP1 treatment (Fig.4A), indicating that HvFCP1 requires HvCLV1 to limit SAM height.

We then analysed the expression of a transcriptional reporter line, *pHvFCP1:mVenus-H2B*, in transgenic barley (Fig.4B-E). During the vegetative phase, *HvFCP1* promoter was active in the SAM, but downregulated in leaf initiation sites (Fig.4B). Later on, activity was found in the IM and from the triple spikelet meristem stage onwards (Fig.4C). Moreover, the activity was polarized at the adaxial side of the developing central spikelet, at the rachilla primordium (RP) and later in the fully formed RM (Fig.4E). In FMs, *HvFCP1* was mainly expressed on the central domain and later in carpel primordia (Fig.4D). Importantly, the *HvFCP1* reporter was more prominently expressed in the RM compared to *HvCLV1* (ExtDataFig.3A-J).

We generated two independent knock-out mutant alleles by CRISPR-Cas9 (*Hvfcp1-1* and *-2)* to study HvFCP1 function. Both *Hvfcp1* alleles are phenotypically indistinguishable, and molecular analysis identifies them as loss-of-function mutants (ExtDataFig.4A). *Hvfcp1* plants, similar to *Hvclv1*, remained shorter with shorter inflorescences and formed fewer viable grains, while tiller or internode number was not affected (ExtDataFig.4B-E). *Hvfcp1* mutant IM height and width increased similarly to those of *Hvclv1* mutants and developed faster than WT (ExtDataFig.4F-H). Ectopic formation of spikelet rows was not observed, but we found multi-floret spikelets as

described for *Hvclv1* (Fig.4F,G; ExtDataFig.4I), indicating that HvFCP1 acts with HvCLV1 to regulate SAM, IM, SM and RM determinacy.

We next analysed the roles of *HvCLV1* and *HvFCP1* in regulating meristem growth and determinacy using confocal imaging and cell segmentation followed by computational 3D reconstructions of WT, *Hvclv1-1* and *Hvfcp1-1* IMs from W4.5 to W6.5 (Fig.4H). After W5 and termination of spikelet formation, the sizes of *Hvclv1* and *Hvfcp1* IMs increased more rapidly than WT, due to enhanced cell proliferation (Fig.4I,J; ExtDataFig.5A-D). Sizes of the RM were also increased at all stages in *Hvclv1-1* and *Hvfcp1-1,* compared to WT (Fig.5A,B), while FMs were less affected (Fig.5C). *Hvfcp1* mutant phenotypes were overall milder than those of *Hvclv1*, and loss of *HvFCP1* activity did not enhance the phenotype of *Hvclv1* in the *Hvclv1;Hvfcp1* double mutant (Fig.5D), indicating that other CLE peptides can partially compensate for the loss of HvFCP1 and signal through HvCLV1. To analyse this further, we crossed the *HvCLV1* and *HvFCP1* reporter lines into the *Hvfcp1* and *Hvclv1* mutant backgrounds (Fig.5E-L). Expression of *pHvCLV1:HvCLV1-mVenus* was unaltered in the *Hvfcp1-1* IM (Fig.5E,F), while *HvFCP1* expression was reduced in *Hvclv1-1* (Fig.5I-L). Interestingly, HvCLV1 protein internalization, which indicates receptor turnover upon ligand binding[22], was still detected in the IM and RM in a *Hvfcp1* background, suggesting that in the absence of HvFCP1, an additional peptide can partially compensate for its function (Fig.5G,H).

3.3 HvFCP1 and HvCLV1 control meristematic proliferation through coordination of cell division, auxin signalling and trehalose-6-phosphate

To investigate the common function of HvCLV1 and HvFCP1, we performed RNA-sequencing of WT, *Hvclv1-1* and *Hvfcp1-1* inflorescences at W3.5. A total of 1,208 genes were upregulated and 1,197 downregulated in *Hvclv1* vs WT, while 521 and 258 were upregulated and downregulated in *Hvfcp1* vs WT respectively. Interestingly, 55.2% (288) of the upregulated and 39.9% (103) of the downregulated genes in *Hvfcp1* vs WT were in common with *Hvclv1* vs WT, suggesting a partially shared function of HvFCP1 in the larger gene regulatory network affected by HvCLV1 (ExtDataFig.6A, B).

Mutation of the HvFCP1/HvCLV1 signalling pathway resulted in an enhanced proliferation of the IM and RM in comparison to WT, which ultimately repressed spikelet formation and promoted inflorescence branching. Within the upregulated genes common to both *Hvclv1* vs WT and *Hvfcp1* vs WT, we found *HvBG1*, ortholog of *Rice Big Grain1* (RBG1), which promotes cell division and auxin accumulation in meristematic and proliferating tissues when overexpressed in rice[23]. Furthermore, upregulation of the P-type cyclin *HvCYCP4-1* and the bicistronic transcript encoding Triphosphate Tunnel Metalloenzyme 3 (HvTTM3) and CELL DIVISION CYCLE PROTEIN26 (HvCDC26), together with upregulation of the auxin response genes *HvIAA13* and *HvIAA31,* indicated a general promotion of cell division and alteration of auxin signalling [24–26].

Inflorescence branching was previously associated with increased levels of Threhalose-6-Phospate (T6P). Mutation of the maize gene *RAMOSA3* (*RA3*), encoding a Threhalose-6-Phospate Phosphatase, led to indeterminate growth of inflorescence auxiliary meristems, that produced long branches bearing additional FMs[12]. Moreover, studies in Arabidopsis linked increased levels of T6P in axillary meristems with enhanced shoot branching via *FLOWERING LOCUS T* (*FT*) and upregulation of the sucrose transporter *Sugars Will Eventually be Exported Transporters11* (*SWEET11*)[27].

In both *Hvclv1* vs WT and *Hvfcp1* vs WT, *SISTER OF RAMOSA3* (*HvSRA*), paralogue of the maize *RA3,* was downregulated, and *HvTPS1*, the closest ortholog of the Arabidopsis Threhalose-6-Phospate Synthase1 (*TPS1*), was upregulated, suggesting an impaired T6P metabolism. Consistent with findings in Arabidopsis, the sucrose transporter *HvSWEET11b* and *HvFT2*, a barley paralogue of FT, were upregulated in both mutants in comparison to WT, indicating a general reallocation of sucrose and alteration of SM identity (Fig.6A, ExtDataFig.6C)[28,29]. Additionally, the barley gene *COM2* was downregulated in Hv*clv1* vs WT, suggesting that HvCLV1 has a role in the upstream regulation of this transcription factor involved in the repression of spike branching.

4. Discussion

In this study, we characterised the function of *CLAVATA* signalling components in coordinating the activity of different meristem types within the barley inflorescence and showed that *HvCLV1*, together with *HvFCP1*, regulates IM and RM proliferation and determinacy.

The localised expression of *HvFCP1* overlapped with only part of the broader expression of *HvCLV1* (Fig.6B), and while both *Hvclv1* and *Hvfcp1* mutants developed multi-floret spikelets as a consequence of their indeterminate and enlarged rachilla, only *Hvclv1* developed crowned spikes. Additionally, the overall weaker phenotype of *Hvfcp1*, together with observation of HvCLV1 protein internalisation in *Hvfcp1* background and the *Hvclv1;Hvfcp1* double mutant phenotype, suggests that additional CLE peptides could interact with HvCLV1, and partially rescue the *Hvfcp1* mutant phenotype. Altogether, our results point toward a more general role of HvCLV1 in mediating the downstream transmission of signals triggered by specifically expressed CLE peptides, thereby regulating the proliferation of different meristems in response to internal or external signals. Transcriptional analyses of *Hvclv1* and *Hvfcp1* highlighted a shared regulatory network between HvCLV1 and HvFCP1, directly or indirectly controlling the expression of genes involved in cell division, auxin signalling and T6P metabolism. Therefore, changes in the proliferation and development of meristems leading to inflorescence growth not only affected inflorescence architecture but also the overall plant architecture. An enhanced activity of the RM came together with upregulation of *HvTPS1* and downregulation of *HvSRA*, which likely results in accumulation of T6P, previously linked with enhanced branching in Arabidopsis, pea, barley and maize[12,27,30,31]. Increased T6P levels were shown to lead to reorganization of sugar transport by transcriptional regulation of *SWEET* genes and upregulation of *FT*-related genes, which are directly involved in spikelet identity and flowering time[27]. *HvFT2* overexpression in barley consistently resulted in early flowering plants with reduced formation of spikelet primordia, similar to the phenotype observed in *Hvclv1* and *Hvfcp1*[32].

Meristem homeostasis is controlled redundantly by different receptors and peptides. In maize, rice, and Arabidopsis, parallel and antagonistic pathways control IM shape and maintenance[16,33,34]. The relatively mild phenotype of *Hvclv1*, in comparison to the

phenotypes described for *td1* in maize or *clv1* in Arabidopsis is probably the result of partial compensation by additional CLV-related receptors acting in parallel[19,35]. Combining *Hvclv1* with mutations in other *HvBAM* genes from the same clade might further enhance the *Hvclv1* phenotype.

Our study shows how the *CLV* signalling pathway coordinates the determinacy and growth of diverse meristems of barley spikes, and that regionally expressed CLE peptides differentially regulate the proliferation of specific meristems. Here we note an underexplored opportunity to redesign and optimise barley inflorescence architecture by manipulating the regulation of distinct meristem activities. The large diversity of inflorescence architectures that already evolved in grasses indicates that the underlying genetic networks offer a vast, yet hidden potential to encode a much wider morpho-space than what is realised in our current cereal varieties.

5. Materials and methods

5.1 Phylogenetic analysis

The CLV1 clade was identified by phylogenetic reconstruction of the protein kinase superfamily of four monocots (*Oryza sativa*, *Triticum turgidum*, *Zea mays*, and *Hordeum vulgare*), and two dicot species (*Arabidopsis thaliana*, *Solanum lycopersicum*). The proteomes of these species were downloaded from Ensembl Plants (https://plants.ensembl.org/index.html). To identify all the protein kinase domain containing proteins in the selected species' proteomes, we conducted HMMscan using HMMER V 3.2 (http://hmmer.org)[36]. HMM profiles of the protein kinase domain (Pfam 10.0) were downloaded from InterPro[37] to carry out the HMM matching. Based on the HMMscan result an E-value threshold of < 1e -10 was imposed to identify the protein kinase domains (PF00069) in the given protein sequences. Protein kinase domains were extracted from all the protein sequences using custom Python scripts and were subjected to HMMalign for protein kinase domain alignment[36]. The multiple sequence alignment was used to construct a Neighbor-joining tree (using the JTT+CAT model and default parameters) using the FastTree package[38]. Based on the constructed protein kinase domain family tree we identified the CLV1 clade. Next, we extracted the protein kinase domain sequences from the operational taxonomic units of the selected CLV1 clade to further examine the phylogenetic relationships of kinase domains of the CLV1 clade. We constructed the receptor-like kinase phylogeny using RAxML (using random seed for tree initiation

and non-parametric bootstrapping) for 1000 bootstrap replicates[39]. This was completed using automated model selection criteria to select the best evolutionary model that fits the dataset.

5.2 Plant material and growth conditions

All barley plants used in this study were *cv.* Golden Promise Fast[40] and were grown in soil (Einheitserde ED73, Einheitserde Werkverband e.V., with 7% sand and 4 g/L Osmocote Exact Hi.End 3-4M, 4th generation, ICL Group Ltd.) under long day (LD) conditions with 16 hours light at 20°C and 8 hours dark at 16 °C. Plants used for microscopy were grown in QuickPot 96T trays (HerkuPlast Kubern GmbH) in a climate chamber, while the plant phenotype was described in plants growing in larger pots (diameter 16.5 cm, height 13 cm) in a greenhouse under the same growing conditions but with temperatures that slightly varied between seasons. Grains were always pregerminated in Petri dishes with water at 4°C for 3 days before being sowed in soil.

5.3 Plasmids construction and plant transformation

The pHvCLV1:HvCLV1-mVenus plasmid was constructed by PCR amplification of a 2,826 bp fragment upstream of the start codon of HvCLV1 (HORVU.MOREX.r3.7HG0747230) as putative regulatory sequence from Morex genomic DNA (gDNA) and cloned by restriction and ligation via a AscI site into a modified pMDC99[41]. The HvCLV1 coding region without stop codon (3,573 bp) was amplified from Morex gDNA and inserted downstream of the promoter by Gateway cloning (Invitrogen). A C-terminal mVENUS was integrated downstream of the gateway site by restriction and ligation via PacI and SpeI (Suppl.table1). The pHvFCP1:VENUS-H2B construct was cloned by amplifying the regulatory sequence including 2,034 bp upstream of the start codon of HvFCP1 (HORVU.MOREX.r3.2HG0174890) and inserted by Gateway cloning (Invitrogen) into the modified pMDC99[41]. This modified pMDC99 contained the gateway cassette, the coding sequence of VENUS and a T3A terminator, which were inserted by restriction via AscI and SacI from pAB114[42]. Furthermore, it contains the coding sequence of Arabidopsis HISTONE H2B (AT5G22880) at the C terminus of VENUS for nuclear localisation, inserted via restriction and ligation at a PacI restriction site (Suppl.table 1). Both pHvCLV1:HvCLV1-mVenus and pHvFCP1:VENUS-H2B constructs were first transformed in the barley cultivar Golden Promise[43] and then crossed into Golden Promise Fast. *Hvclv1* and *Hvfcp1* mutant alleles were generated by CRISPR-Cas9

genome editing. Plasmids were constructed using the vector system and following the established protocol[44]. The HvCLV1 gene was targeted by a single 20bp sgRNA 53bp after the coding sequence started, while two 20bp sgRNAs were cloned to target HvFCP1 298 and 542 bp after the start codon. All the sgRNAs were designed using E-CRISP software[45] and single sgRNA strands were hybridized and cloned into the shuttle vectors pMGE625 or pMGE627 by a BpiI cut/ligation reaction. A second cut/ligation reaction (BsaI) was used to transfer the gRNA transformation units (TUs) to the recipient vector pMGE599[44]. The final vector targeting HvCLV1 was transformed in Golden Promise Fast via embryo transformation[46], while the vector targeting HvFCP1 was transformed in Golden Promise Fast via embryo transformation, but using the transformation protocol by Hensel et al. (2009)[47]. Successful insertion of the transformation vector into the genome was tested by PCR (Suppl.table1) on M0 plants. The Cas9 protein was removed by segregation in M1 plants, and homozygous mutations of HvCLV1 and HvFCP1 were identified in M2 plants by amplification of genomic sequences targeted by the sgRNAs and subsequent Sanger sequencing. (Suppl.table1).

5.4 smRNAfish

Barley inflorescences at W3.5 fixed in 4% PFA were embedded in paraplast (Leica Paraplast X-tra) and tissue sections (10 µm) were placed within the capture areas on Resolve Bioscience slides and incubated on a hot plate for at least 20min at 60°C to attach the samples to the slides. Slides were deparaffinized, permeabilized, acetylated and re-fixed. Sections were mounted with a few drops of SlowFade-Gold Antifade reagent (Invitrogen) and covered with a coverslip to prevent damage during shipment to Resolve BioSciences (Germany).

5.5 Plant phenotyping

WT, *Hvclv1* and *Hvfcp1* plants were phenotyped at the end of their life cycle, when completely dried. Plant measurements and percentage of crowned spikes and multi-grains were performed in all the tillers with no distinction between main stem and lateral branches, since the spike phenotypes raised with the same probability in both main and lateral tillers. Three replicates were performed and three plants per replicate were phenotyped.

5.6 Sample preparation, microscopy and image processing

Barley SAMs and inflorescences were collected by manual removal of all the surrounding leaves. Smaller leaves were dissected under a stereo microscope using a 1.5 mm blade scalpel. Fresh inflorescences were directly imaged for stereo microscope pictures using a Nikon SMZ25 stereo microscope with a Nikon DS-Fi2 camera. For confocal imaging, fresh barley inflorescences were stuck on their side on a double-sided adhesive tape on an objective slide, stained with 4′,6-diamidin-2-phenylindol (DAPI 1 µg/mL) for 3 minutes, washed three times with water and subsequently covered by with a cover slide before being placed under the microscope. Confocal imaging was performed using Zeiss LSM780 and Zeiss LSM880 with a EC PlnN 10x/0.3, Plan-Apochromat 20x/0.8 or Plan-Apochromat 40x/1 objectives. SEM pictures were obtained by direct imaging of fresh inflorescences or by imaging epoxy replicates of barley inflorescences. At first, a negative imprint of the inflorescence was created by mixing the two-component vinyl polysiloxane impression material (Express™ 2Ultra Light Body Quick, 3M ESPE) and pushing the dissected inflorescence into the impression material, which polymerizes a few minutes after having been mixed. After complete polymerization of the negative print, the plant material was removed, and the negative print was filled with epoxy resin. After overnight polymerization, inflorescence replicates were coated with gold using an Agar Sputter Coater and imaged with a Zeiss SUPRA 55VP SEM.

5.7 Peptide treatment

Barley WT and *Hvclv1-1* embryos were dissected at 10 days after pollination when the SAM was exposed, and cultured on gel media. The medium was prepared by mixing 4.4 g/L of MS medium, 2% sucrose, and 500 ul/L of iron chelate. The pH was adjusted to 6.0 before the addition of 1.5 g/L Gelrite. The medium was then autoclaved. Before being poured in cm square plates, after the medium cooled down, 1/1000 v/v ratio of vitamin mix was added. Treated embryos were then grown in medium with HvFCP1 synthetic peptide (REVPTGPDPIHH, by peptides&elephants GmbH) dissolved in 50ul DMSO reaching a final peptide concentration of 30 µM, while control embryos were grown in medium with 50 µl DMSO. Plates with embryos were grown in a Phyto-cabinet for 30 days at 24°C under long-day conditions. After 30 days, when young seedlings developed, vegetative meristems were dissected, fixed in 4% PFA

overnight, washed three times with water and incubated for one week in ClearSee solution[48]. Pictures of the cleared meristems were taken under the Zeiss Axioskop 2 light microscope with AxioCam HRc camera. Images were then analysed in Fiji. SAM width was measured by the length of a horizontal line drawn across the SAM base, just on top of the last visible spikelet primordium. Meristem height was calculated as the distance between the SAM tip and the centre of the horizontal line defining the base of the SAM. Three replicates of this experiment were performed and forty embryos were plated for each replicate, even though not all the embryos germinated.

5.8 IM 3D reconstruction and rachilla vibratome sections

IMs at different W stages were fixed in 4% PFA overnight, then washed three times with water and cleared in ClearSee solution for at least two weeks [48]. One day before imaging, 1/1000 v/v of SR 2200 stain by Renaissance Chemicals was added to the ClearSee solution and the cell wall was stained. After three washing steps in 1X PBS, barley inflorescences at different stages were glued on the bottom of a small petri dish with a drop of super glue and covered in 1X PBS. The petri dish was placed under Zeiss LSM900 confocal microscope and a z-stack of the submerged IM was imaged from the top with a 20x/0.5 water dipping objective. The 3D reconstruction was performed by loading the IM z-stacks in MorphoGraphX 2.0 and analysed according to the protocol [49]. Rachilla central longitudinal sections were obtained by following the same procedure described above for the 3D reconstruction. The fixed, cleared inflorescences at W6.5 were embedded in 6% agarose in Disposable Base Molds (epredia) and 50 µm sections were obtained using a Leica VT1000S vibratome. The sections were stained in a Petri dish in 1X PBS with 1/100 v/v concentration of SR 2200 stain for a few minutes, placed on an objective slide with 1X PBS, and covered with a cover slide. Sections of 10 inflorescences for each genotype were then imaged under an LSM880 confocal microscope.

5.9 RNA sequencing

To detect gene expression changes in *Hvclv1* and *Hvfcp1* inflorescence in comparison to WT, we collected inflorescences of WT, *Hvclv1-1*, and *Hvfcp1-1* at W3.5 for RNA-sequencing. Each replicate contained 40 pooled inflorescences from the main shoot of individual plants. All samples were collected manually under a stereo microscope without surrounding leaves. A total of three biological replicates of each genotype were used for RNA-sequencing. Total RNA was extracted from

inflorescences using the Direct-zol™ RNA, Miniprep Plus following the manufacturer's instructions and digested with DNase I (ZYMO RESEARCH). RNA samples passing a cutoff of RNA Integrity Number (RIN) ≥ 8 were used for mRNA library preparation using poly-A enrichment method. Sequencing was performed on Illumina Novaseq 6000 sequencing platform (PE150), and at least 6G of clean reads data per sample were generated by Biomarker Technologies (BMK) GmbH. To quantify transcripts, all clean reads were mapped to the Morex reference Version 3[50] using Salmon (v. 0.14.1)[51]. We kept transcripts with a minimum of 1 CPM (counts per million) in at least three samples. Analyses were conducted on 22307 expressed genes. To identify differentially expressed genes (DEGs) within *Hvclv1* vs WT and *Hvfcp1* vs WT, a pairwise comparisons was conducted using the count-based Fisher's Exact Test in R package 'EdgeR' (v3.32.1)[52]. The FDR of each gene was adjusted by the Benjamini-Hochberg (BH) procedure, thus the gene with BH.FDR<0.05 and $\log_2$FC ≤ -0.5 or $\log_2$FC ≥ 0.5 was referred to as downregulated or upregulated gene. The heatmap of gene expression (ExtDataFig.6B) was generated on all the differently expressed genes in *Hvclv1* vs WT and *Hvfcp1* vs WT with $-\log_{10}$(TPM + 1) values using 'ThreeDRNAseq' R package[53].

5.10 Quantification and statistical analysis

All the statistical tests were performed using R Studio (RStudio Team 2022). A 2-tailed, unpaired Student's t-test (function t_test from the package rstatix, v0.7.2) was used to determine the significance between two group means, with a P-value cutoff at ≤ 0.05. Significant difference between more than two groups was determined using a one-way ANOVA (function aov from package stats, v3.6.2) and a subsequent Pairwise t-test (function pairwise.t.test from package stats, v3.6.2), P-value cutoff at ≤ 0.05. Symbols: ns= p-value > 0.05, * = p-value <0.05, ** = p-value <0.01, *** = p-value < 0.001.

6. Author contributions

Isaia Vardanega performed most of the work presented here. Jan Eric Maika did the plant screening and imaging for the complementation of *Hvclv1-1* with the HvCLV1 reporter line and helped with the experiments. Edgar Demesa-Aravalo helped with the smRNAfish and with planning the experiments. Tianyu Lan from Maria von Korff Schmising's lab performed the RNA-seq raw data analysis and crossed the HvCLV1 reporter line into the barley cv. Golden Promise Fast. Gwendolyn K. Kirschner cloned the vectors for HvCLV1 and HvFCP1 reporter liones, transformed by Jafargholi Imani in barley *cv*. Golden Promise. Ivan Acosta helped with the transformation of *Hvclv1* mutants and Katarzyna Makowska in Götz Hensel's lab performed the transformation of *Hvfcp1* mutants. Thilanka Ranaweera from Shin-Han Shiu's lab performed the phylogenetic analysis, Thorsten Schnurbusch grew and analysed the *Hvclv1* mutant phenotype in semi-field-like conditions and Rüdiger Simon, with the cooperation of Maria von Korff Schmising, supervised the project and contributed to the overall planning of the experiments.

7. Acknowledgements

We thank Dr. Sebastian Hänsch and the Center for Advanced imaging (CAi) at HHU for microscopy support, Edelgard Wendeler for technical support with barley transformation (MPIPZ), Meik Thiele for providing help with the statistical analysis, and Karine Gustavo Pinto for her help with plant phenotyping. Work in R.S. and M.v.K.S. labs was supported by the DFG through CEPLAS (EXC2048), CSCS (FOR5235), NEXT-PLANT (IRTG2466) and work in I.F.A. lab by the Max Planck Society.

8. References

1. Zhang, D. & Yuan, Z. Molecular Control of Grass Inflorescence Development. *Annual Review of Plant Biology* **65**, 553–578 (2014).
2. Koppolu, R. & Schnurbusch, T. Developmental pathways for shaping spike inflorescence architecture in barley and wheat. *Journal of Integrative Plant Biology* **61**, 278–295 (2019).
3. Kyozuka, J., Tokunaga, H. & Yoshida, A. Control of grass inflorescence form by the fine-tuning of meristem phase change. *Current Opinion in Plant Biology* **17**, 110–115 (2014).
4. Wang, L. *et al.* Coordinated regulation of vegetative and reproductive branching in rice. *Proceedings of the National Academy of Sciences* **112**, 15504–15509 (2015).
5. Bommert, P. & Whipple, C. Grass inflorescence architecture and meristem determinacy. *Seminars in Cell & Developmental Biology* **79**, 37–47 (2018).
6. Shanmugaraj, N. *et al.* Multilayered regulation of developmentally programmed pre-anthesis tip degeneration of the barley inflorescence. *The Plant Cell* **35**, 3973–4001 (2023).
7. Zwirek, M., Waugh, R. & McKim, S. M. Interaction between row-type genes in barley controls meristem determinacy and reveals novel routes to improved grain. *New Phytologist* **221**, 1950–1965 (2019).
8. Poursarebani, N. *et al.* COMPOSITUM 1 contributes to the architectural simplification of barley inflorescence via meristem identity signals. *Nat Commun* **11**, 5138 (2020).
9. Poursarebani, N. *et al.* The Genetic Basis of Composite Spike Form in Barley and 'Miracle-Wheat'. *Genetics* **201**, 155–165 (2015).
10. Zhong, J. *et al.* INTERMEDIUM-M encodes an HvAP2L-H5 ortholog and is required for inflorescence indeterminacy and spikelet determinacy in barley. *Proceedings of the National Academy of Sciences* **118**, e2011779118 (2021).
11. Li, G. *et al.* MADS1 maintains barley spike morphology at high ambient temperatures. *Nat Plants* **7**, 1093–1107 (2021).
12. Satoh-Nagasawa, N., Nagasawa, N., Malcomber, S., Sakai, H. & Jackson, D. A trehalose metabolic enzyme controls inflorescence architecture in maize. *Nature* **441**, 227–230 (2006).

13. Demesa-Arevalo, E., Narasimhan, M. & Simon, R. Intercellular Communication in Shoot Meristems. *Annu Rev Plant Biol.*, 10.1146/annurev-arplant-070523-035342 (2024)
14. Stahl, Y., Wink, R. H., Ingram, G. C. & Simon, R. A signaling module controlling the stem cell niche in Arabidopsis root meristems. *Curr Biol* **19**, 909–914 (2009).
15. Moon, S. *et al.* The Rice FON1 Gene Controls Vegetative and Reproductive Development by Regulating Shoot Apical Meristem Size. *Molecules and cells* vol. 21,1 147-52 (2006).
16. Suzaki, T. *et al.* Conservation and Diversification of Meristem Maintenance Mechanism in Oryza sativa : Function of the FLORAL ORGAN NUMBER2 Gene. *Plant and Cell Physiology* **47**, 1591–1602 (2006).
17. Ohmori, Y., Tanaka, W., Kojima, M., Sakakibara, H. & Hirano, H.-Y. WUSCHEL-RELATED HOMEOBOX4 Is Involved in Meristem Maintenance and Is Negatively Regulated by the CLE Gene FCP1 in Rice. *The Plant Cell* **25**, 229–241 (2013).
18. Je, B. I. *et al.* Signaling from maize organ primordia via FASCIATED EAR3 regulates stem cell proliferation and yield traits. *Nat Genet* **48**, 785–791 (2016).
19. Bommert, P. *et al.* thick tassel dwarf1 encodes a putative maize ortholog of the Arabidopsis CLAVATA1 leucine-rich repeat receptor-like kinase. *Development* **132**, 1235–1245 (2005).
20. Liu, L. *et al.* Enhancing grain-yield-related traits by CRISPR-Cas9 promoter editing of maize CLE genes. *Nat Plants* **7**, 287–294 (2021).
21. Waddington, S. R., Cartwright, P. M. & Wall, P. C. A Quantitative Scale of Spike Initial and Pistil Development in Barley and Wheat. *Annals of Botany* **51**, 119–130 (1983).
22. Jie Wang *et al.* TPLATE complex‐dependent endocytosis attenuates CLAVATA1 signaling for shoot apical meristem maintenance. *EMBO rep* **24**(9), e54709 (2023)
23. Lo, S. *et al.* Rice Big Grain 1 promotes cell division to enhance organ development, stress tolerance and grain yield. *Plant Biotechnol J* **18**, 1969–1983 (2020).
24. Torres Acosta, J. A. *et al.* Molecular characterization of Arabidopsis PHO80-like proteins, a novel class of CDKA;1-interacting cyclins. *Cell Mol Life Sci* **61**, 1485–1497 (2004).

25. Lorenzo-Orts, L. *et al.* Concerted expression of a cell cycle regulator and a metabolic enzyme from a bicistronic transcript in plants. *Nature Plants* **5**, 184–193 (2019)
26. Shimizu-Mitao, Y. & Kakimoto, T. Auxin Sensitivities of All Arabidopsis Aux/IAAs for Degradation in the Presence of Every TIR1/AFB. *Plant and Cell Physiology* **55**, 1450–1459 (2014).
27. Fichtner, F. *et al.* Regulation of shoot branching in arabidopsis by trehalose 6-phosphate. *New Phytologist* **229**, 2135–2151 (2021).
28. Radchuk, V. *et al.* SWEET11b transports both sugar and cytokinin in developing barley grains. *The Plant Cell* **35**, 2186–2207 (2023).
29. Kikuchi, R., Kawahigashi, H., Ando, T., Tonooka, T. & Handa, H. Molecular and Functional Characterization of PEBP Genes in Barley Reveal the Diversification of Their Roles in Flowering. *Plant Physiol* **149**, 1341–1353 (2009).
30. Fichtner, F. *et al.* Functional Features of TREHALOSE-6-PHOSPHATE SYNTHASE1, an Essential Enzyme in Arabidopsis[OPEN]. *The Plant Cell* **32**, 1949–1972 (2020).
31. Koppolu, R. et al. Six-rowed spike4 (Vrs4) controls spikelet determinacy and row-type in barley. *Proceedings of the National Academy of Sciences* U S A 110, 13198–13203 (2013).
32. Shaw, L. M. et al. FLOWERING LOCUS T2 regulates spike development and fertility in temperate cereals. *J Exp Bot* 70, 193–204 (2019).
33. Je, B. I. et al. The CLAVATA receptor FASCIATED EAR2 responds to distinct CLE peptides by signaling through two downstream effectors. *eLife* 7, e35673 (2018).
34. Schlegel, J. et al. Control of Arabidopsis shoot stem cell homeostasis by two antagonistic CLE peptide signalling pathways. *eLife* 10, e70934 (2021).
35. Müller, R., Borghi, L., Kwiatkowska, D., Laufs, P. & Simon, R. Dynamic and Compensatory Responses of Arabidopsis Shoot and Floral Meristems to CLV3 Signaling. *The Plant Cell* **18**, 1188–1198 (2006).
36. Sean R. Eddy Accelerated Profile HMM Searches. *PLoS Comput Biol* **7**(10): e1002195 (2011).
37. Paysan-Lafosse, T. *et al.* InterPro in 2022. *Nucleic Acids Res* **51**, D418–D427 (2023).

38. Price, M. N., Dehal, P. S. & Arkin, A. P. FastTree: computing large minimum evolution trees with profiles instead of a distance matrix. *Mol Biol Evol* **26**, 1641–1650 (2009).
39. Stamatakis, A. RAxML version 8: a tool for phylogenetic analysis and post-analysis of large phylogenies. *Bioinformatics* **30**, 1312–1313 (2014).
40. Gol, L., Haraldsson, E. B. & von Korff, M. Ppd-H1 integrates drought stress signals to control spike development and flowering time in barley. *J Exp Bot* **72**, 122–136 (2021).
41. Curtis, M. D. & Grossniklaus, U. A gateway cloning vector set for high-throughput functional analysis of genes in planta. *Plant Physiol* **133**, 462–469 (2003).
42. Bleckmann, A., Weidtkamp-Peters, S., Seidel, C. A. M. & Simon, R. Stem Cell Signaling in Arabidopsis Requires CRN to Localize CLV2 to the Plasma Membrane. *Plant Physiol* **152**, 166–176 (2010).
43. Imani, J., Li, L., Schäfer, P. & Kogel, K.-H. STARTS – A stable root transformation system for rapid functional analyses of proteins of the monocot model plant barley. *The Plant Journal* **67**, 726–735 (2011).
44. Galli, M. *et al.* CRISPR/SpCas9-mediated double knockout of barley Microrchidia MORC1 and MORC6a reveals their strong involvement in plant immunity, transcriptional gene silencing and plant growth. *Plant Biotechnol J* **20**, 89–102 (2022).
45. Heigwer, F., Kerr, G. & Boutros, M. E-CRISP: fast CRISPR target site identification. *Nat Methods* **11**, 122–123 (2014).
46. Amanda, D. *et al.* Auxin boosts energy generation pathways to fuel pollen maturation in barley. *Current Biology* **32**, 1798-1811.e8 (2022).
47. Hensel, G., Kastner, C., Oleszczuk, S., Riechen, J. & Kumlehn, J. Agrobacterium-mediated gene transfer to cereal crop plants: current protocols for barley, wheat, triticale, and maize. *Int J Plant Genomics* **2009**, 835608 (2009).
48. Kurihara, D., Mizuta, Y., Sato, Y. & Higashiyama, T. ClearSee: a rapid optical clearing reagent for whole-plant fluorescence imaging. *Development* **142**, 4168–4179 (2015).
49. Strauss, S. *et al.* Using positional information to provide context for biological image analysis with MorphoGraphX 2.0. *eLife* **11**, e72601 (2022).

50. Mascher, M. *et al.* Long-read sequence assembly: a technical evaluation in barley. *The Plant Cell* **33**, 1888–1906 (2021).
51. Patro, R., Duggal, G., Love, M. I., Irizarry, R. A. & Kingsford, C. Salmon: fast and bias-aware quantification of transcript expression using dual-phase inference. *Nat Methods* **14**, 417–419 (2017).
52. Robinson, M. D., McCarthy, D. J. & Smyth, G. K. edgeR: a Bioconductor package for differential expression analysis of digital gene expression data. *Bioinformatics* **26**, 139–140 (2010).
53. Guo, W. *et al.* 3D RNA-seq: a powerful and flexible tool for rapid and accurate differential expression and alternative splicing analysis of RNA-seq data for biologists. *RNA Biol* **18**, 1574–1587 (2021).

9. Figures

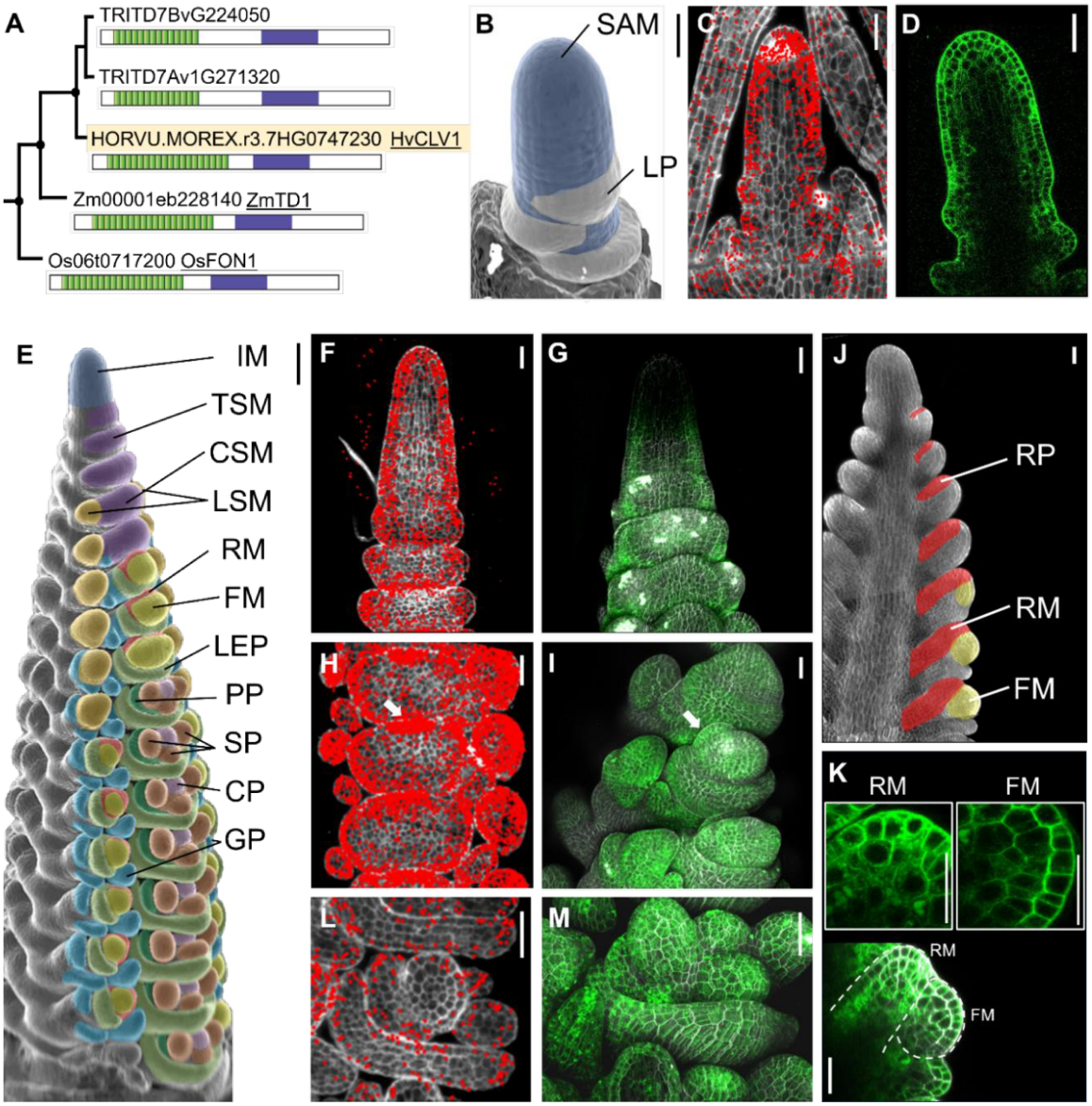

Fig.1: Identification and expression pattern of HvCLV1 in meristems composing the barley inflorescence

(A) Maximum likelihood tree of *HvCLV1* subclade. Dots indicate nodes with bootstrap value higher than 80. Gene identifiers are shown next to a schematic representation of protein structures. Kinase domain in purple and LRRs in green. *HvCLV1* is highlighted in light orange. **(B)** SEM picture of barley vegetative meristem. Color code: shoot apical meristem meristem (SAM) in blue, leaf primordia (LP) in white. **(C)** smRNAfish detection of *HvCLV1* transcripts (red dots) at the vegetative stage, calcofluor stained cell wall in grey. **(D)** HvCLV1 protein localisation in a central longitudinal section of the SAM at vegetative stage, HvCLV1 proteins tagged with mVenus in green**.** **(E)** *Hordeum vulgare* inflorescence cv. Golden Promise Fast, W3.5. Colour code: inflorescence meristem (IM) in blue, triple spikelet meristem (TSM) and central spikelet meristem (CSM) in purple, lateral spikelet meristem (LSM) in orange, rachilla meristem (RM) in red, flower meristem (FM) in yellow, lemma primordia (LEP) in light green, palea primordia (PP) in dark green, stamen primordia (SP) in brown, carpel primordium (CP) in pink and glumes primordia (GP) in cyan. **(F,G)** Transcripts and proteins localisation of HvCLV1 in the IM and TSMs, **(H,I)** in spikelet primordia at the FM initiation stage. The white arrows indicate the RM **(J)** Schematic representation of rachilla development. The rachilla primordium (RP) become RM after formation of the FM. **(K)** central longitudinal section of SM. Segmented lines indicate RM and FM. The close-up pictures show HvCLV1 proteins internalised in the vacuole in the RM (top left) and HvCLV1 proteins localised on the plasma membrane in the FM (top right). **(L,M)** HvCLV1 transcripts and proteins localisation in stamens and carpel primordia. *HvCLV1* transcripts in red and HvCLV1 proteins in green. Scale bars = 50 µm, in (E) = 100 µm.

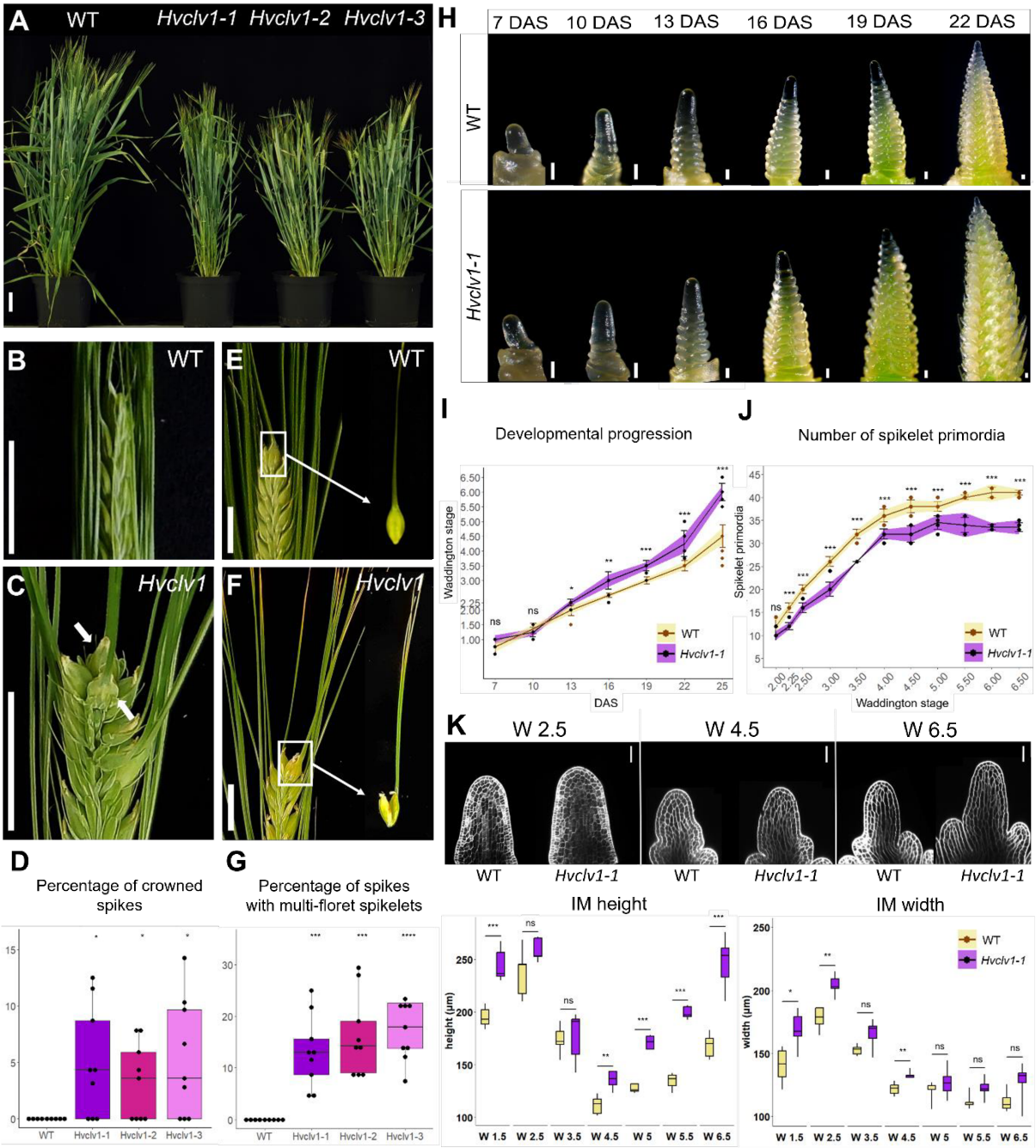

Fig.2: HvCLV1 plays a role in plant and spike architecture, delays inflorescence development and promotes spikelet formation

(A) Mature plants of Hordeum vulgare cv. Golden Promise Fast (WT) versus three selected *Hvclv1* mutant alleles (*Hvclv1-1*, *Hvclv1-2*, *Hvclv1-3*) **(B, C)** WT inflorescence and *Hvclv1-1* crowned spike phenotype respectively, ectopic grains are indicated by white arrows. **(D)** Percentage of crowned spikes in WT and *Hvclv1* mutant alleles. Dots represent the percentage per plant and asterixis indicate the significant difference to WT. n=9 **(E,F)** Close up respectively on WT single grain and *Hvclv1-1* multi-grain developed from multi-floret spikelets. **(G)** Percentage of spikes with multi-grain in WT plants and *Hvclv1* mutant alleles. Dots represent the percentage per plant and asterixis indicate the significant difference to WT. n=9 **(H)** Stereo microscope pictures of WT and *Hvclv1-1* SAM development from 7 to 22 days after sowing (DAS). **(I,J)** Developmental progression and number of spikelet primordia. WT in yellow, *Hvclv1-1* in purple. Dots represent single measurements; error bars represent standard deviation and the coloured ribbon the interval of confidence. n=10 (I) n =7 (J). **(K)** On the top, examples of WT and *Hvclv1-1* IM at W2.5, 4.5 and 6.5. The pictures were taken by confocal microscope, in white the cell wall stained with renaissance blue. The two plots on the bottom were generated by measuring meristem tip height and width at different W. Five samples per genotype were measured for every W. **(I)** Scale bars = 5 cm in (A), 1.5 cm (B, C, E, F), 100 µm (H) and 50 µm (K).

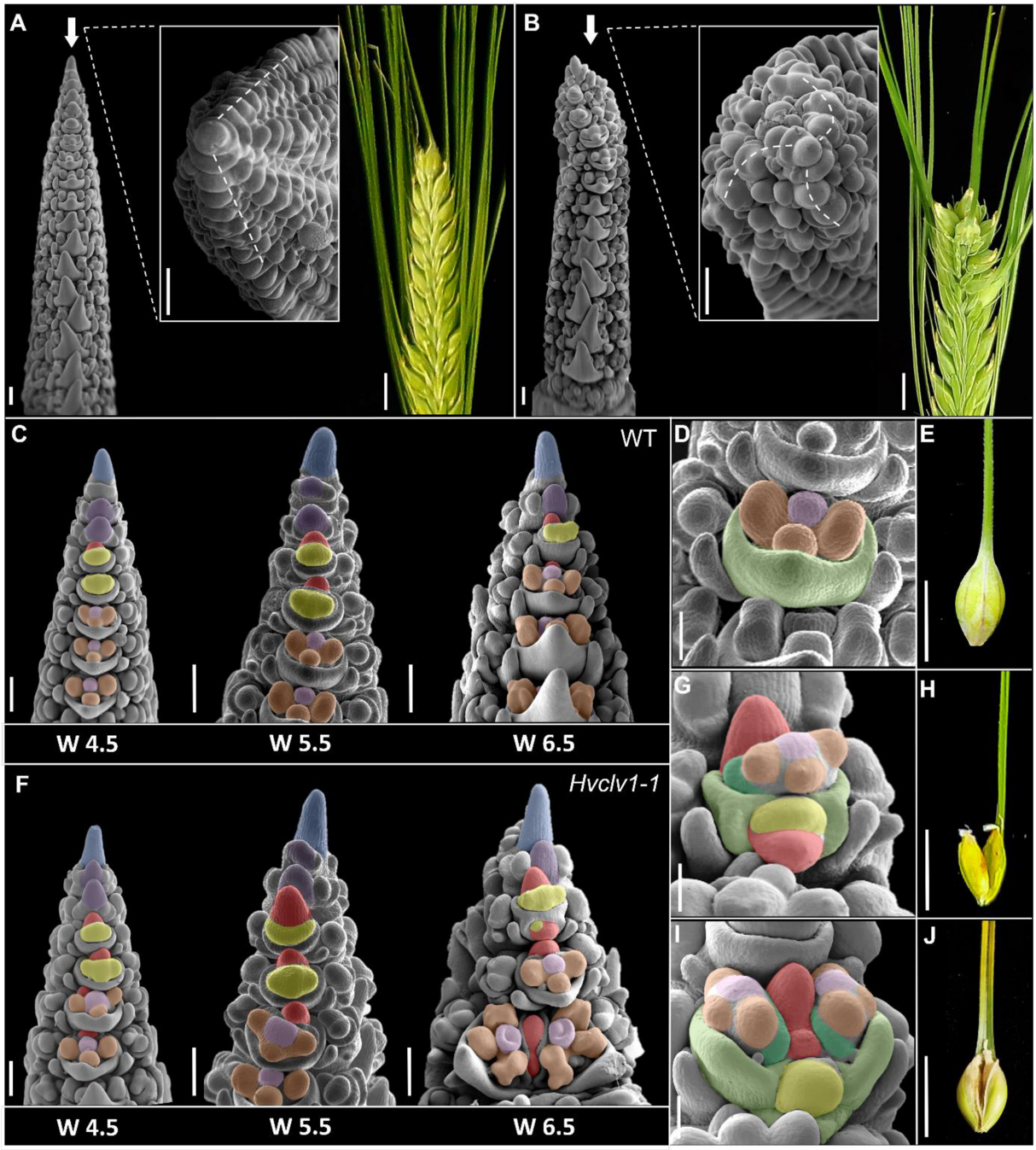

Fig.3: Origins of crowned spikes and multi-floret spikelets

(A,B) SEM pictures of WT and *Hvclv1-1* inflorescence meristems at W4.5 respectively. Frontal view on the left and close-up of the top view in the centre. Segmented lines indicate spikelet primordia phyllotaxis. On the right pictures of representative spike phenotypes. Crowned spikes were found in 6/38 *Hvclv1-1* inflorescences from W5.5 to W6.5 **(C)** Developmental progression of WT inflorescences at W4.5, 5.5 and 6.5. Colour code as described in Fig.1E **(D,E)** Close up on WT floret and WT single grain respectively. **(F)** Developmental progression of *Hvclv1-1* inflorescences at W4.5, 5.5 and 6.5. Colour code as described in Fig.1E. Multi-floret spikelets were found in 27/38 *Hvclv1-1* inflorescences from W5.5 to W6.5. **(G-J)** Close up on *Hvclv1-1* multi-floret spikelet and the resulting multi-grain disposed vertically (G,H) and horizontally (I,J). Colour code (G-J): RM and secondary rachilla meristem (SRM) in red, FM in yellow, LP in light green, PP in dark green, SP in brown and CP in pink. Scale bars: A, B, C, F = 200 µm; D, G, I = 100 µm; E, H, J = 1 cm.

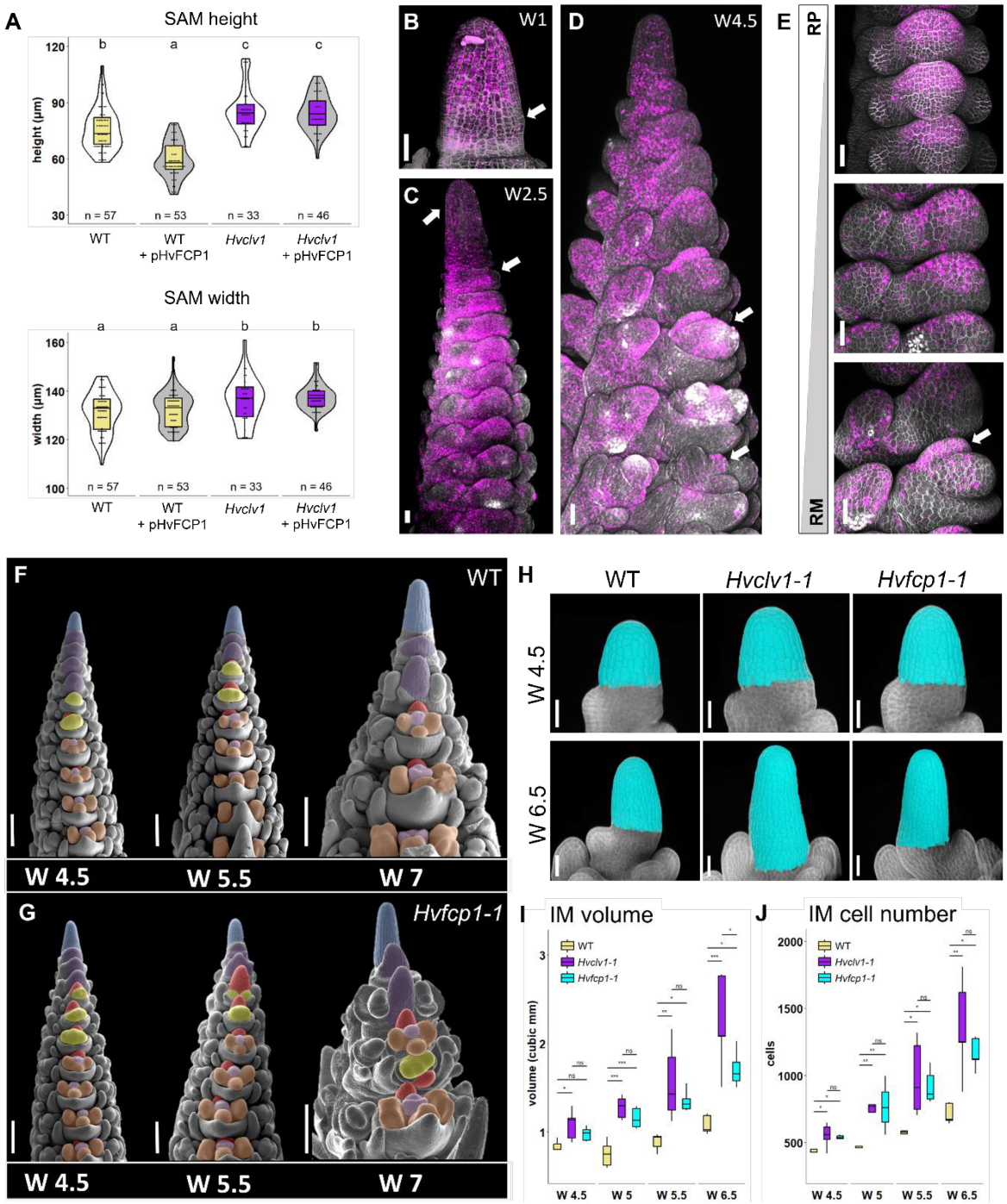

Fig.4: HvFCP1 interacts with HvCLV1 to regulate IM proliferation and RM determinacy

(A) Vegetative SAM height and width in control samples (white) and samples treated with HvFCP1 synthetic peptide (pHvFCP1) (grey). WT SAMs in yellow and *Hvclv1-1* in purple. Dots represent single measurements, n = number of samples. Letters on top of each boxplot represent the results of the ANOVA test. **(B-D)** Confocal images of barley SAM and inflorescence expressing *HvFCP1* transcriptional reporter line (pHvFCP1:mVenus-H2B) at different developmental stages and organ primordia. SAM at vegetative stage (B), at W2.5 (C) and at W3.5 (D). **(E)** *HvFCP1* transcriptional reporter line along rachilla development. From rachilla primordium (RP) to rachilla meristem (RM). **(F,G)** Inflorescence phenotype in late stages of development (W4.5, W5.5, W7) in WT (F) and *Hvfcp1-1* (G). Multi-floret spikelets were found in 12/35 *Hvfcp1-1* inflorescences from W5.5 to W6.5. Colour code as described in Fig.1E **(H-J)** 3D reconstruction of WT, *Hvclv1-1* and *Hvfcp1-1* IMs at W4.5 and W6.5 (H). Cells in cyan were selected for the IM measurements in (I) and (J), where boxplots display IM volume and cell number respectively. WT (yellow), *Hvclv1-1* (purple), *Hvfcp1-1* (cyan). Scale bars: 50 µm; F and G = 200 µm.

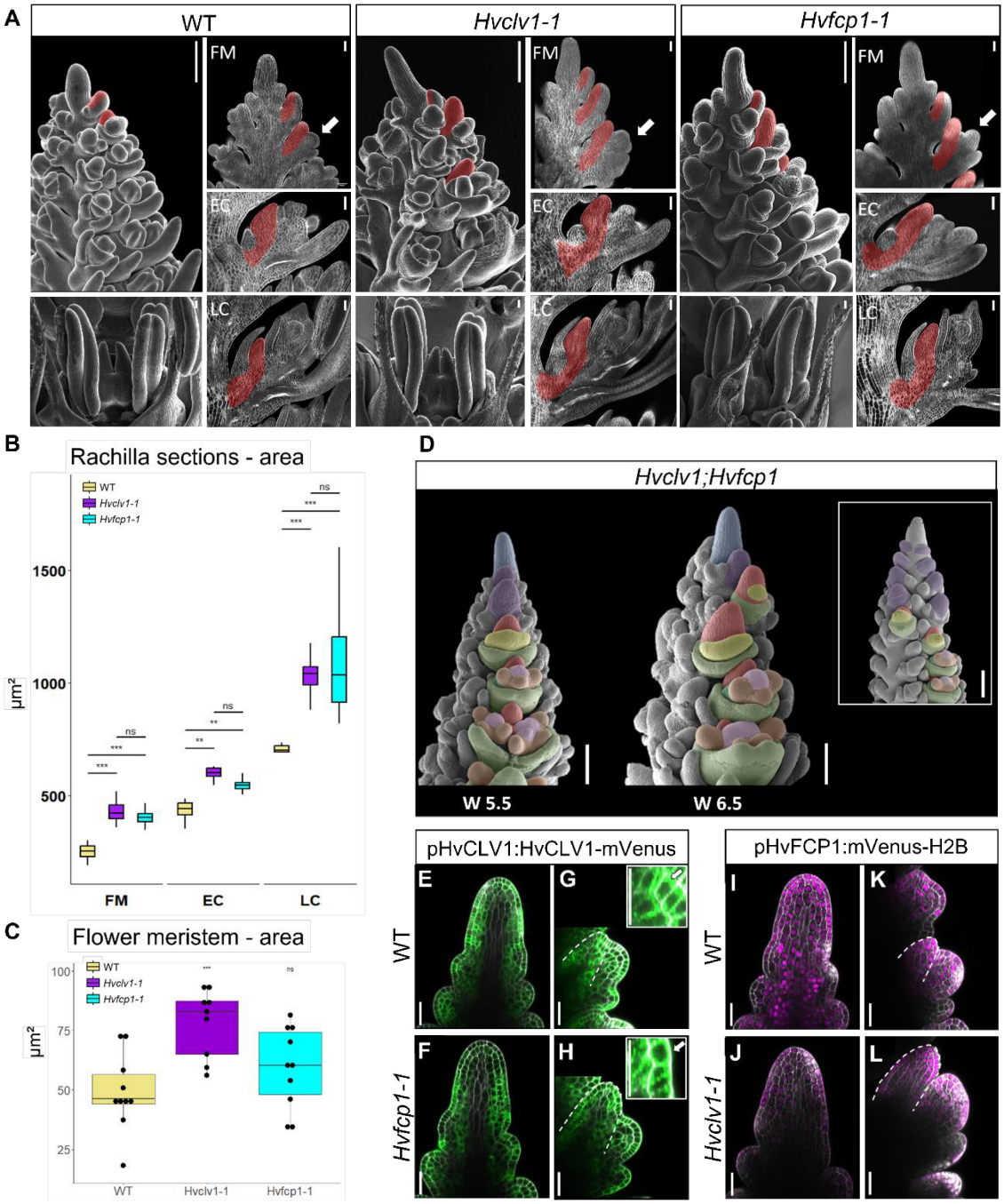

Fig.5: HvCLV1 and HvFCP1 repress RM elongation, *Hvclv1;Hvfcp1* double mutant and reporter lines in the respective mutant backgrounds

(A) SEM pictures of WT, *Hvclv1-1* and *Hvfcp1-1* inflorescence meristems at W6.5 were used as reference for matching longitudinal sections on their right. The RM in three stages of flower development is highlighted in red. Spikelet with floret meristem (FM), early carpel stage (EC), and late carpel stage (LC). White arrows indicate the considered spikelet stage described as FM **(B)** Boxplots displaying rachilla area from central longitudinal sections in WT (yellow), *Hvclv1-1* (purple), *Hvfcp1-1* (cyan). **(C)** Measurements of FM area from SEM frontal pictures of barley inflorescences at W5.5 in WT, *Hvclv1-1* and *Hvfcp1-1*. Dots represent biological replicates and asterixis indicate the significant difference to WT. n=10. **(D)** Inflorescence phenotype of *Hvclv1;Hvfcp1* double mutant at W5.5 and W6.5. On the top right crowned tip phenotype. Color code as described in Fig.1E. **(E-H)** HvCLV1 proteins localisation (green) in WT (E,G) and *Hvfcp1-1* (F,H) IM and RM (segmented line) respectively. **(I, L)** *HvFCP1* expression pattern (magenta) respectively in WT and *Hvclv1-1* IM. (R, S) *HvFCP1* expression pattern (magenta) in WT (I,K) and *Hvfcp1-1* (J,L) IM and RM (segmented line) respectively. Scale bars in A: SEM pictures of the inflorescence tip = 200 µm; SEM pictures of flowers and all sections = 50 µm, in D = 200 µm, in E-L = 50 µm.

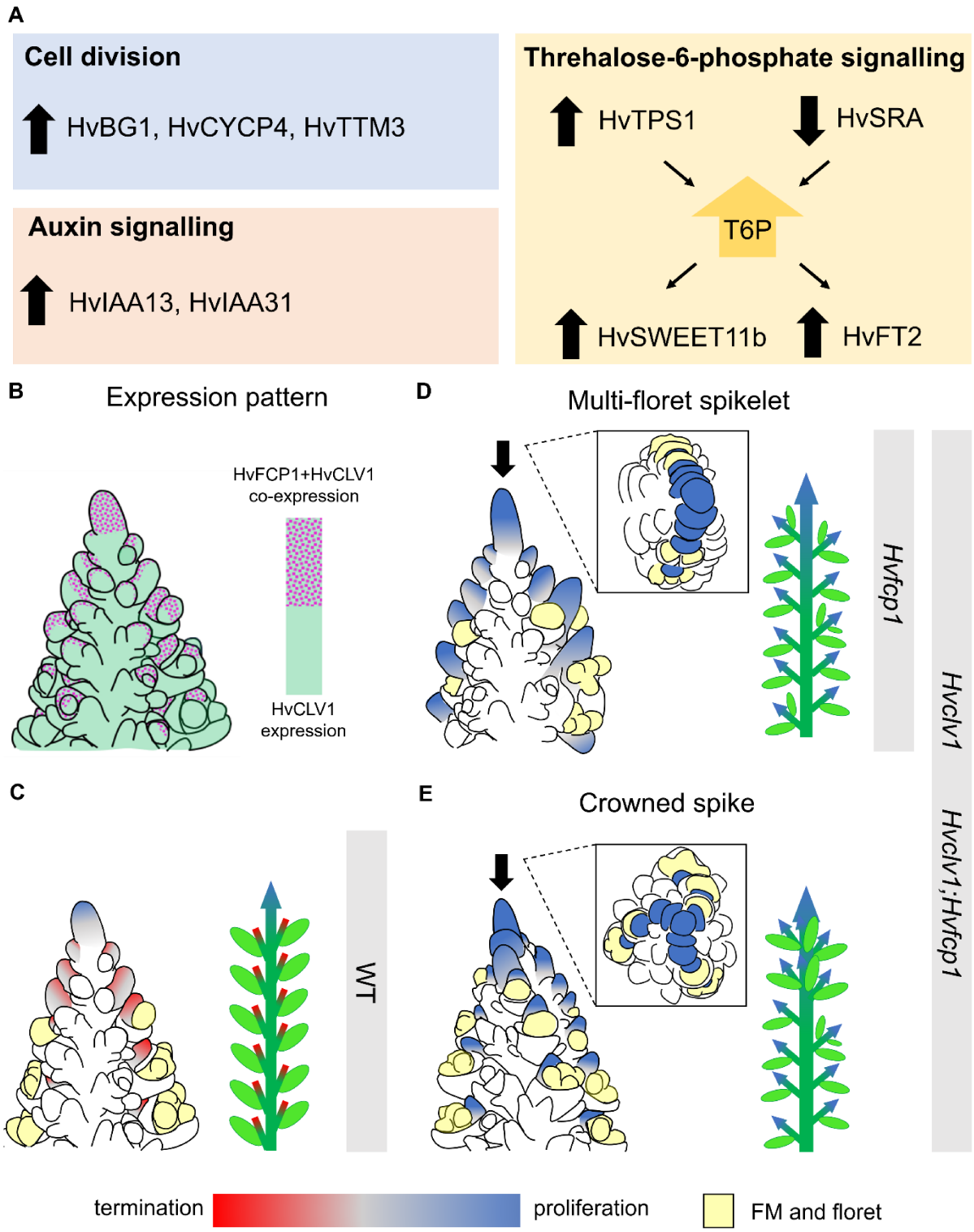

Fig.6: Comparative transcriptome analysis of common gene regulation in *Hvclv1* and *Hvfcp1* vs WT, and schematic summary

(A) Commonly regulated genes in *Hvclv1* vs WT and *Hvfcp1* vs WT from RNA-sequencing results. Black arrows pointing upward indicate commonly upregulated genes, while arrows pointing downward indicate commonly downregulated genes. **(B)** Schematic representation of HvCLV1 (green) and *HvFCP1* (magenta dots) expression patterns in barley inflorescence at W5.5. **(C-E)** Schematic representation of barley inflorescences at W5.5 (left) and mature spikes (right) in WT (C), *Hvfcp1*, *Hvclv1* and *Hvclv1;Hvfcp1* (D,E). Grey bars indicate the observed spike phenotypes (multi-floret spikelets and crowned spikes) in the respective genetic backgrounds. Colour code: IM and RMs are marked in red or blue to indicate meristematic proliferation or termination respectively. FM and floral organs are marked in yellow, main rachis and grains in dark and light green.

10. Extended Data Figures

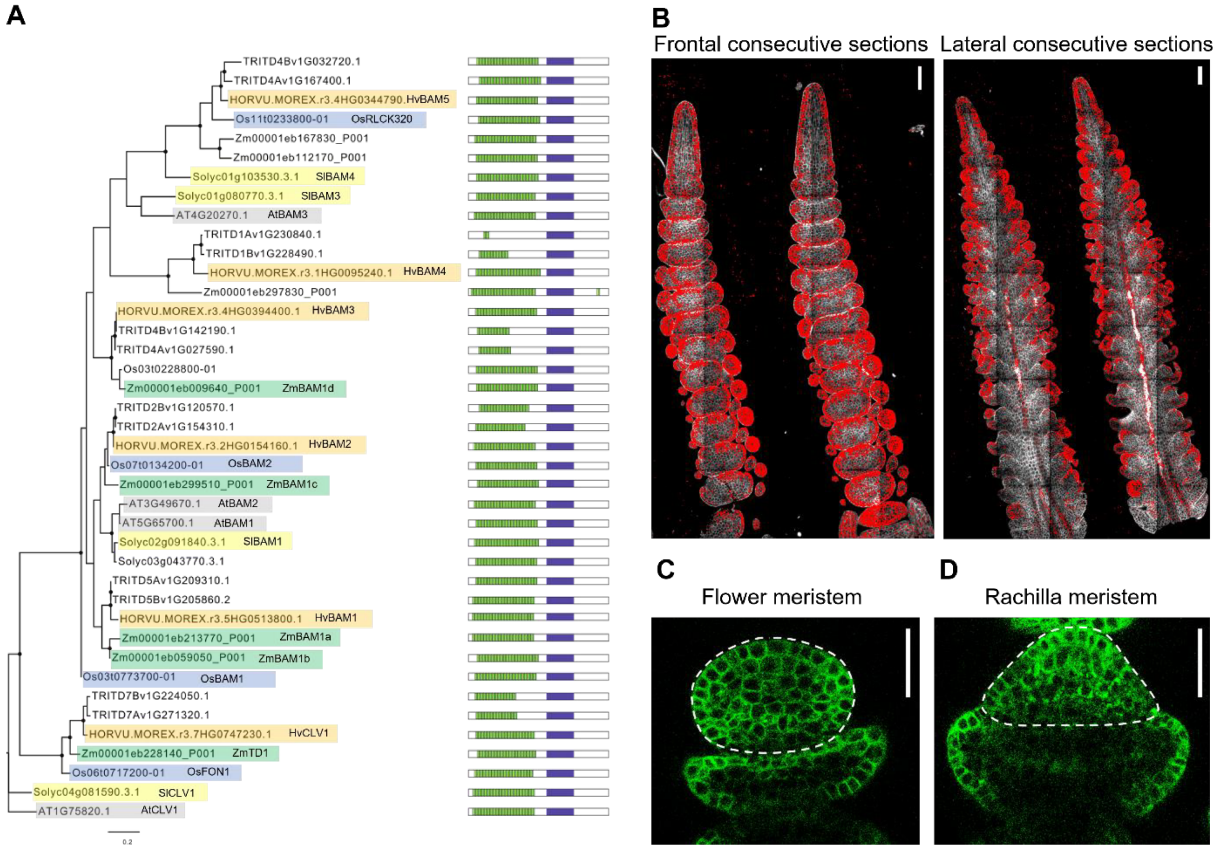

ExtDataFig1: HvCLV1 clade, expression pattern and protein localisation

(A) Maximum likelihood tree of the CLV1 clade based on protein kinase domains. Black dots indicate nodes with a bootstrap value higher than 80. Genes identifiers and names of already described genes are highlighted in different colours based on the species [*Arabidopsis thaliana* (grey), *Solanum lycopersicum* (yellow), *Zea mays* (green), *Oryza sativa japonica* (blue) and *Hordeum vulgare* (orange)] are coupled with a schematic representation of the protein structure. Kinase domain as purple rectangles and LRRs as green rectangles. **(B)** Results from smRNAfish (Molecular CartographyTM, Resolve Biosciences) experiment. The fluorescent signal in red shows the localisation of HvCLV1 transcripts in dorsal and lateral sections of the barley inflorescence at W3.5. Scalebar: 100 µm **(C,D)** HvCLV1 protein localisation (green) in dorsal sections of the floret meristem and rachilla meristem respectively. Scale bars: 50 µm.

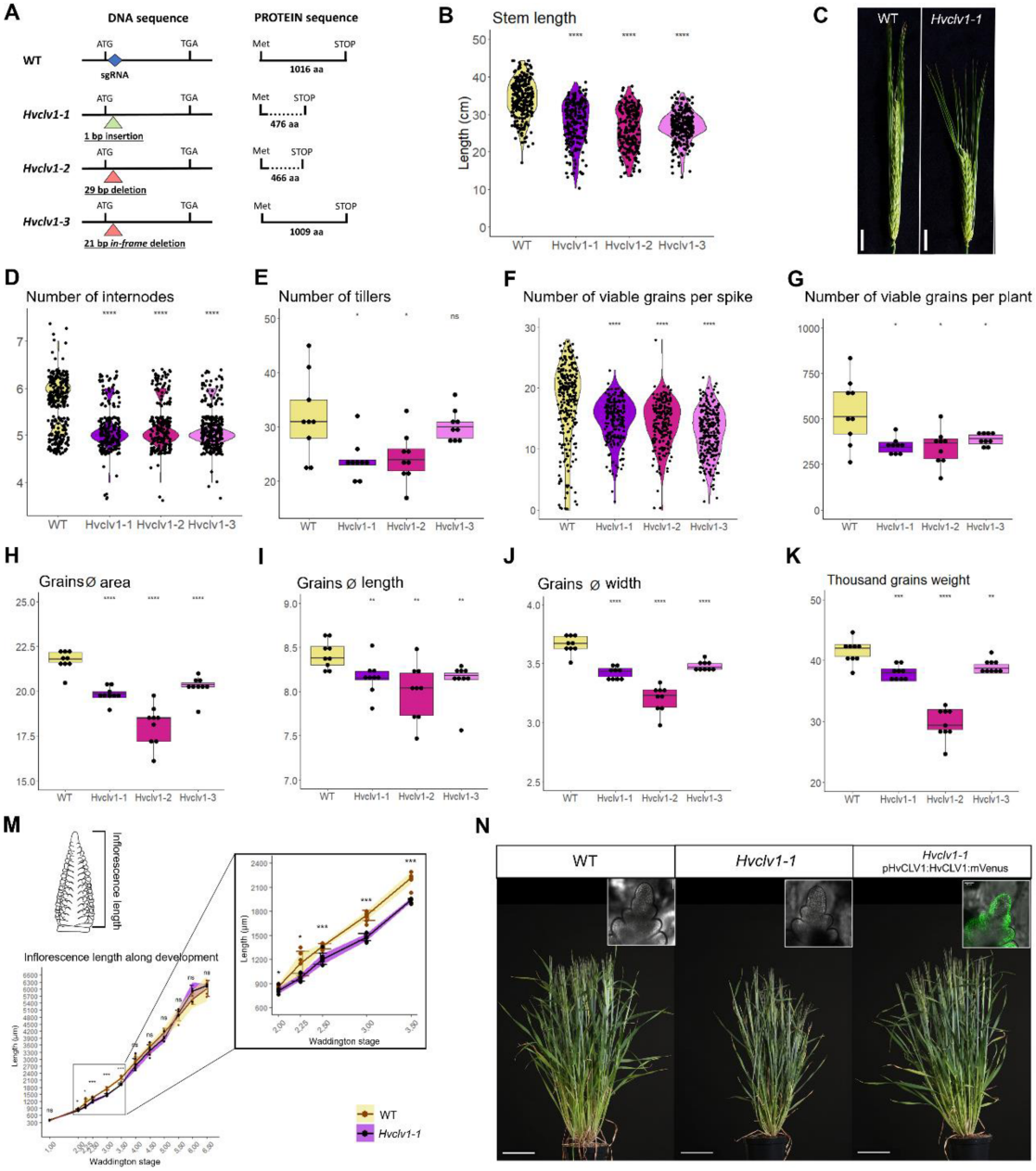

ExtDataFig2: *Hvclv1* mutant alleles phenotype and complementation with HvCLV1 reporter line

(A) Schematic representation of the HvCLV1 DNA and protein sequence in WT and *Hvclv1-1, Hvclv1-2, Hvclv1-3* mutant alleles. The blue square indicates the region targeted by the sgRNA, the triangles indicate the position of the selected mutation (insertions in green, deletions in red). The dotted lines indicate a different protein sequence to WT. **(B-G)** Plant and spike phenotype. Measurements of stem length (B), spike phenotype of WT and *Hvclv1-1* 60 DAS. Scale bar: 1.5 cm (C), number of internodes (D), number of tillers (E), number of viable grains per spike (F) and per plant (G). Dots indicate single measurement performed in nine mature plants, and asterisks indicate the significant difference in comparison to WT. **(H-K)** Grain phenotype and weight: measurements of grain area (H), grain length (I), grain width (J) and Thousand grains weight (TGW) (K). Dots indicate the average of value of measurements taken in 150 mature grains from nine different plants, asterisks indicate the significant difference in comparison to WT. **(M)** Inflorescence length of WT (yellow) and *Hvclv1-1* (purple). Measurements were taken from W1 to W6.5. Zoom-in plot between W2 and W3.5 on the right. Dots represent single measurements; error bars represent standard deviation and the colored ribbons the interval of confidence. Asterisks indicate the significant difference to WT for each W. **(N)** Complementation of *Hvclv1-1* plant phenotype with HvCLV1 translational reporter line. From left to right WT plant, *Hvclv1-1* and *Hvclv1-1* carrying pHvCLV1:HvCLV1:mVenus plasmid (60 DAS). Pictures on the top right show HvCLV1:mVenus expression (green) in the IM in the relative genetic background. Scale bars: 10 cm (plants), 50 µm (IMs).

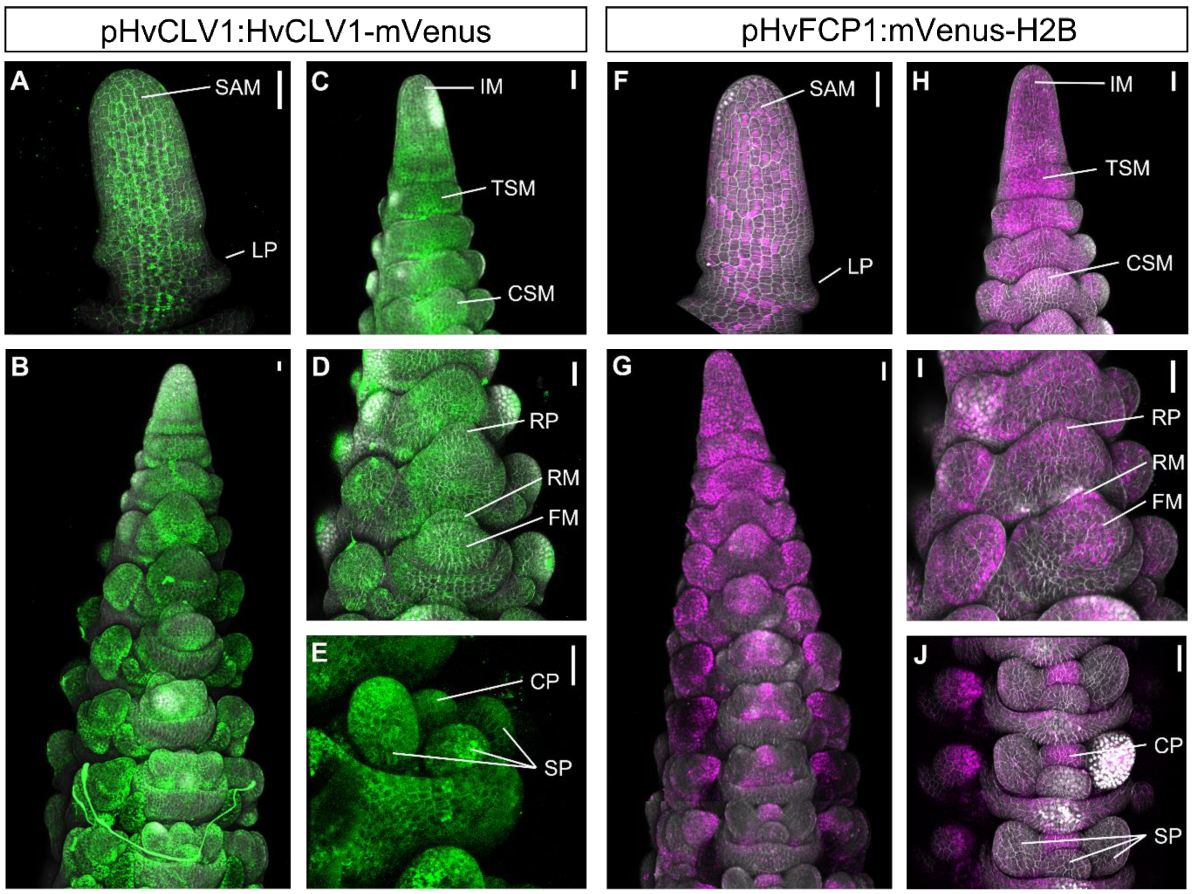

ExtDataFig3: Comparison between HvCLV1 protein localisation and HvFCP1 promoter activity in barley inflorescence

(A-E) HvCLV1 translational reporter line in barely inflorescence at W1 (A) and W3.5 (B). Close-ups on HvCLV1 protein localisation in IM, TSM and CSM (C), RP, RM and FM (D) and CP, SP (E). HvCLV1 proteins in green, DAPI-stained cell wall in grey. **(F-J)** HvFCP1 transcriptional reporter line in barely inflorescence at W1 (F) and W3.5 (G). Close-ups on HvFCP1 expression in IM, TSM and CSM (H), RP, RM and FM (I) and CP, SP (J). Nuclear-localised HvFCP1 expression in magenta, DAPI-stained cell wall in grey. Scale bars: 50 µm.

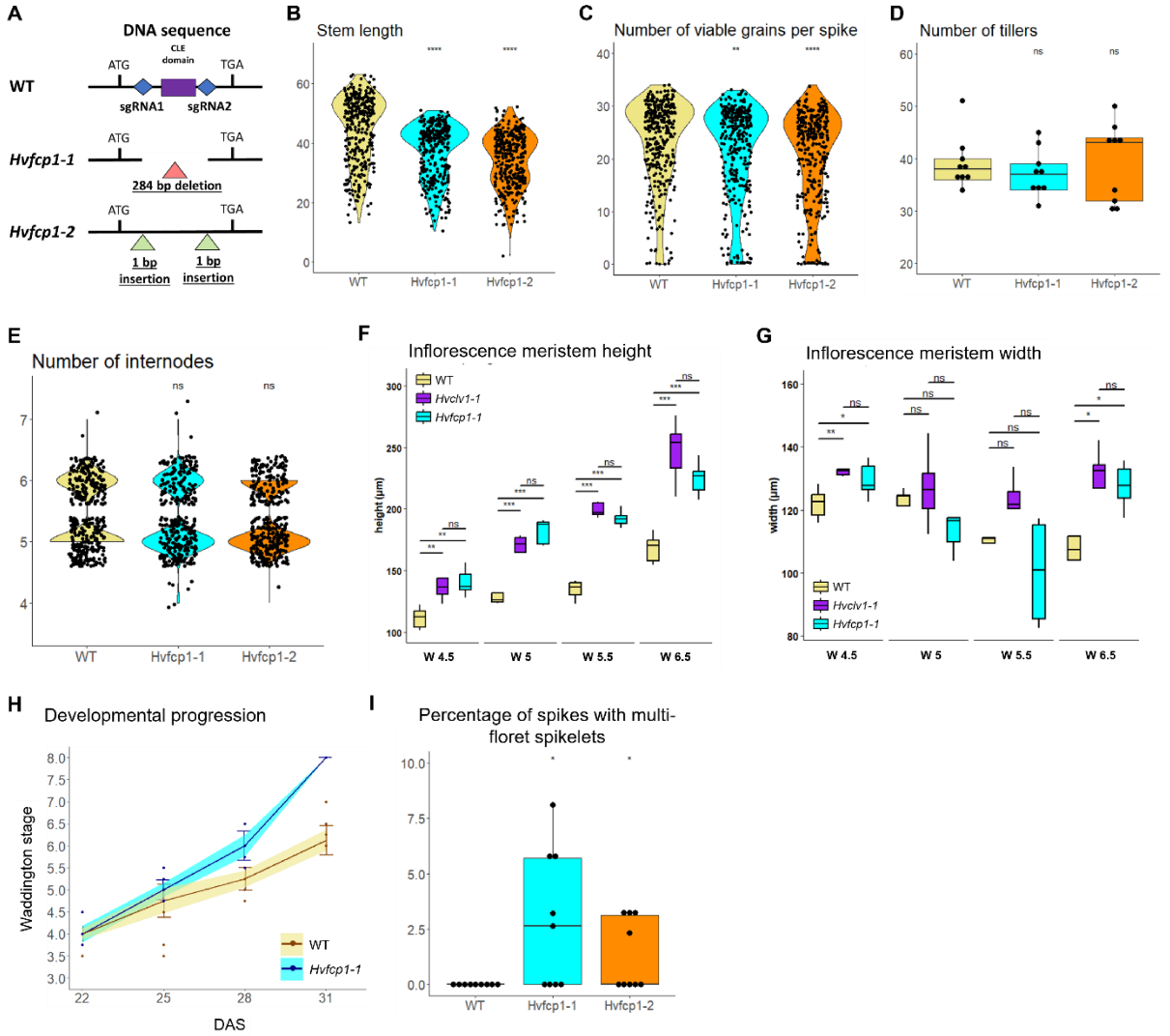

ExtDataFig4: *Hvfcp1* mutant alleles phenotype and IM shape

(A) Schematic representation of the HvFCP1 DNA sequence in WT and *Hvfcp1-1* and *Hvfcp1-2* mutant alleles. The blue squares indicate the regions targeted by the sgRNAs, the purple rectangle indicates the position of the HvFCP1 CLE domain, and triangles indicate the position of the selected mutation (insertions in green, deletions in red). **(B-E)** Plant phenotype: measurements of stem length (B), number of viable grains per spike (C), number of tillers (D), number of internodes (E). Dots indicate single measurements performed in nine mature plants and asterisks indicate the significant difference in comparison to WT. **(F, G)** Developmental progression and number of spikelet primordia respectively. WT in yellow, *Hvclv1-1* in purple and *Hvfcp1-1* in cyan. Dots represent single measurements; error bars represent standard deviation and the coloured ribbons the interval of confidence. **(H)** Developmental progression in WT (yellow) and *Hvfcp1-1* (cyan). Dots represent single measurements; error bars represent standard deviation and the coloured ribbon is the interval of confidence. n=10. **(I)** Percentage of spikes with multi-floret spikelets in WT plants and *Hvfcp1* mutant alleles. Dots represent the percentage per plant and asterixis indicate the significant difference to WT. n=9.

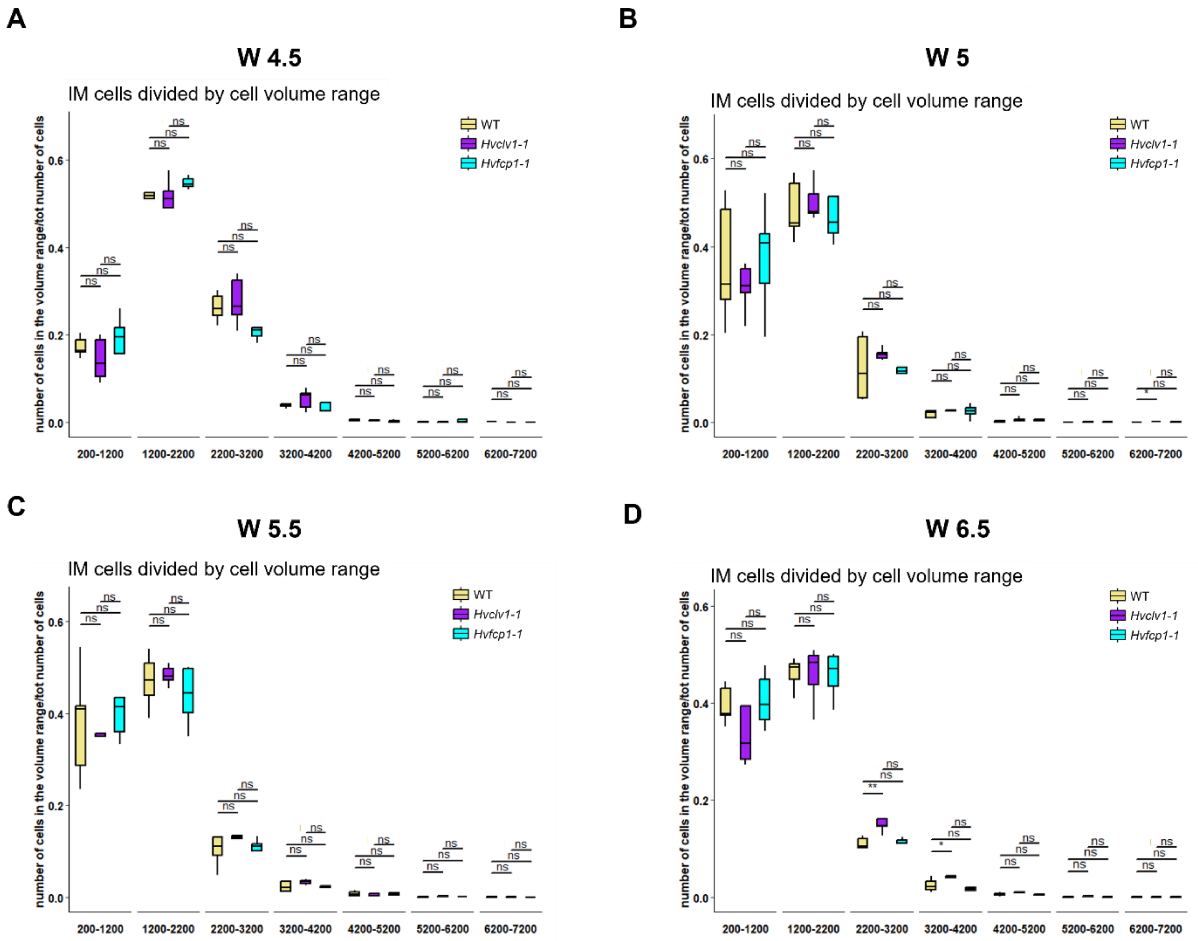

ExtDataFig5: cell volume is unaffected in *Hvclv1* and *Hvfcp1* IM

(A, B, C, D) Quantification of the Cell Volume Ratio (CVR) in WT (yellow), *Hvclv1-1* (purple) and *Hvfcp1-1* (cyan) in barley inflorescences at W4.5, W5, W6 and W6.5. In the y-axis CVR (ratio between number of IM cells in a specific volume range and total number of cells of the IM), in the x-axis cell volume ranges in cubic micrometres. Boxplots show the CVR of 5 IMs per Waddington stage.

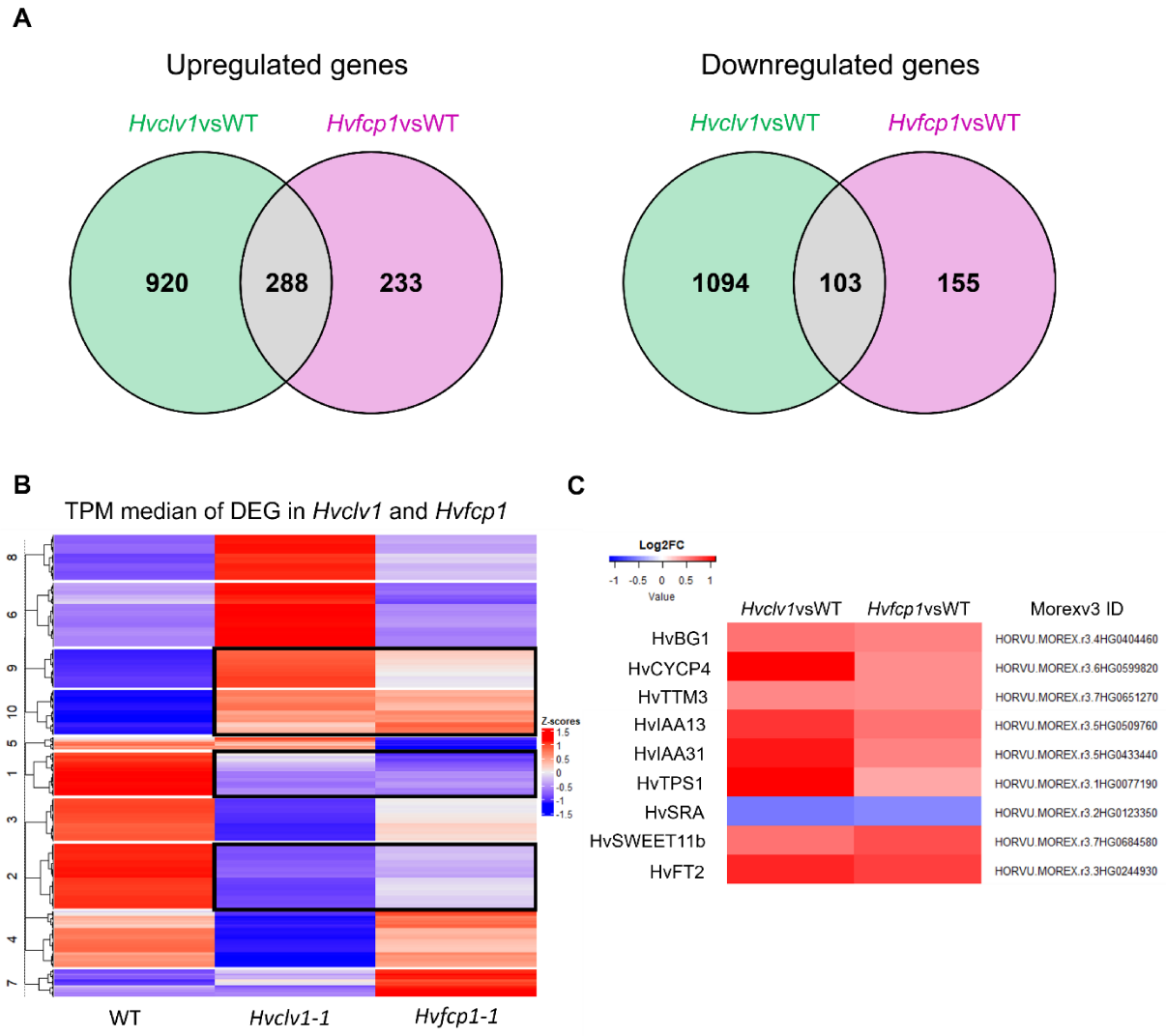

ExtDataFig6: RNA-seq in *Hvclv1* vs WT and *Hvfcp1* vs WT revealed a common gene regulatory network

(A) Venn diagrams illustrating the number of upregulated (Log2FC > 0.5) and downregulated (Log2FC < -0.5) genes in *Hvclv1* vs WT (green) and *Hvfcp1* vs WT (magenta). Commonly regulated genes in grey. **(B)** Heatmap illustrating the z-score of median transcripts per million (TPM) values for each of the differentially expressed genes (DEG) in *Hvclv1* vs WT and *Hvfcp1* vs WT. Clusters on the y-axis group genes with a similar expression trend between genotypes. Black rectangles highlight genes that are similarly regulated in *Hvclv1-1* and *Hvfcp1-1*. (C) Heatmap displaying Log2FC values of genes mentioned in Fig.6A in *Hvclv1* vs WT and *Hvfcp1* vs WT.

11. Supplementary information

Suppl.Info1: *Hvclv1* mutant alleles

HvCLV1 (HORVU.MOREX.r3.7HG0747230) Location: Chr7H 618,787,699 - 618,791,569

Hvclv1-1 carries a 1bp insertion after 70bp that caused a shift in the reading frame and an early stop codon after 476 amino acids (aa), generating a misfolded protein which only shares the first 23aa with the WT sequence (1016aa). *Hvclv1-2* carries a 29bp deletion 41bp after the coding start that caused a shift in the reading frame and an early stop codon after 466 aa. *Hvclv1-3* carries an in-frame deletion of 21 bp after 63bp from the coding start, which allowed the formation of a protein almost identical to the WT apart from 7 missing amino acids (SGSPDRD) in position 22 to 28 in the N-terminal region that disrupts the signal peptide sequence.

Alignment: sgRNA target sequence (blue), insertion (green), deletion (red)

```
HvCLV1          ATGCCGCCACCTCACCTGCTCACCATCCTCCTACCTCTCCTCCTCCTCCCGGCCCCT
Hvclv1-1        ATGCCGCCACCTCACCTGCTCACCATCCTCCTACCTCTCCTCCTCCTCCCGGCCCCT
Hvclv1-2        ATGCCGCCACCTCACCTGCTCACCATCCTCCTACCTCTCCTCC-----------------
Hvclv1-3        ATGCCGCCACCTCACCTGCTCACCATCCTCCTACCTCTCCTCCTCCTCC-----------

                ******************************************

HvCLV1          TCCTCCGGCT-CCCCGGACCGCGACATCTACGCGCTCGCCAAGATCAAGGCCGCCCT…
Hvclv1-1        TCCTCCGGCTTCCCCGGACCGCGACATCTACGCGCTCGCCAAGATCAAGGCCGCCCT…
Hvclv1-2        -------------CCGGACCGCGACATCTACGCGCTCGCCAAGATCAAGGCCGCCCT…
Hvclv1-3        ----------CCCCGGACCGCGACATCTACGCGCTCGCCAAGATCAAGGCCGCCCT…
                             *******************************************
```

Signal peptide and cleavage position prediction (PredSi)

Matrix:	Eukarya
Truncation:	70 residues
Cleavage position:	23
Score:	0.9205
Secreted protein:	**predicted for secretion**

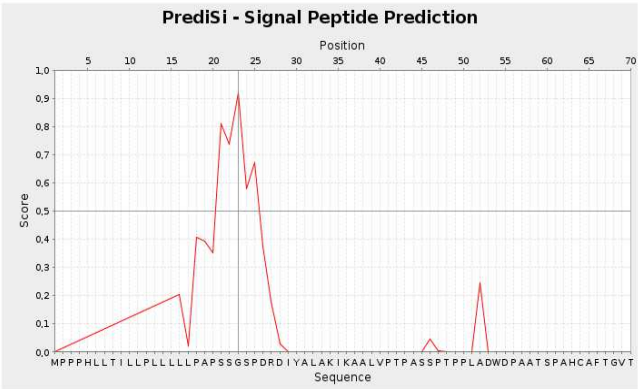

HvCLV1:

```
MPPPHLLTILLPLLLLLPAPSSGSPDRDIYALAKIKAALVPTPASSPTPPLADWDPAATSPAHCAFTGVT
|   |   |   |   |   |   |   |   |   |   |   |   |   |   |   |   |   |
1       10      20      30      40      50      60      70
```

HvCLV1 WT protein sequence

MPPPHLLTILLPLLLLLPAPSSGSPDRDIYALAKIKAALVPTPASSPTPPLADWDPAATSPAHCAFTG
VTCDAATSRVVAINLTALPLHAGTLPPELALLDSLTNLTIAACSLPGRVPAGLPSLPSLRHLNLSNNN
LSGPFPAGDGQTTLYFPSIEVLDCYNNNLSGPLPPFGAAHKAALRYLHLGGNYFSGPIPVAYGDVASL
EYLGLNGNALSGRIPPDLARLGRLRSLYVGYFNQYDGGVPPEFGGLRSLVLLDMSSCNLTGPIPPELG
KLKNLDTLFLLWNRLSGEIPPELGELQSLQLLDLSVNDLAGEIPATLAKLTNLRLLNLFRNHLRGGIP
GFVADLPDLEVLQLWENNLTGSLPPGLGRNGRLRNLDVTTNHLTGTVPPDLCAGGRLEMLVLMDNAFF
GPIPESLGACKTLVRVRLSKNFLSGAVPAGLFDLPQANMLELTDNLLTGGLPDVIGGGKIGMLLLGNN
GIGGRIPPAIGNLPALQTLSLESNNFTGELPPEIGRLRNLSRLNVSGNHLTGAIPEELTRCSSLAAVD
VSRNRLTGVIPESITSLKILCTLNVSRNALSGELPTEMSNMTSLTTLDVSYNALTGDVPMQGQFLVFN
ESSFVGNPGLCGGPLTGSSNDDACSSSSNHGGGGVLSLRRWDSKKMLVCLAAVFVSLVAAFLGGRKGC
EAWREAARRRSGAWKMTVFQQRPGFSADDVVECLQEDNIIGKGGAGIVYHGVTRGGGAELAIKRLVGR
GVGGDRGFSAEVGTLGRIRHRNIVRLLGFVSNRETNLLLYEYMPNGSLGEMLHGGKGGHLGWDARARV
ALEAARGLCYLHHDCAPRIIHRDVKSNNILLDSAFEAHVADFGLAKFLGGAAGASECMSAIAGSYGYI
APEYAYTLRVDEKSDVYSFGVVLLELITGRRPVGGFGDGVDIVHWVRKATAELPDTAAAVLAVADCRL
SPEPVPLLVGLYDVAMACVEEASTDRPTMREVVHMLSQPALVAPTAVVDENTARPDDDLILSF*

Hvclv1 mutant alleles protein sequence

Hvclv1-1

MPPPHLLTILLPLLLLLPAPSSGFPGPRHLRARQDQGRPRAHPRILPDAAARRLGPGGDIPSPLRIHR
RHMRRRHLPRRRHQPHRPPAPRRHAAPGARPPRLPNQPHHRRLLPPRPRPRGPPVPAIPPPPQPLQQQ
PLRPLPRRRRTDNVVLPVHRGPRLLQQQPLRPAPALRRRAQGRAPLPPPRRELLLRPHPGGLRRRRQP
RVPRPQRQRALRQDPAGPGPAGPAPEPLRRLLQPVRRRRAARVRRAAQPRAARHEQLQPHRPHPARAR
QAQEPRHALPPLEPIVWRDSARAGGAPEPPVAGPVRQRPRRRDTGDPGQAHEPQAAQPVPEPPPRRDT
RVRRRPAGPRGAAALGEQPHRQPPAGTRAQRPAQEPRRHHQPPHRHRAAGPLRGREARDARAHGQRLL
RPHPGVAGRVQDAGARPPQQELPQRRRAGRALRPAAGQHARAHRQPAHGRPPRRDRRRQDRHAAAGE*

Hvclv1-2

MPPPHLLTILLPLLPGPRHLRARQDQGRPRAHPRILPDAAARRLGPGGDIPSPLRIHRRHMRRRHLPR
RRHQPHRPPAPRRHAAPGARPPRLPNQPHHRRLLPPRPRPRGPPVPAIPPPPQPLQQQPLRPLPRRRR
TDNVVLPVHRGPRLLQQQPLRPAPALRRRAQGRAPLPPPRRELLLRPHPGGLRRRRQPRVPRPQRQRA
LRQDPAGPGPAGPAPEPLRRLLQPVRRRRAARVRRAAQPRAARHEQLQPHRPHPARARQAQEPRHALP
PLEPIVWRDSARAGGAPEPPVAGPVRQRPRRRDTGDPGQAHEPQAAQPVPEPPPRRDTRVRRRPAGPR
GAAALGEQPHRQPPAGTRAQRPAQEPRRHHQPPHRHRAAGPLRGREARDARAHGQRLLRPHPGVAGRV
QDAGARPPQQELPQRRRAGRALRPAAGQHARAHRQPAHGRPPRRDRRRQDRHAAAGE*

Hvclv1-3

MPPPHLLTILLPLLLLLPAPSIYALAKIKAALVPTPASSPTPPLADWDPAATSPAHCAFTGVTCDAAT
SRVVAINLTALPLHAGTLPPELALLDSLTNLTIAACSLPGRVPAGLPSLPSLRHLNLSNNNLSGPFPA
GDGQTTLYFPSIEVLDCYNNNLSGPLPPFGAAHKAALRYLHLGGNYFSGPIPVAYGDVASLEYLGLNG
NALSGRIPPDLARLGRLRSLYVGYFNQYDGGVPPEFGGLRSLVLLDMSSCNLTGPIPPELGKLKNLDT
LFLLWNRLSGEIPPELGELQSLQLLDLSVNDLAGEIPATLAKLTNLRLLNLFRNHLRGGIPGFVADLP
DLEVLQLWENNLTGSLPPGLGRNGRLRNLDVTTNHLTGTVPPDLCAGGRLEMLVLMDNAFFGPIPESL
GACKTLVRVRLSKNFLSGAVPAGLFDLPQANMLELTDNLLTGGLPDVIGGGKIGMLLLGNNGIGGRIP
PAIGNLPALQTLSLESNNFTGELPPEIGRLRNLSRLNVSGNHLTGAIPEELTRCSSLAAVDVSRNRLT
GVIPESITSLKILCTLNVSRNALSGELPTEMSNMTSLTTLDVSYNALTGDVPMQGQFLVFNESSFVGN
PGLCGGPLTGSSNDDACSSSSNHGGGGVLSLRRWDSKKMLVCLAAVFVSLVAAFLGGRKGCEAWREAA
RRRSGAWKMTVFQQRPGFSADDVVECLQEDNIIGKGGAGIVYHGVTRGGGAELAIKRLVGRGVGGDRG
FSAEVGTLGRIRHRNIVRLLGFVSNRETNLLLYEYMPNGSLGEMLHGGKGGHLGWDARARVALEAARG
LCYLHHDCAPRIIHRDVKSNNILLDSAFEAHVADFGLAKFLGGAAGASECMSAIAGSYGYIAPEYAYT
LRVDEKSDVYSFGVVLLELITGRRPVGGFGDGVDIVHWVRKATAELPDTAAAVLAVADCRLSPEPVPL
LVGLYDVAMACVEEASTDRPTMREVVHMLSQPALVAPTAVVDENTARPDDDLILSF*

Suppl.Info2: *Hvclv1-1* growing in semi-field-like conditions

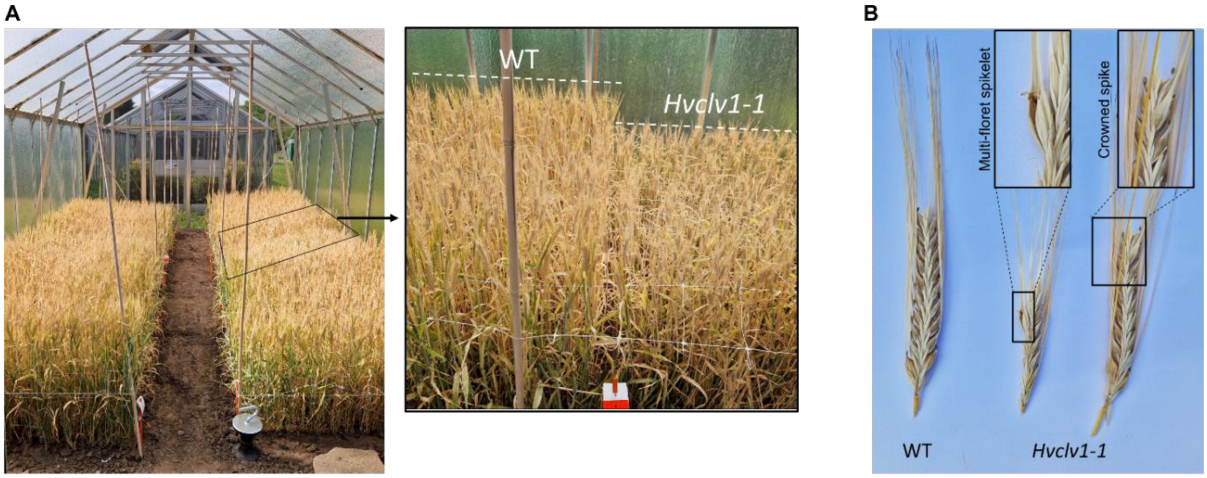

In picture (A): semi-field setup and zoom-in in WT and *Hvclv1-1* plants. In every plot, twelve rows of 44 grains were sown 11 cm apart (528 grains per 1.3mx1.35m =~300 grains per m^2) and grown between March and August 2023. In (B) examples of spikes from WT and *Hvclv1-1* mutants showing multi-floret spikelets and crowned spikes. The average plot yield was 851.7 +- 85 grams for WT plants and 466.4 +- 20.4 grams for *Hvclv1-1.* Thousand grain weight (TGW) was 41.9 +- 0.1 for WT plants and 38.0 +- 1.4 for *Hvclv1-1* plants.

Suppl.Info3: *Hvfcp1* mutant alleles

HvFCP1 (HORVU.MOREX.r3.2HG0174890) Location: Chr2H 523,068,208 - 523,069,031

We generated two independent knock-out mutant alleles by CRISPR-Cas9, called *Hvfcp1-1* and *Hvfcp1-2*. The 284bp deletion in *Hvfcp1-1* removed part of the first exon and the entire second exon, which normally carries the conserved CLE domain. *Hvfcp1-2*, carries two1bp insertions at the +298bp and +543bp positions. The first insertion caused a shift in the reading frame that altered the entire amino acid sequence of the predicted peptide.

<u>FCP1 CLE domain sequence in barley, maize and rice</u>

```
HORVU.MOREX.r3.2HG0174890(HvFCP1)    REVPTGPDPIHHH
Zm00001d003320(ZmFCP1)               REVPTGPDPIHHH
Os04t0473800(OsFCP1)                 REVPTGPDPIHHH
```

sgRNAs target sequences (blue), insertion (green), deletion (red)

```
HvFCP1          ATGGCTCATGCCGCCGACGCGAGGTCGCGCTGCGTCGTCGCGGTGCTCTTCGCCGTAGCC
Hvfcp1-1        ATGGCTCATGCCGCCGACGCGAGGTCGCGCTGCGTCGTCGCGGTGCTCTTCGCCGTAGCC
Hvfcp1-2        ATGGCTCATGCCGCCGACGCGAGGTCGCGCTGCGTCGTCGCGGTGCTCTTCGCCGTAGCC
                ************************************************************

HvFCP1          GTCTTCCTCGCCTGCTTGCCGCCCGCCGCCGCCTCCTCCTCGTCTTCCCGGGCAGGTACG
Hvfcp1-1        GTCTTCCTCGCCTGCTTGCCGCCCGCCGCCGCCTCCTCCTCGTCTTCCCGGGCAGGTACG
Hvfcp1-2        GTCTTCCTCGCCTGCTTGCCGCCCGCCGCCGCCTCCTCCTCGTCTTCCCGGGCAGGTACG
                ************************************************************

HvFCP1          TGCGTCGTCCCGTCCGCCATGCGTTCGTTGCTCTCTACAACCCCCGCCGCAAGGCCACCT
Hvfcp1-1        TGCGTCGTCCCGTCCGCCATGCGTTCGTTGCTCTCTACAACCCCCGCCGCAAGGCCACCT
Hvfcp1-2        TGCGTCGTCCCGTCCGCCATGCGTTCGTTGCTCTCTACAACCCCCGCCGCAAGGCCACCT
                ************************************************************

HvFCP1          CCCTGGTTCTCGCGCCGCACGGGAATCTCCTGCGCTCTTTGACGCCTTTGTTGGTCATCT
Hvfcp1-1        CCCTGGTTCTCGCGCCGCACGGGAATCTCCTGCGCTCTTTGACGCCTTTGTTGGTCATCT
Hvfcp1-2        CCCTGGTTCTCGCGCCGCACGGGAATCTCCTGCGCTCTTTGACGCCTTTGTTGGTCATCT
                ************************************************************

HvFCP1          CCCTCGCAGCGGCGGCGGCGGCATTGCAACGAGTCGAGATGGCGGCCATGTACACCCCGC
Hvfcp1-1        CCCTCGCAGCGGCGGCGGCGGCATTGCAACGAGTCGAGAT--------------------
Hvfcp1-2        CCCTCGCAGCGGCGGCGGCGGCATTGCAACGAGTCGAGATGGCGGCCATGTACACCCCGC
                ****************************************
HvFCP1          AGGACCTGCAGGAGAAG-CCGGATGTGACCAAGGTACGTACGCGGCCGCCATGTTACGGC
Hvfcp1-1        ------------------------------------------------------------
Hvfcp1-2        AGGACCTGCAGGAGAAAGCCGGATGTGACCAAGGTACGTACGCGGCCGCCATGTTACGGC

HvFCP1          TTCGGGCCGAAGGAAAGGCGGCTCCTTTGGTGGTTTCTTGCTGTCGTGTTTCGAGCTCAT
Hvfcp1-1        ------------------------------------------------------------
Hvfcp1-2        TTCGGGCCGAAGGAAAGGCGGCTCCTTTGGTGGTTTCTTGCTGTCGTGTTTCGAGCTCAT

HvFCP1          GGGGTTTTGATTTTCGATGCGCAGGACGCGGAGGAGGACGTGAGCACGACGGGGTTCGGC
Hvfcp1-1        ------------------------------------------------------------
Hvfcp1-2        GGGGTTTTGATTTTCGATGCGCAGGACGCGGAGGAGGACGTGAGCACGACGGGGTTCGGC

HvFCP1          GCGGAGGAGGAGAGGGAGGTGCCCACCGGGCCGGACCCCATCCACCACCACGGCAGGGGA
Hvfcp1-1        ------------------------------------------------------------
Hvfcp1-2        GCGGAGGAGGAGAGGGAGGTGCCCACCGGGCCGGACCCCATCCACCACCACGGCAGGGGA

HvFCP1          CCCAGG-CGCCGGCAGTCGCCCTGATCGCGCGGCAGGTGGAGGATGCTTCCGTGGGTCG…
Hvfcp1-1        --------------------------CGCGCGGCAGGTGGAGGATGCTTCCGTGGGTCG…
Hvfcp1-2        CCCAGGGCGCCGGCAGTCGCCCTGATCGCGCGGCAGGTGGAGGATGCTTCCGTGGGTCG…
                                         *********************************
```

HvFCP1 WT protein sequence (CLE domain highlighted in yellow)

MAHAADARSRCVVAVLFAVAVFLACLPPAAASSSSSRAAAAAALQRVEMAAMYTPQDLQE

KPDVTKDAEEDVSTTGFGAEEEREVPTGPDPIHHHGRGPRRRQSP*

Hvfcp1 mutant alleles protein sequence

Hvfcp1-1

MAHAADARSRCVVAVLFAVAVFLACLPPAAASSSSSRAGTCVVPSAMRSLLSTTPAARPPPWFSRRTG
ISCAL*

Hvfcp1-2

MAHAADARSRCVVAVLFAVAVFLACLPPAAASSSSSRAAAAAALQRVEMAAMYTPQDLQEKAGCDQGR
GGGREHDGVRRGGGEGGAHRAGPHPPPRQGTQGAGSRPDRAAGGGCFRGSVHPA*

Suppl.Table1 – list of primers

Construct		Primer	Primer sequence
pHvCLV1:HvCLV1-mVenus	amplifying promoter	GK-HvpCLV1-fw-AscI	AAAGGCGCGCCGTTTATTTATTGAAGTATTAATCA
		GK-HvpCLV1-rv3	GCAGGTGAGGTGGCGGCATTGTG
	amplifying CDS	GK-HvCLV1-fw+CACC	CACCATGCCGCCACCTCACCTGC
		GK-HvCLV1-rv-stop2	GAAGGAGAGGATGAGGTCGTCGTCGG
pHvFCP1:mVenus-H2B	amplifying promoter	GK-HvpCLE402-fw+CACC	CACCCATGCGACGTTCCCCAACAGCCT
		GK-HvpCLE402-rv	CCAATCCGGCCTTGGCCCTAGCG
p35sHyg-Cas9_HvCLV1	sgRNA	HvCLV1_sgRNA_Fw	agcaGGCCCCTTCCTCCGGCTCCC
		HvCLV1_sgRNA_Rv	aaacGGGAGCCGGAGGAAGGGGCC
p35sHyg-Cas9_HvFCP1	sgRNA_1	HvFCP1_sgRNA1_Fw	agcaGCAGGACCTGCAGGAGAAGC
		HvFCP1_sgRNA1_Rv	aaacGCTTCTCCTGCAGGTCCTGC
	sgRNA_2	HvFCP1_sgRNA2_Fw	agcaCAGGGCGACTGCCGGCGCCT
		HvFCP1_sgRNA2_Rv	aaacAGGCGCCGGCAGTCGCCCTG
p35sHyg-Cas9_HvCLV1	mutant selection by genotyping	HvCLV1_gene_Fw	CGTGCCACTCACATCACATC
		HvCLV1_gene_Rv	TGGTGAGGTTGGTTAGGGAGT
p35sHyg-Cas9_HvFCP1	mutant selection by genotyping	HvFCP1_gene_Fw	CATGCGTTCGTTGCTCTCTA
		HvFCP1_gene_Rv	CCTCAGAATGGACCCAACAC
	Selection of Cas9-free plants	Fl_Cas9_Fw	TTGATGTGGGTTTTACTGATGC
		Fl_Cas9_Rv	CTTGTAGCCTCGGCTGTCTC
		Fl_Hyg_Fw	ATTTCGGCTCCAACAATGTC
		Fl_Hyg_Rv	GCAGGTCACTGGATTTTGGT

Chapter 2

CLAVATA Receptors HvBAM1, HvBAM2, and HvCLV1 shape barley inflorescence architecture through synergistic and antagonistic regulation of meristems activity and identity

Isaia Vardanega[1], Edgar Demesa-Arevalo[1,4], Tianyu Lan[2], Edelgard Wendeler[3], Ivan F. Acosta[3], Maria von Korff Schmising[2,4], Rüdiger Simon[1,4]

[1] Institute of Developmental Genetics, H-einrich-Heine University, Düsseldorf, Germany

[2] Institute of Plant Genetics, Heinrich-Heine University, Düsseldorf, Germany

[3] Max Planck Institute for Plant Breeding Research, Cologne, Germany

[4] CEPLAS, Center of Excellence in Plant Sciences, Heinrich-Heine University, Düsseldorf, Germany

1. Abstract

Grasses have evolved diverse inflorescence architectures, ranging from the complex branching patterns of panicle inflorescences to the simpler organisation of the barley spike. Inflorescence shape is determined in early stages of plant development by activity, determinacy, and identity of meristems leading to the growth of the main rachis and lateral branches. The receptor-like kinase HvCLV1 has been shown to orchestrate the activity and determinacy of both inflorescence and rachilla meristems in barley, promoting the formation of spikelets in the main rachis and repressing auxillary branching. Here, we investigated the function of two additional CLAVATA signalling pathways mediated by the receptor-like kinases *Hordeum vulgare* BARELY ANY MERISTEM 1 (HvBAM1) and HvBAM2, and explored their genetic interaction with HvCLV1 by the generation of higher-order mutants. While the single mutants didn't show a strong effect on the inflorescence phenotype, mutant combinations displayed branches and multi-floret spikelets, resembling inflorescence architectures characteristic of different grass species. Transcriptome analysis of mutant combinations, by bulk and single-cell RNA sequencing, revealed perturbance of multiple pathways, involving genes that regulate cell division, auxin signalling, trehalose-6-phosphate metabolism, and sucrose synthesis. With this study, we confirmed the role of CLAVATA receptors in the regulation of different meristem types comprising the barley spike and demonstrated the potential to engineer inflorescence architecture through the specific regulation of meristem activities.

2. Main

The grass family emerged approximately 55–77 million years ago and progressively developed the various inflorescence architectures characteristic of modern grass species[1,2]. Over time, the complex branching structures of panicle-like inflorescences gradually simplified, giving rise to diverse inflorescence shapes that range from the branched inflorescences in the *Oryzeae* (rice) and *Andropogoneae* (maize) tribes to the simple spike found in *Triticeae*, including barley (*Hordeum vulgare* L.) and wheat (*Triticum* ssp.)[3]. The architecture of these inflorescences is determined in early plant development by shape, size, and determinacy of the shoot apical meristem (SAM) and the lateral meristems positioned on its flanks[4]. The SAM transitions from a vegetative meristem, that only produces leaf primordia, to an inflorescence meristem (IM) that, in dicot species like *Arabidopsis Thaliana*, ultimately produces floral meristems (FMs). However, the categorisation of Arabidopsis meristem types is too simple to explain the more complex inflorescence architecture displayed by grass species, where florets and all the organs that comprise grains or kernels develop from specialised units called spikelets[3]. Spikelets develop from spikelet meristems (SMs), whose placement, morphology, and phyllotaxis can vary between grass species or even between different inflorescence types in the same plant (Fig.1A)[5]. In the panicle inflorescence of rice, the IM produces primary branch meristems in a spiral phyllotaxis, which further generates secondary branch meristems. Spikelet meristems are later produced only on branch meristems (BMs)[3,6]. In maize, the SAM develops the tassel inflorescence along the vertical axis, which only contains the male reproductive organs. In contrast, the female reproductive organs are produced by axillary inflorescences known as ears. The tassel IM first initiates branch meristems bearing spikelet pair meristems (SPMs), but later produces SPMs directly on its main rachis. The auxiliary ear IM produces multiple rows of spirally distributed SMPs directly on its flanks[7].

Within the *Triticeae* tribe, we see the evolution of the spike-type simple inflorescences, where SMs develop directly on the main rachis. In wheat, each SM can form up to 12 florets, while in barley, each SM forms a single floret. The difference lies in the determinacy of the rachilla meristem (RM), a short vestigial axis directing SM growth. In wheat, the RM proliferates indeterminately, giving rise to multiple florets, while the determinate barley rachilla terminates after forming a single floret (Fig.1A)[8]. The barley spikelet develops from a triple spikelet meristem (TSM), that later splits into a central spikelet meristem (CSM) flanked by two lateral spikelet meristems (LSMs).

In six-rowed barley cultivars, each CSM and LSM develops a grain, while in two-rowed cultivars lateral spikelets arrest their development before flower organs are fully developed[9]. The SM is composed of an adaxial RM bearing the subtending floret meristem (FM), lemma primordium (LEP), and glume primordia (GP). The GP eventually develops into two bract-like structures called glumes. The LEP and the later-formed palea primordium generate two leaf-like structures that enclose the FM-generated reproductive organs, the stamens and carpel[3,8,9].

Different molecular pathways play a role in determining the activity of meristems within the barley inflorescence, promoting or repressing meristem proliferation. For instance, SIX-ROWED SPIKE (VRS) genes are responsible for the repression of lateral spikelet development in two-row barley cultivars. Mutation of any of the five characterized VRS genes converts a two-rowed barley spike into a six-row one[10]. Interestingly, mutation of VRS4, the barley ortholog of the LOB domain transcription factor RA2 in maize, generates branched inflorescences. This effect was attributed to the VRS4 regulation of *Hv SISTER OF RAMOSA 3* (*HvSRA*), a putative trehalose-6-phosphate phosphatase, paralog of the maize *RAMOSA 3* (*RA3*), that maintains trehalose-6-phosphate (T6P) homeostasis, controlling SM identity[11]. In maize, *ra3* develops branched ears, from spikelet pair meristems (SPMs) converted into branch meristems (BMs)[12].

Moreover, loss of function of the TCP transcription factor COMPOSITUM1 (COM1) and the AP2/ERF transcription factor COMPOSITUM2 (COM2) enables prolonged activity of the RM through independent pathways, allowing its further elongation and transformation into an actual branch, bearing multiple spikelets[13,14]. The SEPALLATA MADS-box protein HvMADS1 maintains the barley spike in an unbranched state at height ambient temperatures, while the AP2-like transcription factor (HvAP2-L-H5/INTERMEDIUM-m), restricts floret number per spikelet and maintains the indeterminate state of the IM causing, when mutated, its differentiation into a terminal spikelet meristem[15,16].

In our recent study, we discovered the role of a CLAVATA-signalling pathway composed of the RLK HvCLV1 and the CLAVATA3/ENDOSPERM SURROUNDING REGION (CLE) peptide FON2-LIKE CLE PROTEIN1 (HvFCP1), that repress IM and RM meristem proliferation[17]. *Hvclv1* and *Hvfcp1* mutants exhibited enhanced activity in both IM and RM, which resulted in a reduced formation of spikelet meristems (SMs)

and the development of additional florets, resembling the indeterminate multi-floret spikelet of wheat[3]. Transcriptional analysis indicated that the HvFCP1-HvCLV1 signalling pathway influences the barley spike architecture by regulating cell division, auxin signalling, and trehalose-6-phosphate (T6P) metabolism[17]. Genes associated with cell division, such as *HvCyclin P4-1* (*HvCYCP4-1*)[18], *HvBG1* (the ortholog of *Rice Big Grain1*)[19], and *CELL DIVISION CYCLE PROTEIN26* (*HvCDC26*)[20], were upregulated, along with the auxin response factors *HvIAA13* and *HvIAA31*[21]. Additionally, potential effects on T6P homeostasis were suggested by the upregulation of *HvTPS1*, the ortholog of Arabidopsis Trehalose-6-Phosphate Synthase 1 (TPS1)[22], and the downregulation of *HvSRA*. These changes may lead to increased T6P levels, which were associated with the upregulation of *HvFLOWERING LOCUS T 2* (*HvFT2*) and *HvSugars Will Eventually be Exported Transporters 11b* (*HvSWEET11b*)[17,23–25].

This finding revealed the potential to engineer barley spike architecture by manipulating the activity of different meristems. However, the *Hvclv1;Hvfcp1* double mutant phenotype, and indications of HvCLV1 signalling in *Hvfcp1* mutant background, suggested the presence of additional peptides interacting with HvCLV1. Additionally, the overall mild phenotype of *Hvclv1* and *Hvfcp1* indicated a possible compensatory effect on the inflorescence phenotype by additional CLAVATA-related pathways regulating IM and RM activity[17].

Here we investigate the function of two barley receptor-like kinases (RLKs), Hv BARELY ANY MERISTEM1 (HvBAM1) and HvBAM2, and their genetic interaction with the closely related HvCLV1[17]. Studies in Arabidopsis showed that BAM genes play a role in the regulation of stem cell homeostasis in the SAM, which is maintained by negative feedback regulation of WUSCHEL (WUS) expression. In the central zone, the CLE peptide CLV3 interacts with CLV1 to repress WUS expression, while the CLE peptide CLE40 acts through BAM1 from the meristem periphery, influencing the meristem shape[26].

Three BAM genes were found in Arabidopsis, as part of the same monophyletic group as CLV1, and named BAM1, BAM2, and BAM3. BAM receptors had an opposite function to CLV1, therefore higher-ordered *bam* mutants displayed a reduced IM and FM size[27]. Even though *bam* mutants display an opposite IM phenotype to *clv1* mutants, expression of CLV1 under the ERACTA promoter, which directs CLV1 expression to the meristem and young developing tissues, fully rescues the

bam1;bam2 double mutant phenotype. Moreover, BAM1 and BAM2 expression in the meristematic zone can partially rescue the *clv1* phenotype[27], and *BAM1* was found to be upregulated in the meristem centre in the absence of CLV1 signalling[28]. Further genetic studies on various combinations of *bam* and *clv*1 mutants revealed a range of phenotypic outcomes. Among these, the *bam1;bam2;clv1* triple mutant exhibited the most severe synergistic defects in stem cell homeostasis compared to wild-type and other mutant combinations. The triple mutant was notably smaller and had small leaves, an increased number of rosette leaves, and thick stems. The double mutants, *bam1;clv1* and *bam2;clv1*, significantly amplified the *clv1* phenotype, showing enlarged IMs and, an increased number of organ primordia and carpels[29]. The role of BAM1 and BAM2 is not only limited to the SAM but extends to vascular development, leaf shape and symmetry, ovule specification[27], and early anther development, affecting cell division and differentiation[30]. Additionally, BAM1 plays a role in the root apical meristem, where it forms heteromeric complexes with RECEPTOR-LIKE PROTEIN KINASE 2 (RPK2) to modulate cell proliferation[31]. In maize, the BAM1 ortholog ZmBAM1d was shown to regulate kernel size and weight, suggesting a role of BAM genes in regulating grain development in grasses[32].

Overall, the understanding of BAM functions in grasses is limited. In this study, we investigate the roles of HvBAM1 and HvBAM2 in relation to the previously characterised HvCLV1, with the specific aim of understanding their functions in regulating different meristem types within the barley inflorescence and further exploring the potential for engineering barley spike architecture by modulating specific meristem activities.

3. Results

3.1 Identification of the barley BAM gene family and complementary expression of HvBAM1 and HvCLV1 in vegetative and inflorescence meristems

Within the *CLV1* clade, we identified a sub-clade comprising paralogs of *BAM* genes in six different species, the two dicotyledons *Arabidopsis thaliana* and *Solanum lycopersicum* (tomato) and the four monocotyledon grasses *Zea mays* (maize), *Oryza sativa japonica* (rice), *Triticum turgidum* (durum wheat) and *Hordeum vulgare* (barley)[17].

Although Arabidopsis has three *BAM* genes, four *BAM* orthologs are found in both tomato and rice, five in barley, seven in maize, and twelve in tetraploid durum wheat. The two barley genes HORVU.MOREX.r3.5HG0513800 and HORVU.MOREX.r3.2HG0154160 were the most closely related to the Arabidopsis BAM1 and 2, and therefore named HvBAM1 and HvBAM2 respectively (Fig.1B). The three additional barley genes in the clade were most closely related to AtBAM3 and named HvBAM3, HvBAM4, and HvBAM5. As for all the Arabidopsis BAMs, HvBAM1, 2, 3, and 5 had 21 leucine-rich repeats (LRRs) and one kinase domain, while HvBAM4 had an additional LRR[17]. In this study, we started by characterizing the function of HvBAM1 and HvBAM2 and their genetic interaction with the previously described HvCLV1. Results from smRNAfish (Molecular Cartography™, Resolve Biosciences) on sectioned SAMs at the vegetative and inflorescence phases revealed the expression pattern of *HvBAM1* (Fig.1C-M). Unfortunately, no results were retrieved for *HvBAM2*.

In both vegetative SAM and IM, *HvBAM1* transcripts were mostly localized to the apical meristem and corpus, while mostly absent in leaf primordia and early spikelet primordia (Fig.1 C-F). The corpus, which represents the inner cell layers of meristems comprising the inflorescence, is surrounded by an outer cell layer known as the tunica/epidermis[33]. When compared with the expression pattern of *HvCLV1*, *HvBAM1* transcripts were localized in a mostly complementary pattern, but the two genes were co-expressed at the very tip of both SAM and IM (Fig.1 D,F). In barley inflorescences at Waddington stage (W) 3.5[34] (Fig.1H), *HvBAM1* transcripts were nearly absent in the TSM but gradually accumulated in the corpus of the SM just before the formation of the floret meristem (FM) (Fig.1 H-G). This was in contrast to *HvCLV1* transcripts,

which were predominantly localized in the three outer cell layers (Fig.1 I). *HvBAM1* transcripts were found in the RM, FM, LEP, and GP. Conversely, regions with high *HvCLV1* transcript localisation coincided with the absence of *HvBAM1* expression, and vice versa (Fig.1 J-M).

3.2 HvBAM1 and HvBAM2 regulate IM size and plant height

To characterize the functions of HvBAM1 and HvBAM2 and explore their genetic relationship with HvCLV1 in coordinating the activities of different meristems within the barley inflorescence, we generated transgenic plants with CRISPR-Cas9-induced mutations in *HvCLV1*, *HvBAM1*, and *HvBAM2* (Fig.2 A). A plasmid carrying the Cas9 coding sequence expressed under the ZmUBIQUITIN promoter and three 20bp sgRNAs targeting *HvCLV1*, *HvBAM1*, and *HvBAM2* was generated and transformed in the barley cultivar Golden Promise Fast[35]. The sgRNA targeting *HvCLV1* was the same as the one previously used for the generation of *Hvclv1*[17]. Consequently, we selected a transgenic line carrying the *Hvclv1-1* mutation along with heterozygous mutations in the *HvBAM1* and *HvBAM2* genes. The Cas9 sequence was then removed through segregation, and the plants were back-crossed to WT, producing a segregating population that allowed the selection of all possible mutant combinations within the three genes (Suppl.Info 1).

The single mutants *Hvbam1* and *Hvbam2* had a similar phenotype and showed only small differences in comparison to WT. Even though more precise measurements are needed, preliminary observations of the plant and spike phenotypes showed a reduction in plant height and spike length in comparison to WT. The mutated spikes of *Hvbam1* and *Hvbam2* didn’t show any obvious alteration in their morphology (Fig.2 B). Still, they produced a slightly reduced grain yield and thousand grains weight (TGW) in comparison to WT in plants grown in semi-field-like conditions in Germany from March to the end of July 2023 (Fig.2 C,D). Scanning electron microscope (SEM) pictures of inflorescences at W 4.5 didn’t show any difference along spikelet development in *Hvbam1* and *Hvbam2*, while the IM appeared to be shorter than WT in *Hvbam1*, and higher in *Hvbam2* (Fig.2 E).

3.3 HvCLV1, HvBAM1, and HvBAM2 act through independent pathways to shape spike architecture by regulating IM and RM activity, and SM identity

All possible mutant combinations were recovered except for the *Hvbam1;Hvbam2* double mutant (*Db1b2*), which was recently obtained through crossing *Hvbam1* and *Hvbam2*. While *Db1b2* plants are not presented in this study, preliminary observations of their phenotype did not reveal any obvious differences in plant and spike morphology compared to the WT. However, the double mutants *Hvclv1;Hvbam1* (*Dc1b1*), *Hvclv1;Hvbam2* (*Dc1b2*) and the triple mutant *Hvclv1;Hvbam1;Hvbam2* (*Tc1b1b2*) were increasingly shorter than WT. *Dc1b1* was shorter than *Hvbam1* and higher than *Hvclv1*, while *Dc1b2* had a similar height to *Hvclv1*. The triple mutant *Tc1b1b2* showed the strongest dwarf phenotype (Fig.3A).

Spikes of *Dc1b1* were more similar to the ones of *Hvclv1* than to WT, *Hvbam1,* or *Hvbam2* (Fig3 B-F), and developed crowned spikes and muti-floret spikelets (Fig.3 F). Crowned spikes formed an additional row of spikelets in a spiral phyllotaxis at the tip of the inflorescence, while muti-floret spikelets developed secondary RMs and additional florets. SEM pictures of *Dc1b1* inflorescences at W4.5, 5.5, and 6.5 showed an additive phenotype in comparison to *Hvclv1*. The IM was elongated compared to WT and the RM appeared larger and longer than in WT and *Hvclv1*. The morphology and development of multi-florets spikelets in *Dc1b1* reproduced what was previously described for *Hvclv1*, but the enlarged RM allowed a more frequent formation of three florets per spikelet when *Hvclv1* mostly formed two (Fig.3F).

More drastic was the inflorescence phenotype of *Dc1b2,* which displayed fasciation of the upper half of the inflorescence (Fig.3G). The main rachis was enlarged and formed disorganized supernumerary spikelet meristems. The development of crowned spikes was also observed in *Dc1b2* and an enhanced proliferation of SMs on the upper part of the inflorescence generated branch-like structures. In *Dc1b2,* spikelet meristems on the upper part of the inflorescence not only enlarged but their morphology suggests a change in their identity to branch meristem (BM). In *Dc1b2,* SMs weren't only produced directly on the main rachis, but also from the newly formed BMs. Only part of the spikelet meristems ultimately developed into viable grains and the mature spike appeared shorter than WT and ramified on its tip, with branches bearing a variable number of disorganized grains (Fig.3G).

The triple mutant *Tc1b1b2* inflorescences displayed a further enhanced branching phenotype (Fig.3H). SMs on the upper part of the main spike developed into long BMs bearing multiple rows of spikelets disposed in a spiral phyllotaxis. Interestingly, lateral tillers developed a spherical-shaped inflorescence as result of a strong fasciation. Tillers' inflorescences had very short and enlarged rachis and produced two large branches on their flanks, completely covered by disorganized SMs (Fig.3H).

3.4 Transcriptome analysis revealed synergic and antagonistic regulation of genes involved in cell division, auxin signalling, inflorescence development, trehalose-6-phosphate metabolism, and sucrose synthesis

Bulk RNA-sequencing in *Hvclv1* vs WT and *Hvfcp1* vs WT indicated a common gene regulatory network affecting cell division, auxin signalling, and T6P signalling[17]. Phenotypic analysis of *Hvclv1*, *Hvbam1,* and *Hvbam2* mutant combinations showed how these receptors work in parallel pathways to regulate the activity of different meristems within the barley inflorescence.

To further explore the genetic pathways involved in the generation of the described inflorescence phenotypes we performed RNA-sequencing of inflorescences at W3.5 in all the recovered mutant combinations and compared them.

Mutation of *HvCLV1* had a greater impact on the inflorescence transcriptional profile compared to the single mutants *Hvbam1* and *Hvbam2*. In *Hvclv1* vs WT, 1,208 genes were upregulated and 1,198 genes were downregulated. In contrast, *Hvbam1* vs WT showed 446 upregulated genes and 170 downregulated genes, while 504 genes were upregulated and 219 genes downregulated in *Hvbam2* vs WT. Even though the double mutant *Dc1b1* had an enhanced inflorescence phenotype in comparison to *Hvclv1*, *Dc1b1* vs WT showed a lower number of DEGs than *Hvclv1* vs WT. A total of 777 genes were indeed upregulated and 601 downregulated in *Dc1b1* vs WT. *Dc1b1* plants were higher than *Hvclv1* (see above), suggesting that the additional mutation of HvBAM1 can partially rescue the shorter stems of *Hvclv1-1* in comparison to WT. *Dc1b2* vs WT showed 1,367 upregulated and 1,009 downregulated genes, while the triple mutant *Tc1b1b2* showed 1,598 upregulated and 1,223 downregulated genes (ExtDataFig.1A,B).

When compared, the transcriptional profiles of *Hvclv1* vs WT, *Hvbam1* vs WT, *Hvbam2* vs WT, and the respective double mutants, highlighted an opposite trend of

Hvbam1 vs WT and *Hvbam2* vs WT in the transcriptional regulation of most DEGs in comparison to *Hvclv1* vs WT (ExtDataFig.1C,D). *Hvbam1* vs WT and *Hvclv1* vs WT shared only 7 upregulated genes and 2 downregulated genes, while 15 and 10 genes were commonly up and down-regulated in Hv*bam*2 vs WT and *Hvclv1* vs WT respectively (ExtDataFig.1A,B). Consistently with the inflorescence phenotype, the transcriptional profile of *Dc1b1* vs WT, *Dc1b2* vs WT, and *Tc1b1b2* vs WT were more similar to *Hvclv1* vs WT than to *Hvbam1* vs WT and *Hvbam2* vs WT, and all the three higher-order mutants shared a higher number of DEGs with *Hvclv1* vs WT than with *Hvbam1* vs WT or *Hvbam2* vs WT (ExtDataFig.1A,B,E).

Upregulation of the closely related *HvBAM5* and the LRR receptor *HvFEA6*, a paralog of *HvFEA3*[36], in *Hvclv1* vs WT and *Dc1b1* vs WT, suggests that additional CLV-like receptors might partially compensate for the inflorescence phenotype of these mutants. Additionally, another paralog of *HvFEA3*, termed *HvFEA5*, was upregulated in *Hvbam2* vs WT. Moreover, downregulation of *HvRPK2* in *Dc1b2* vs WT and *Tc1b1b2* vs WT, the closest barley ortholog of the Arabidopsis gene *RPK2*[37], suggests regulation of *HvRPK2* by HvCLV1 and HvBAM2. In Arabidopsis roots, RPK2 forms heteromeric complexes with BAM1 to regulate cell proliferation[31]. A similar function could have been conserved between the closely related RLKs in the regulation of meristems composing the barley inflorescence. Further insights into the regulation of meristem homeostasis came from the *Tc1b1b2* vs WT comparison, which revealed the upregulation of the undescribed CLE peptides *HvCLV3*, whose name is based on protein sequence similarity to *At*CLV3, and *HvCLE18*, along with the WUSCHEL ortholog *HvWUS1*, and downregulation of the WUSCHEL-related gene *HvWOX3b* (Fig.4, purple areas; ExtDataFig.2).

The previously observed increase in cell division rates in *Hvclv1* and *Hvfcp1* IMs has been linked to the common upregulation of *HvBG1*, *HvTMM3*, and Hv*Cyclin-P4-1*[17–20]. Additionally, *Hvclv1* vs WT showed upregulation of two more cyclins: *HvCyclin-P2-1* and *HvCyclin-B1-5*. Interestingly, *HvBG1* and *Cyclin-P4-1* were upregulated in *Hvbam2* vs WT, *Dc1b1* vs WT, and *Tc1b1b2* vs WT. *Dc1b2* vs WT showed upregulation of *HvTMM3* and *Cyclin-P2-1*, which were also upregulated in *Tc1b1b2* vs WT. Upregulation of these cell division-related genes correlated with the increased IM size in these mutants. In contrast, the downregulation of *HvCyclin-B1-5* in *Hvbam1* vs WT possibly correlates with the reduced IM size observed in *Hvbam1* (Fig.4, blue areas; ExtDataFig.2). Moreover, upregulation of the auxin response factors *HvIAA13*

and *HvIAA31* in *Hvclv1* vs WT, *Dc1b1* vs WT, and *Tc1b1b2* vs WT, along with the upregulation of *HvIAA13* in Hv*bam2* vs WT, in addition to the consistent downregulation of *HvPIN1* in all mutant combinations except Hv*bam1* vs WT, suggests a direct or indirect effect of these mutants on auxin signalling and transport (Fig.4, orange areas; ExtDataFig.2).

Various genes previously described as important regulators of barley inflorescence architecture were differently regulated in our mutant combinations. *HvCOM2*, a transcription factor repressing inflorescence branching in barley[14], was interestingly downregulated in *Hvclv1* vs WT and *Dc1b2* vs WT, together with downregulation of *HvLEAFY*[38], which was oppositely regulated in *Hvbam1* vs WT. Additionally, *HvCRABS CLAW*, expressed in the lemma and suppressed bracts[39], was downregulated in *Hvclv1* vs WT, *Dc1b2* vs WT, and *Tc1b1b2* vs WT. *HvFUL2* was upregulated in both *Dc1b2* and *Tc1b1b2* mutants and possibly involved in the change of SM identity observed in these two mutant combinations[55]. Within the VRS genes, involved in lateral spikelets development, *VRS3* was downregulated in *Hvclv1* vs WT and *VRS4*, the barley homolog of the maize RA2[11], in *Hvbam2* vs WT, and both were downregulated in the double mutant *Dc1b2* in comparison to WT. Interestingly, the triple mutant *Tc1b1b2* showed downregulation of different VRS genes: *VRS1* and *VRS5*[10] (Fig.4, grey areas; ExtDataFig.2).

Indications of increased levels of trehalose-6-phosphate, previously suggested in *Hvclv1* and *Hvfcp1*[17], were consistent in Hv*bam2* vs WT, but not in Hv*bam1* vs WT. *HvTPS1* was indeed upregulated in all the mutant combinations apart from *Hvbam1* vs WT. *HvSRA* was downregulated in both *Hvclv1* vs WT and *Tc1b1b2* vs WT, providing additional indications of increased T6P levels in the inflorescence of these mutants. Consistent with this, studies in Arabidopsis showed that increased levels of T6P lead to upregulation of *SWEET* genes and *Flowering Locus T* (*FT*)[23]. As described for *Hvclv1* and *Hvfcp1*[17], in *Hvbam2* vs WT and *Dc1b2* vs WT, *HvSWEET11b* and *HvFT2* were also upregulated. *HvSWEET15*, an additional close paralog of SWEET11 in Arabidopsis, was instead upregulated in *Tc1b1b2* vs WT and *HvFT2* was upregulated in all the considered mutant combinations, while downregulated in *Hvbam1* vs WT (Fig.4, yellow areas; ExtDataFig.2).

Interestingly, *FCS-Like Zinc finger 6* (*HvFLZ6*), a starvation-induced protein, ortholog of the homonymous FLZ6 in Arabidopsis, that was previously shown to affect

T6P accumulation[40], was upregulated in all the mutant combinations except for *HvDc1b1* vs WT and accompanied by upregulation of eleven additional paralogous *FCS-Like Zinc finger* genes in *Tc1b1b2* vs WT. Downregulation of *TARGET OF RAPAMYCIN* (*HvTOR*) in *Tc1b1b2* vs WT, a fundamental metabolic regulator that integrates energy sensing with various aspects of plant growth and development[41], indicates a general state of energy and carbon starvation in the inflorescence cells, while upregulation of genes involved in sucrose synthesis, like *Fructose-Bisphosphate Aldolase* (*HvFBA*), *Fructose-1,6-Bisphosphatase* (*HvFBP*), and *Sucrose-Phosphate Synthase 5 (HvSPS5)* suggests an increased sucrose production (Fig.4, cyan areas; ExtDataFig.2)[42–44].

3.5 Phenotyping *Tc1b1b2* inflorescences at a cellular resolution by single-cell RNA sequencing

Transcriptome analysis suggested that the drastic phenotype of *Tc1b1b2* is due to a cascade of gene expression changes, affecting not only the size of the IM but also the identity of the RMs, which transforms into actual branch meristems.

To investigate the mechanisms underlying the reorganization of the simple barley spike into the branched inflorescence of this mutant, we performed single-cell RNA sequencing (scRNA-seq) on *Tc1b1b2* inflorescences at stage W3.5. We then compared these results with an unpublished dataset that integrated scRNA-seq data from cv. Golden Promise inflorescences with transcripts spatial informations from smRNAfish (Demesa-Arevalo et al. 2024, unpublished).

Twenty-five *Tc1b1b2* inflorescences at W3.5 were protoplasted and sequenced using the BD Rhapsody™ microwell-based single-cell partitioning system. All the sequenced cells were divided into 29 clusters, which grouped into cells with a characteristic expression imprint, that defines specific organs within the barley inflorescence and cells undergoing cell division (Fig.5A-C).

A preliminary description of each cluster was achieved through analysis of the smRNAfish results. Genes with specific expression patterns were selected as marker genes. The broad expression of *HvKNOTTED1* generally defined clusters comprising cells from vascular tissues and corpus of the IM and SM within the barley inflorescence (ExtDataFig.3 A,A')[45]. The corpus clusters were further delineated by the expression pattern of more specifically expressed genes. For instance, *HvMADS1* was expressed in the IM corpus and during early spikelet development but not in later-developed floret

organs, which specifically expressed *HvMADS7*, a floral organ marker that defined the origin of cells in clusters 3 and 24 (ExtDataFig.3 B-C')[15,46]. *VRS4*, expressed at the LSM and SM base, was predominantly present in clusters 1, 19, 22, and 25 (ExtDataFig.3 D,D')[11]. Clusters 19 and 25 also expressed *COM1*, whose expression defines RM and organ boundaries(ExtDataFig.3 E,E')[13]. Additionally, *HvCRABS CLAW*, specifically expressed in leaf-like primordia such as repressed bracts, lemmas, and glumes, was mostly present in clusters 4, 27, and 0 (ExtDataFig.3 F,F')[39]. Cluster 0, along with clusters 10, 16, 25, 26, and 28, comprised cells from the epidermal layer, as these clusters expressed the undescribed *HvOCL8* and *Homeobox Domain Transcription Factor* (*HvHDTF*), which expression specifically marked the inflorescence epidermis (ExtDataFig.3 G-H')[47]. Expression of *HvMND1* and *HvCONSTANS-like* marker genes allowed the identification of clusters 8 and 22 as representative of vascular bundles, and a *Cysteine proteinase* (*HvCYSP*) marking the xylem was expressed in cluster 27 (ExtDataFig.3I,K')[48–50]. Finally, an eisosome protein was specifically expressed in the cell cycle clusters representative of dividing cells in the M phase (ExtDataFig.3 L,L')[51].

When comparing the percentage of cells in each cluster between *Tc1b1b2* and WT (Fig.5C), we observed an increase in the cell populations of clusters 8, 12, and 23. The increased number of dividing vascular cells in the S-phase (cluster 23) mirrored the rise in the cell population from vascular tissue in cluster 8, and an overall heightened proliferation of cells from the corpus. On the other hand, the reduced number of cells in clusters 3, 4, and 19, specific for floral organs, leaf-like structures, and rachilla meristems, indicated a tendency of *Tc1b1b2* in the proliferation of the main rachis and vascular tissues at stage W3.5, with a lower ratio of cells that differentiate into the specialised primordia composing the spikelets (Fig.5C). These findings mirror the inflorescence phenotype of *Tc1b1b2* at W3.5. At this stage, *Tc1b1b2* inflorescence developed an enlarged main rachis that ramified into branch-like structures (Fig.3H). Inflorescence branches reflect the organisation of the main rachis. Unlike barley WT, where SMs are produced directly on the main rachis at W3.5, in *Tc1b1b2*, SMs on the upper half of the inflorescence are formed on branches only at later stages. Therefore, the expression profile of cells composing branches likely resembles that of cells from the main rachis. This explains the reduced number of cells with SM identity we recovered in *Tc1b1b2* in comparison to WT, and the increased number of cells with rachis-like identity, expressing marker genes for corpus and vascular tissues.

3.6 scRNA-Seq results provided an insight into the spatial expression of differentially regulated genes in *Tc1b1b2* in comparison to WT

The integrated results from scRNA-seq and smRNA-fish in *cv.* Golden Promise inflorescences at W3.5 (Fig.6A) were previously used to generate a database linked to an online platform named Barvista. This platform can impute the expression pattern of 48,904 genes at cellular resolution with an accuracy of 84 ± 10% (Demesa-Arevalo et al. 2024, unpublished). We utilized the unpublished Barvista platform to verify the expression patterns of some DEGs previously identified by bulk RNA-seq in *Tc1b1b2* vs WT. We then used the integrated scRNA-seq results from both *Tc1b1b2* and WT *cv*. Golden Promise to validate their differential regulation and to obtain spatial information about their expression within the defined clusters.

Among the CLV pathway-related genes differentially regulated in *Tc1b1b2* vs WT, the receptor-like kinase *HvRPK2* was notably downregulated. Results from scRNA-seq confirmed its downregulation in *Tc1b1b2* compared to WT. In *Tc1b1b2*, *HvRPK2* expression was no longer detected in clusters 1, 14, and 19, which include cells from the corpus of the TSM, SM, and RM. The predicted expression pattern from Barvista localized *HvRPK2* expression in early spikelet primordia and RM, suggesting its possible involvement in the regulation of SM and RM proliferation. Regulation that likely occurs in parallel or in conjunction with HvCLV1, HvBAM2, and possibly HvBAM5 (Fig.6B).

HvCyclin-P4-1, previously proposed to be important for the enhanced cell proliferation rate observed in *Hvclv1* IM[17], was upregulated in *Tc1b1b2* vs WT. Consistently, the Barvista platform predicted its expression primarily in the IM corpus and the subtending portion of the main rachis, which coincides with the upper portion of the inflorescence that enlarged in *Hvclv1* crowned spikes and formed BMs in *Tc1b1b2*. Results from scRNA-seq showed its upregulation in clusters 1, 8, 12, 14, and 24, which include cells from the meristem corpus, TSM, SM, and vascular tissues (Fig.6C). Additionally, *HvIAA13*, an auxin response factor upregulated in both *Hvclv1* vs WT and *Tc1b1b2* vs WT, was also increasingly expressed in the same clusters, reinforcing the hypothesis of impaired auxin signalling in *Tc1b1b2* (Fig.6D).

Bulk RNA sequencing results showed differential regulation of genes involved in T6P signalling in *Tc1b1b2*. Consistently, *HvTPS1* was upregulated in scRNA-seq results

from *Tc1b1b2* compared to WT, especially in clusters defining inflorescence corpus, vascular tissue, and tunica cells. The predicted expression of *HvTPS1* in the inflorescence at W3.5 was notably restricted to a specific cell population located at the base of the SM, at the boundary of the corpus, adjacent to the vascular bundles (Fig.6E). The predicted expression pattern of *HvSRA* (T6P-phosphatase), was consistent with the expression pattern of *RA3* and *SRA* in maize[12] and overlapped with *HvTPS1*-expressing cells. *HvSRA* was additionally expressed in vascular tissue and RM and downregulated in clusters comprising cells from TSM, SM, and RM (Fig.5F).

HvFT2 and *HvSWEET15* were putatively upregulated in response to increased T6P levels[17,23]. *HvFT2* was upregulated across all clusters in *Tc1b1b2* compared to WT, with pronounced expression in clusters 8, 12, and 24, which contain cells from vascular tissue, TSM, SM, and corpus (Fig.6G). Its predicted expression pattern notably resembled that of *HvCyclin-P4-1*, particularly in the SM and IM corpus and the subtending region of the main stem. *HvSWEET15* is putatively expressed in the SM but not in the IM and FM. Its expression overlaps with that of *HvFT2*, suggesting a possible role for this sucrose transporter in the transport of sugars into the developing spikelets (Fig.6H).

4. Discussion

Here we investigated the function of the barley RLKs HvBAM1 and HvBAM2, which act with HvCLV1 through independent but redundant pathways to regulate shape and proliferation of the IM while also influencing RM determinacy and SM identity. *Hvbam1* and *Hvbam2* single mutants exhibited only minor alterations in plant and inflorescence architecture compared to WT, although notable differences in IM shape were observed. *Hvbam1* showed a reduction in IM size, while *Hvbam2* IM was elongated, similar to the *Hvclv1* IM[17]. The previously described *Hvclv1* inflorescence phenotype was exacerbated by additional mutations in *HvBAM1* and *HvBAM2*, resulting in an increasingly additive branching phenotype in double and triple mutants. This indicates that independent CLAVATA-related pathways collaborate in the regulation of different meristem types to maintain the simple barley spike architecture.

Interestingly, the impact on IM size and shape in various mutant combinations, though evident, was not as pronounced as previously observed for related CLAVATA-receptor mutants in Arabidopsis and maize[29,52,53]. Instead, a major effect was detected at the base of the IM, specifically in the upper portion of the developing rachis, which enlarged in *Hvclv1*, *Dc1b1*, and *Tc1b1b2* mutants. This enlargement caused an occasional change in spikelet phyllotaxis from distichous to spiral in these mutants. The most pronounced effect, however, was on RM determinacy and SM identity. The elongated RM of *Hvclv1* was further enlarged in *Dc1b1*, allowing the formation of FM triplets and supporting the correlation between RM size and FM number, consistent with the multi-floret spikelet formed by the indeterminate rachilla of wheat. In *Dc1b2* and *Tc1b1b2* mutants, a different effect was observed: not only was the RM enlarged, but the SMs in the upper portion of the main rachis changed identity to become BMs, which developed either spirally distributed or disorganized SMs on their flanks.

While *Hvclv1* and *Dc1b1* inflorescences resembled the organization of wheat spikelets, *Dc1b2* and *Tc1b1b2* resembled the branched inflorescences of rice and maize[3]. The spherical-shaped tiller inflorescences developed by *Tc1b1b2* exhibited a completely new architecture, comparable to the drastic transformation seen in the axillary ears of maize from its ancestor, Teosinte[54]. These phenotypes suggest that CLV-related genes may have played a crucial role in the evolution of the diverse inflorescence architectures displayed by the grass family.

Results from bulk and single-cell RNA sequencing suggested that additional RLKs might be involved in similar processes. For instance, the upregulation of *HvBAM5* in *Hvclv1* vs WT and *Dc1b1* vs WT suggests its possible compensatory function in the absence of functional HvCLV1 proteins. Moreover, *HvRPK2*, whose Arabidopsis ortholog forms a heteromeric complex with BAM1 to regulate cell proliferation in the root apical meristem[31], was putatively expressed in the RM and downregulated in *Dc1b2* vs WT and *Tc1b1b2* vs WT. This suggests that a similar mechanism involving HvRPK2, HvCLV1, and HvBAM2 may be conserved in regulating RM activity in barley inflorescence and indicates cross-regulation between these receptors. Such cross-regulation is further indicated by the downregulation of *HvBAM1* in *Dc1b2* vs WT. *HvBAM1* not only exhibited a complementary expression pattern compared to *HvCLV1* but also showed a reduced IM size in its mutant, with an opposite effect on most of the DEGs identified in *Hvclv1* vs WT. Altogether, these results point toward an antagonistic pathway mediated by HvBAM1, in comparison to HvCLV1, that positively regulates IM activity, similar to what was previously described in Arabidopsis[26].

Transcriptome analysis of *Tc1b1b2* vs WT revealed additional insights into the potential players involved in the HvCLV1, HvBAM1, or HvBAM2 pathways. The CLE peptides *HvCLV3* and *HvCLE18* were upregulated in *Tc1b1b2* vs WT, while the WUSCHEL-like genes *HvWUS1* and *HvWOX3b* were upregulated and downregulated, respectively. These results align with the regulation of SAM homeostasis proposed for Arabidopsis, where different CLE peptides are perceived by CLV-like receptors that trigger synergistic or antagonistic signals, ultimately regulating the expression of WUS-related transcription factors[26,27,29]. However, the role of these parallel CLV-related pathways in barley extends to the regulation of RM proliferation and SM identity. The increased number of genes involved, along with their varied expression patterns and milder single mutant phenotypes, suggest an enhanced complexity and redundancy in the regulation of different meristem activities in barley, as well as the acquisition of new functions involving the regulation of SM identity and the repression of spike branching.

In line with the gene regulatory network regulated by the HvFCP1/HvCLV1 pathway[17], the transcriptional profile of inflorescences from all the mutant combinations revealed a direct or indirect effect in the regulation of genes involved in cell division, auxin signalling, spikelet identity, trehalose-6-phosphate metabolism, and sucrose biosynthesis. Upregulation of different genes involved in cell division was

consistently found in all the mutant combinations with enhanced IM or rachilla proliferation, while in *Hvbam1* vs WT, the cyclin *CYCB5-1* was downregulated, suggesting an opposite effect in the regulation of cell division. Of most interest was the upregulation of an undescribed type P cyclin *HvCYCP4-1* in most of the mutant combinations. ScRNA-seq results showed its upregulation in clusters containing cells from meristem corpus, TSM, SM, and vascular tissues, and its putative expression was enhanced in the IM corpus and in the subtending upper portion of the main rachis, which coincides with the region where *Hvclv1*, double, and triple mutants showed an increased cell proliferation and the formation of additional rows of SM. Also expressed in the same region were the auxin response factor *HvIAA13* and the FT paralog *HvFT2*, which were similarly upregulated in most of the mutant combinations in comparison to WT, except *Hvbam1*, suggesting an integrated regulation of these genes by HvCLV1 and HvBAM2 and their important contribution on the formation of the described inflorescence phenotypes. Within the genes described as important for inflorescence architecture, *HvFUL2*[55] was interestingly upregulated in both *Dc1b2* and *Tc1b1b2* and possibly involved in the change of SM identity we found in these two mutant combinations. Additionally, the downregulation of *VRS3* in *Hvclv1* vs WT, *VRS4* in *Hvbam2* vs WT, and both in *Dc1b2*, indicated specific and independent repression of different VRS genes by the HvCLV1 and HvBAM2 signalling pathways.

The barley *vrs4* mutant displayed a change in the SM identity, which became a BM[11], similar to the effect we saw in *Dc1b2* and *Tc1b1b2* inflorescences. The branching phenotype of *vrs4* was previously linked with downregulation of the trehalose-6-phosphate phosphatase *HvSRA*[11]*. HvSRA* was downregulated in *Hvclv1* and *Tc1b1b2*, and *HvTPS1* was upregulated in all the mutant combinations except for *Hvbam1* vs WT. Both the T6P synthase and phosphatase are putatively colocalized at the spikelet base and were up and down-regulated in the TSM and SM clusters respectively. Their expression pattern, together with the ears branching phenotype of *ra3* in maize and the increased shoot branching in Arabidopsis plant with enhanced levels of T6P, suggests a role of T6P signalling in the determination of SMs identity and axillary meristems outgrowth in our branched mutant combinations. Moreover, the upregulation of *SWEET* genes and *HvFT2* we observed, is consistent with the previously described effect of increased T6P levels in Arabidopsis. The putative expression pattern of *HvSWEET15* and *HvFT2* and their strong upregulation in *Tc1b1b2* clusters containing cells from TSM, SM, meristem corpus, and vasculature,

indicates their possible involvement in the determination of SM identity and sugar transport to the BMs developed by *Tc1b1b2*.

Results from scRNA-seq in *Tc1b1b2* showed an enhanced proliferation of cells belonging to the inflorescence corpus and vascular tissues, which are necessary to feed the newly formed branches. In general, over-proliferation and new organogenesis come with increased energy demand, reflected by the upregulation of the starvation-induced Hv*FLZ6* and other genes of the same family, downregulation of *HvTOR*, and upregulation of genes such as *HvFBA*, *HvFBP*, and *HvSPS5*, encoding for enzymes necessary for sucrose synthesis[42–44].

With this study, we confirmed the involvement of HvBAM1 and HvBAM2 in addition to HvCLV1 in the regulation of proliferation, determinacy, and identity of different meristem types within the barley inflorescence, affecting the transcription of a wide number of genes, whose functions range from regulation of cell division to T6P metabolism and sucrose synthesis and reallocation. Our findings demonstrate how targeted regulation of meristems in grass inflorescences can pave the way for future engineering of spike architecture and suggest that differential regulation of CLAVATA-related pathways could have played an important role in the evolution of different inflorescence architectures within grasses.

5 Materials and methods

5.1 Plant material and growth conditions

All plants used for this study were barley *cv.* Golden Promise Fast[56]. Plants were grown in soil (Einheitserde ED73, Einheitserde Werkverband e.V., with 7% sand and 4 g/L Osmocote Exact Hi.End 3-4M, 4th generation, ICL Group Ltd.) under long day (LD) conditions with 16 hours light at 20°C and 8 hours dark at 16 °C. Plants dissected for scanning electron microscope imaging were grown in QuickPot 96T trays (HerkuPlast Kubern GmbH) in a climate chamber, while plants used to show differences in plant height were grown in large pots (diameter 16.5 cm, height 13 cm) in a greenhouse under the same growing conditions. However, temperatures could have varied between seasons. Dried barley grains were placed in Petri dishes with distilled water and pregerminated at 4°C for 3 days before sowing.

5.2 Plasmids construction and plant transformation

A construct including three sgRNA that specifically targeted *HvCLV1*, *HvBAM1*, and *HvBAM2* was generated by following the protocol of a previously established CRISPR-Cas9 vector system (Suppl.Info1)[57]. All the sgRNAs were designed using E-CRISP software[58]. Single sgRNA strands were first hybridised and then cloned into the shuttle vectors pMGE625 or pMGE627 using the restriction enzyme BpiI. The second step consisted of a cut/ligation reaction (BsaI) and allowed the insertion of the sgRNA units (TUs) into the recipient vector pMGE599[57]. The vector targeting *HvCLV1*, *HvBAM1* and *HvBAM2* was transformed into the barley *cv.* Golden promise Fast via *Agrobacterium Tumefaciens*-mediated embryo transformation[59]. Successful transformation was tested by PCR using vector-specific primers (Suppl.table1) on M0 plants. The Cas9 protein was subsequently removed from the plant's genome by segregation in the M1 generation, and mutants carrying the *Hvclv1-1* mutation and heterozygous mutation of *HvBAM1* and *HvBAM2* were selected in M2 plants by PCR and subsequent Sanger sequencing (Suppl.table1).

5.3 smRNAfish

Barley inflorescences at W3.5 were first fixed in 4% PFA and embedded in paraplast (Leica Paraplast X-tra). Microtome sections (10 µm) of the inflorescence were placed on Resolve Bioscience slides and incubated on a heating plate at 60°C for a few minutes to attach the samples to the slides. Slides were further deparaffinized, permeabilized, acetylated, and re-fixed with 4% PFA. Slides were mounted with SlowFade-Gold Antifade reagent (Invitrogen) and covered with a coverslip before being shipped to Resolve BioSciences (Germany).

5.4 Sample preparation, microscopy, and image processing

Barley SAMs and inflorescences were collected at the desired stage by manual dissection. Small leaves were removed under a stereo microscope with a 1.5 mm blade scalpel. SEM pictures were obtained either by direct imaging of fresh inflorescences or by imaging of epoxy replicates of barley inflorescences. A negative imprint of the inflorescence was generated by mixing the two-component vinyl polysiloxane impression material (Express™ 2Ultra Light Body Quick, 3M ESPE) and imprinting the dissected inflorescence into the impression material. Once the polymerization of the negative imprints was completed the plant material was removed. Inflorescence replicates were generated by filling the negative imprints with epoxy resin, that polymerized overnight. Inflorescence replicates were then coated with gold using an Agar Sputter Coater and imaged under the scanning electron microscope Zeiss SUPRA 55VP.

5.5 Bulk RNA sequencing

Gene expression changes in *Hvclv1*, *Hvbam1*, *Hvbam2*, *Dc1b1*, *Dc1b2,* and *Tc1b1b2* inflorescence in comparison to WT, were detected by RNA-sequencing on WT and mutant inflorescences at W3.5. For each of the three analysed replicates per sample, a total of 40 inflorescences were manually dissected and collected in a 1.5 ml tube. Total RNA from each replicate was extracted using the Direct-zol™ RNA, Miniprep Plus kit, following the manufacturer's instructions, and digested with DNase I (ZYMO RESEARCH). RNA samples with RNA Integrity Number (RIN) ≥ 8 were selected for mRNA library preparation using the poly-A enrichment method. Sequencing was performed on the Illumina Novaseq 6000 sequencing platform (PE150), and at least 6G of clean reads data per sample were generated by Biomarker Technologies (BMK) GmbH. All the reads were then mapped to the Morex reference

Version 3[60] using Salmon (v. 0.14.1)[61]. Transcripts with a minimum of 1 CPM (counts per million) in at least three samples were kept and the analysis was conducted on 22,307 expressed genes. The identification of differentially expressed genes (DEGs) within WT and mutant combinations was conducted by pairwise comparisons using the count-based Fisher's Exact Test in R package 'EdgeR' (v3.32.1)[62]. Gene with BH.FDR<0.05 and $\log_2$FC ≤ -0.5 or $\log_2$FC ≥ 0.5 was considered as downregulated or upregulated. The FDR of each gene was adjusted by the Benjamini-Hochberg (BH) procedure. Heatmaps of gene expression (ExtDataFig.1 C-E) were generated on the summed differentially expressed genes of the compared genotypes, with $-\log_{10}$(TPM + 1) values using the R package '3DRNAseq' [63].

5.6 Single-cell RNA-sequencing and integration

Single-cell RNA sequencing was performed on cells from 25 pooled inflorescences at W3.5, manually dissected from main shoots of *Tc1b1b2.* Protoplasts were obtained following a previously established protocol with minor modifications[64] and sequenced by the BD Rhapsody™ microwell-based single-cell partitioning system. A total of 6,960 cells were successfully sequenced, analysed, and integrated with unpublished data from Demesa-Arevalo et al. 2023, where scRNA-seq of inflorescences from the barley *cv.* Golden Promise was performed in three replicates. Golden Promise replicates were merged and integrated with results from *Tc1b1b2* inflorescences at the same stage using the Seurat package v5.0.3. Low quality cells were removed with a threshold of 800< Genes <9000 and log-normalized. Differentially expressed genes from protoplasting were later removed from the merged object. The *FindIntegrationAnchors* function was then used to identify the anchors to integrate the three experiments from Golden Promise and the one from *Tc1b1b2* using 30 dimensions. The integrated expression matrix was retrieved by the *IntegrateData* Function. Then, dimensionality reduction was performed by scaling the expression matrix with *ScaleData* function and then with a principal component analysis (PCA). Cells were clustered using a *k*-nearest neighbours and SNN graph method. The functions *FindNeighbors* and *FindClusters* were applied with a resolution of 1.3. Then, dimensional reduction was performed using the UMAP algorithm with the top 40 principal components and a minimal distance of 0.01. Gene enriched in each cluster were identified using *FindAllmarkers* function in *Seurat* using as a threshold: Log.FC = 0.25, pct1 >0.25, pct2<0.3, P-value$_{adj}$ < 0.001. Differential gene expression was calculated by using the function *FindAllMarkers* and a Model-based Analysis of Single-

cell Transcriptomics (MAST). The markers identified were used to manually annotate the cluster identity. The featureplots in Fig.5 compare results from one WT and one *Tc1b1b2* replicate, comprising results from 6,238 and 6,960 cells respectively. The colored heatmap displaying expression intensity in each Featureplot was calculated by dividing counts (per gene) for each cell by the total counts in that cell and then multiplied by the scale factor (10,000) to do a log transformation. Values were scaled and normalized prior to any comparison.

6. Author contributions

Isaia Vardanega did most of the work presented here, together with Edgar Demesa-Aravalo who performed the scRNA-seq data analysis and helped with the smRNAfish. Tianyu Lan from Maria von Korff Schmising's lab performed the RNA-seq raw data analysis. Edelgard Wendeler from Ivan Acosta's lab performed the *Tc1b1b2* transformation, from where all the mutant combinations were selected by Isaia Vardanega. Rüdiger Simon supervised the project and contributed to the overall planning of the experiments.

7. Acknowledgements

We thank the Center for Advanced imaging (CAi) at HHU for microscopy support. Work in R.S. and M.v.K.S. labs was supported by the DFG through CEPLAS (EXC2048), CSCS (FOR5235), NEXT-PLANT (IRTG2466) and work in I.F.A. lab by the Max Planck Society.

8. References

1. Jacobs, B. F., Kingston, J. D. & Jacobs, L. L. The Origin of Grass-Dominated Ecosystems. *Annals of the Missouri Botanical Garden* **86**, 590–643 (1999).
2. Kellogg, E. A. Evolutionary History of the Grasses1. *Plant Physiology* **125**, 1198–1205 (2001).
3. Koppolu, R. & Schnurbusch, T. Developmental pathways for shaping spike inflorescence architecture in barley and wheat. *Journal of Integrative Plant Biology* **61**, 278–295 (2019).
4. Kyozuka, J., Tokunaga, H. & Yoshida, A. Control of grass inflorescence form by the fine-tuning of meristem phase change. *Current Opinion in Plant Biology* **17**, 110–115 (2014).
5. Bonnett, O. T. *Inflorescences of Maize, Wheat, Rye, Barley, and Oats: Their Initiation and Development*. University of Illinois, College of Agriculture, Agricultural Experiment Station, (1966).
6. Wang, L. *et al.* Coordinated regulation of vegetative and reproductive branching in rice. *Proceedings of the National Academy of Sciences* **112**, 15504–15509 (2015).
7. Bommert, P., Satoh-Nagasawa, N., Jackson, D. & Hirano, H.-Y. Genetics and Evolution of Inflorescence and Flower Development in Grasses. *Plant and Cell Physiology* **46**, 69–78 (2005).
8. Bommert, P. & Whipple, C. Grass inflorescence architecture and meristem determinacy. *Seminars in Cell & Developmental Biology* **79**, 37–47 (2018).
9. Clayton, W. D. The spikelet. *Reproductive versatility in the grasses*, 32-51 (1990).
10. Zwirek, M., Waugh, R. & McKim, S. M. Interaction between row-type genes in barley controls meristem determinacy and reveals novel routes to improved grain. *New Phytologist* **221**, 1950–1965 (2019).
11. Koppolu, R. *et al.* Six-rowed spike4 (Vrs4) controls spikelet determinacy and row-type in barley. *Proc Natl Acad Sci U S A* **110**, 13198–13203 (2013).
12. Satoh-Nagasawa, N., Nagasawa, N., Malcomber, S., Sakai, H. & Jackson, D. A trehalose metabolic enzyme controls inflorescence architecture in maize. *Nature* **441**, 227–230 (2006).

13. Poursarebani, N. *et al.* COMPOSITUM 1 contributes to the architectural simplification of barley inflorescence via meristem identity signals. *Nat Commun* **11**, 5138 (2020).
14. Poursarebani, N. *et al.* The Genetic Basis of Composite Spike Form in Barley and 'Miracle-Wheat'. *Genetics* **201**, 155–165 (2015).
15. Li, G. *et al.* MADS1 maintains barley spike morphology at high ambient temperatures. *Nat. Plants* **7**, 1093–1107 (2021).
16. Zhong, J. *et al.* INTERMEDIUM-M encodes an HvAP2L-H5 ortholog and is required for inflorescence indeterminacy and spikelet determinacy in barley. *Proceedings of the National Academy of Sciences* **118**, e2011779118 (2021).
17. Vardanega, I. *et al.* CLAVATA signalling shapes barley inflorescence architecture by controlling activity and determinacy of shoot apical and rachilla meristems. *bioRxiv*, https://doi.org/10.1101/2024.05.28.595952 (2024).
18. Torres Acosta, J. A. *et al.* Molecular characterization of Arabidopsis PHO80-like proteins, a novel class of CDKA;1-interacting cyclins. *Cell Mol Life Sci* **61**, 1485–1497 (2004).
19. Lo, S. *et al.* Rice Big Grain 1 promotes cell division to enhance organ development, stress tolerance and grain yield. *Plant Biotechnol J* **18**, 1969–1983 (2020).
20. Lorenzo-Orts, L. *et al.* Concerted expression of a cell cycle regulator and a metabolic enzyme from a bicistronic transcript in plants. *Nature Plants* **5**, 184–193 (2019).
21. Shimizu-Mitao, Y. & Kakimoto, T. Auxin Sensitivities of All Arabidopsis Aux/IAAs for Degradation in the Presence of Every TIR1/AFB. *Plant and Cell Physiology* **55**, 1450–1459 (2014).
22. Dijken, A. J. H. van, Schluepmann, H. & Smeekens, S. C. M. Arabidopsis Trehalose-6-Phosphate Synthase 1 Is Essential for Normal Vegetative Growth and Transition to Flowering. *Plant Physiol* **135**, 969–977 (2004).
23. Fichtner, F. *et al.* Regulation of shoot branching in arabidopsis by trehalose 6-phosphate. *New Phytologist* **229**, 2135–2151 (2021).
24. Shaw, L. M. *et al.* FLOWERING LOCUS T2 regulates spike development and fertility in temperate cereals. *J Exp Bot* **70**, 193–204 (2019).

25. Radchuk, V. *et al.* SWEET11b transports both sugar and cytokinin in developing barley grains. *Plant Cell* **35**, 2186–2207 (2023).
26. Schlegel, J. *et al.* Control of Arabidopsis shoot stem cell homeostasis by two antagonistic CLE peptide signalling pathways. *eLife* **10**, e70934 (2021).
27. DeYoung, B. J. *et al.* The CLAVATA1-related BAM1, BAM2 and BAM3 receptor kinase-like proteins are required for meristem function in Arabidopsis. *The Plant Journal* **45**, 1–16 (2006).
28. Nimchuk, Z. L. CLAVATA1 controls distinct signalling outputs that buffer shoot stem cell proliferation through a two-step transcriptional compensation loop. *PLOS Genetics* **13**, e1006681 (2017).
29. DeYoung, B. J. & Clark, S. E. BAM Receptors Regulate Stem Cell Specification and Organ Development Through Complex Interactions With CLAVATA Signaling. *Genetics* **180**, 895–904 (2008).
30. Hord, C. L. H., Chen, C., DeYoung, B. J., Clark, S. E. & Ma, H. The BAM1/BAM2 Receptor-Like Kinases Are Important Regulators of Arabidopsis Early Anther Development. *The Plant Cell* **18**, 1667–1680 (2006).
31. Shimizu, N. *et al.* BAM 1 and RECEPTOR-LIKE PROTEIN KINASE 2 constitute a signaling pathway and modulate CLE peptide-triggered growth inhibition in Arabidopsis root. *New Phytologist* **208**, 1104–1113 (2015).
32. Yang, N. *et al.* Genome assembly of a tropical maize inbred line provides insights into structural variation and crop improvement. *Nat Genet* **51**, 1052–1059 (2019).
33. Reeve, R. M. The 'Tunica-Corpus' Concept and Development of Shoot Apices in Certain Dicotyledons. *American Journal of Botany* **35**, 65–75 (1948).
34. Waddington, S. R., Cartwright, P. M. & Wall, P. C. A Quantitative Scale of Spike Initial and Pistil Development in Barley and Wheat. *Annals of Botany* **51**, 119–130 (1983).
35. Gol, L., Haraldsson, E. B. & Von Korff, M. *Ppd-H1* integrates drought stress signals to control spike development and flowering time in barley. *Journal of Experimental Botany* **72**, 122–136 (2021).

36. Wang, C. *et al.* Barley FASCIATED EAR genes determine inflorescence meristem size and yield traits. *The Crop Journal* **11**, 679–691 (2023).
37. Kinoshita, A. *et al.* RPK2 is an essential receptor-like kinase that transmits the CLV3 signal in Arabidopsis. *Development* **137**, 3911–3920 (2010).
38. Jin, R. *et al.* LEAFY is a pioneer transcription factor and licenses cell reprogramming to floral fate. *Nat Commun* **12**, 626 (2021).
39. Lee, J.-Y. *et al.* Recruitment of CRABS CLAW to promote nectary development within the eudicot clade. *Development* **132**, 5021–5032 (2005).
40. Jamsheer K, M. *et al.* FCS-like zinc finger 6 and 10 repress SnRK1 signalling in Arabidopsis. *Plant J* **94**, 232–245 (2018).
41. Morales-Herrera, S., Paul, M. J., Dijck, P. V. & Beeckman, T. SnRK1/TOR/T6P: three musketeers guarding energy for root growth. *Trends in Plant Science* **0**, (2024).
42. Lv, G.-Y. *et al.* Molecular Characterization, Gene Evolution, and Expression Analysis of the Fructose-1, 6-bisphosphate Aldolase (FBA) Gene Family in Wheat (Triticum aestivum L.). *Front Plant Sci* **8**, 1030 (2017).
43. Lee, S.-K. *et al.* Loss of cytosolic fructose-1,6-bisphosphatase limits photosynthetic sucrose synthesis and causes severe growth retardations in rice (Oryza sativa). *Plant, Cell & Environment* **31**, 1851–1863 (2008).
44. Solís-Guzmán, M. G. *et al.* Arabidopsis thaliana sucrose phosphate synthase (sps) genes are expressed differentially in organs and tissues, and their transcription is regulated by osmotic stress. *Gene Expr Patterns* **25–26**, 92–101 (2017).
45. Jackson, D., Veit, B. & Hake, S. Expression of maize KNOTTED1 related homeobox genes in the shoot apical meristem predicts patterns of morphogenesis in the vegetative shoot. *Development* **120**, 405–413 (1994).
46. Thiel, J. *et al.* Transcriptional landscapes of floral meristems in barley. *Science Advances* **7**, eabf0832 (2021).
47. Ingram, G. C., Magnard, J. L., Vergne, P., Dumas, C. & Rogowsky, P. M. ZmOCL1, an HDGL2 family homeobox gene, is expressed in the outer cell layer throughout maize development. *Plant Mol Biol* **40**, 343–354 (1999).

48. Walla, A. *et al.* An Acyl-CoA N-Acyltransferase Regulates Meristem Phase Change and Plant Architecture in Barley. *Plant Physiol* **183**, 1088–1109 (2020).
49. Griffiths, S., Dunford, R. P., Coupland, G. & Laurie, D. A. The Evolution of CONSTANS-Like Gene Families in Barley, Rice, and Arabidopsis. *Plant Physiol* **131**, 1855–1867 (2003).
50. Avci, U., Earl Petzold, H., Ismail, I. O., Beers, E. P. & Haigler, C. H. Cysteine proteases XCP1 and XCP2 aid micro-autolysis within the intact central vacuole during xylogenesis in Arabidopsis roots. *The Plant Journal* **56**, 303–315 (2008).
51. Olivera-Couto, A. *et al.* Eisosomes Are Dynamic Plasma Membrane Domains Showing Pil1-Lsp1 Heteroligomer Binding Equilibrium. *Biophys J* **108**, 1633–1644 (2015).
52. Bommert, P. *et al.* thick tassel dwarf1 encodes a putative maize ortholog of the Arabidopsis CLAVATA1 leucine-rich repeat receptor-like kinase. *Development* **132**, 1235–1245 (2005).
53. Je, B. I. *et al.* The CLAVATA receptor FASCIATED EAR2 responds to distinct CLE peptides by signaling through two downstream effectors. *eLife* **7**, e35673 (2018).
54. Chen, Q. *et al.* The genetic architecture of the maize progenitor, teosinte, and how it was altered during maize domestication. *PLoS Genet* **16**, e1008791 (2020).
55. Li, C. *et al.* Wheat VRN1, FUL2 and FUL3 play critical and redundant roles in spikelet development and spike determinacy. *Development* **146**, dev175398 (2019).
56. Gol, L., Haraldsson, E. B. & von Korff, M. Ppd-H1 integrates drought stress signals to control spike development and flowering time in barley. *Journal of Experimental Botany* **72**, 122–136 (2021).
57. Galli, M. *et al.* CRISPR/SpCas9-mediated double knockout of barley Microrchidia MORC1 and MORC6a reveals their strong involvement in plant immunity, transcriptional gene silencing and plant growth. *Plant Biotechnol J* **20**, 89–102 (2022).
58. Heigwer, F., Kerr, G. & Boutros, M. E-CRISP: fast CRISPR target site identification. *Nat Methods* **11**, 122–123 (2014).
59. Amanda, D. *et al.* Auxin boosts energy generation pathways to fuel pollen maturation in barley. *Current Biology* **32**, 1798-1811.e8 (2022).

60. Mascher, M. *et al.* Long-read sequence assembly: a technical evaluation in barley. *The Plant Cell* **33**, 1888–1906 (2021).
61. Patro, R., Duggal, G., Love, M. I., Irizarry, R. A. & Kingsford, C. Salmon: fast and bias-aware quantification of transcript expression using dual-phase inference. *Nat Methods* **14**, 417–419 (2017).
62. Robinson, M. D., McCarthy, D. J. & Smyth, G. K. edgeR: a Bioconductor package for differential expression analysis of digital gene expression data. *Bioinformatics* **26**, 139–140 (2010).
63. Guo, W. *et al.* 3D RNA-seq: a powerful and flexible tool for rapid and accurate differential expression and alternative splicing analysis of RNA-seq data for biologists. *RNA Biol* **18**, 1574–1587.
64. Xu, X. *et al.* Single-cell RNA sequencing of developing maize ears facilitates functional analysis and trait candidate gene discovery. *Dev Cell* **56**, 557-568.e6 (2021).

9. Figures

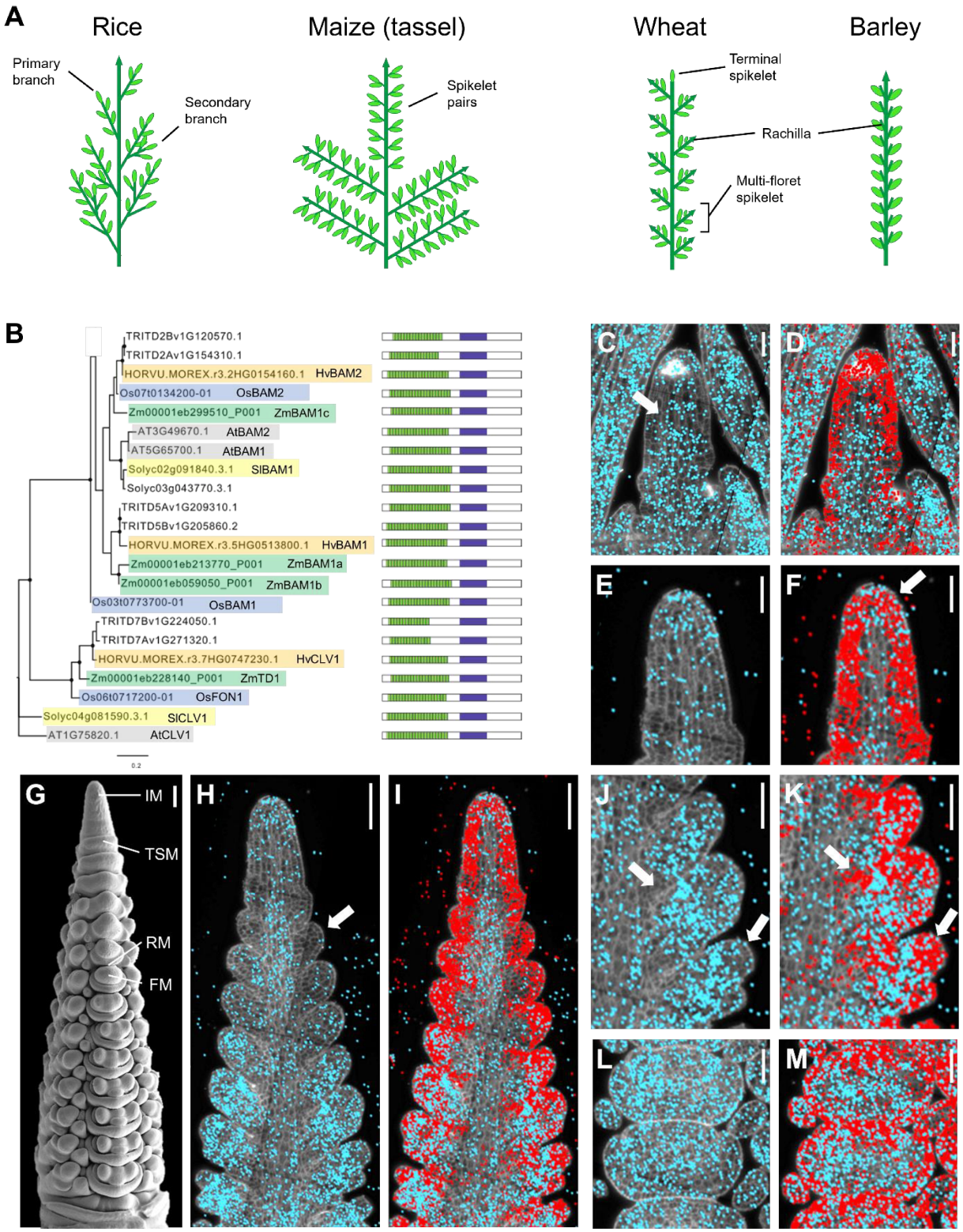

Fig.1: Grass inflorescences, HvBAM1 and HvBAM2 phylogenetic tree and *HvBAM1* expression pattern compared to *HvCLV1*

(A) Schematic representation of different inflorescence architectures among grasses. **(B)** Maximum likelihood tree of the BAM1 and BAM2 clades based on protein kinase domains. Black dots indicate nodes with bootstrap value higher than 80. Genes identifiers and names of already described genes are highlighted in different colours based on the species [*Arabidopsis Thaliana* (grey), *Solanum lycopersicum* (yellow), *Zea mays* (green), *Oryza sativa japonica* (blue) *and Hordeum vulgare* (orange)]

are coupled with a schematic representation of the protein structure. Kinase domain as purple rectangles and LRRs as green rectangles. **(C-F)** smRNAfish detection of *HvBAM1* transcripts (cyan dots) and *HvCLV1* transcripts (red dots) of SAM at vegetative stage (C,D) and IM (E,F), calcofluor stained cell wall in grey. White arrow in (C) indicates a primordium initiation site and in (F) the IM tip. **(G)** Scanning electron microscope picture of barley *cv.* Golden Promise Fast inflorescence at W3.5. IM, TSM, RM, and FM are indicated bt white lines **(H-M)** smRNAfish detection of *HvBAM1* transcripts (cyan dots) and *HvCLV1* transcripts (red dots) throughout spikelet development, calcofluor stained cell wall in grey. White arrows indicate a TSM in (H) and *HvBAM1* and *HvCLV1* complementary expression patterns in (J,K). Scale bars in (C-F) and (J-M) = 50 µm, in (G-I) = 100 µm.

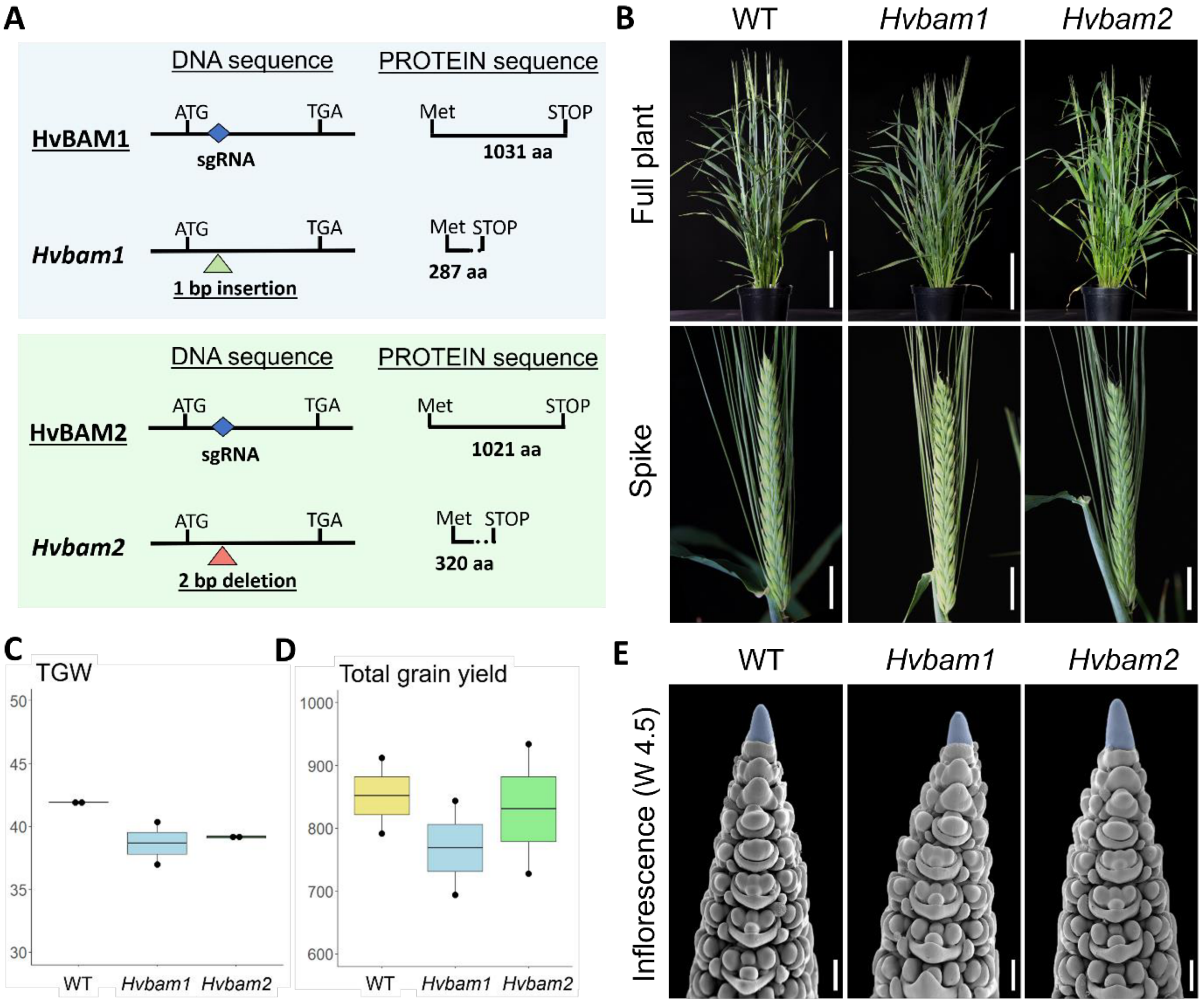

Fig.2: Plant and inflorescence phenotype of *Hvbam1* and *Hvbam2*

(A) Schematic representation of HvBAM1 and HvBAM2 DNA and protein sequence in WT, *Hvbam1*, and *Hvbam2* mutant alleles. The blue square indicates the region targeted by the sgRNA, and the triangles indicate the position of the selected mutation (insertions in green, deletions in red). The dotted lines indicate a different protein sequence to WT. **(B)** WT, *Hvbam1,* and *Hvbam2* plant and spike phenotype. **(C,D)** Thousand Grain Weight (TGW) and total grain yield of WT, *Hvbam1,* and *Hvbam2* grown in semi-field-like conditions. Dots represent data from two plots per genotype, where twelve rows of 44 grains were sown 11 cm apart (528 grains per 1.3mx1.35m =~300 grains per m2). Calculation of statistical differences between genotypes was not possible given the two measurements per genotype. **(E)** SEM pictures of WT, *Hvbam1,* and *Hvbam2* inflorescences at W 4.5. Scale bars: in (A) full plants pictures = 15 cm and spike pictures = 1.5 cm. in (E) = 100 µm.

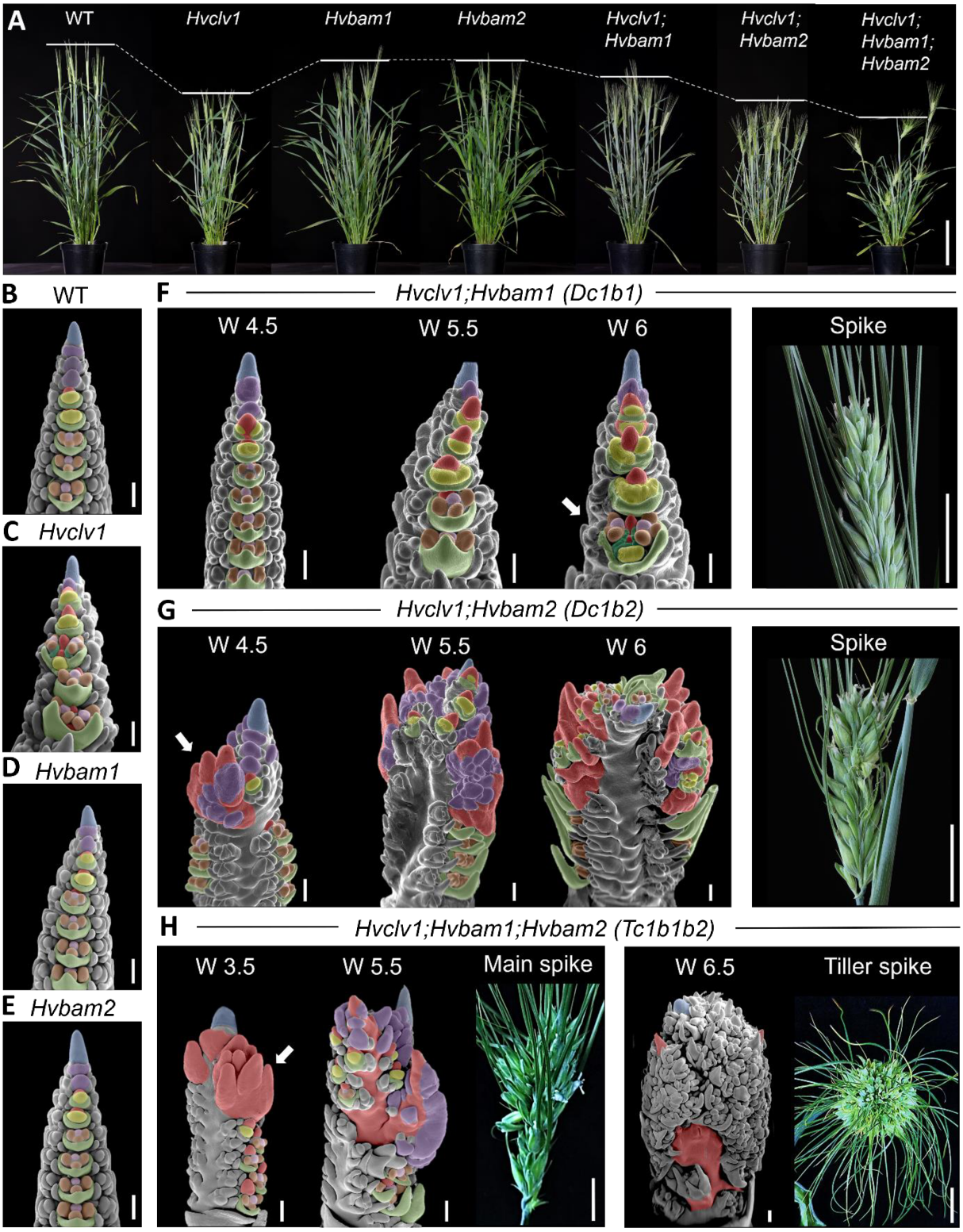

Fig.3: Plant and inflorescence phenotype of all mutant combinations

(A) Plant height comparison of all the mutant combinations. **(B-H)** SEM pictures of WT and mutant inflorescences at different developmental stages (W) and their mature spike phenotype. Color code: inflorescence meristem (IM) in blue, triple spikelet meristem (TSM) and central spikelet meristem (CSM) in purple, rachilla meristem (RM) and branch meristem (BM) in red, floret meristem (FM) in yellow, lemma primordia (LEP) in light green, palea primordia in dark green, stamen primordia (SP) in brown and carpel primordium (CP) in pink. Arrows indicate BMs. Scale bars: in (A) = 15 cm, in all SEM pictures = 200 µm and in mature spike pictures = 1.5 cm.

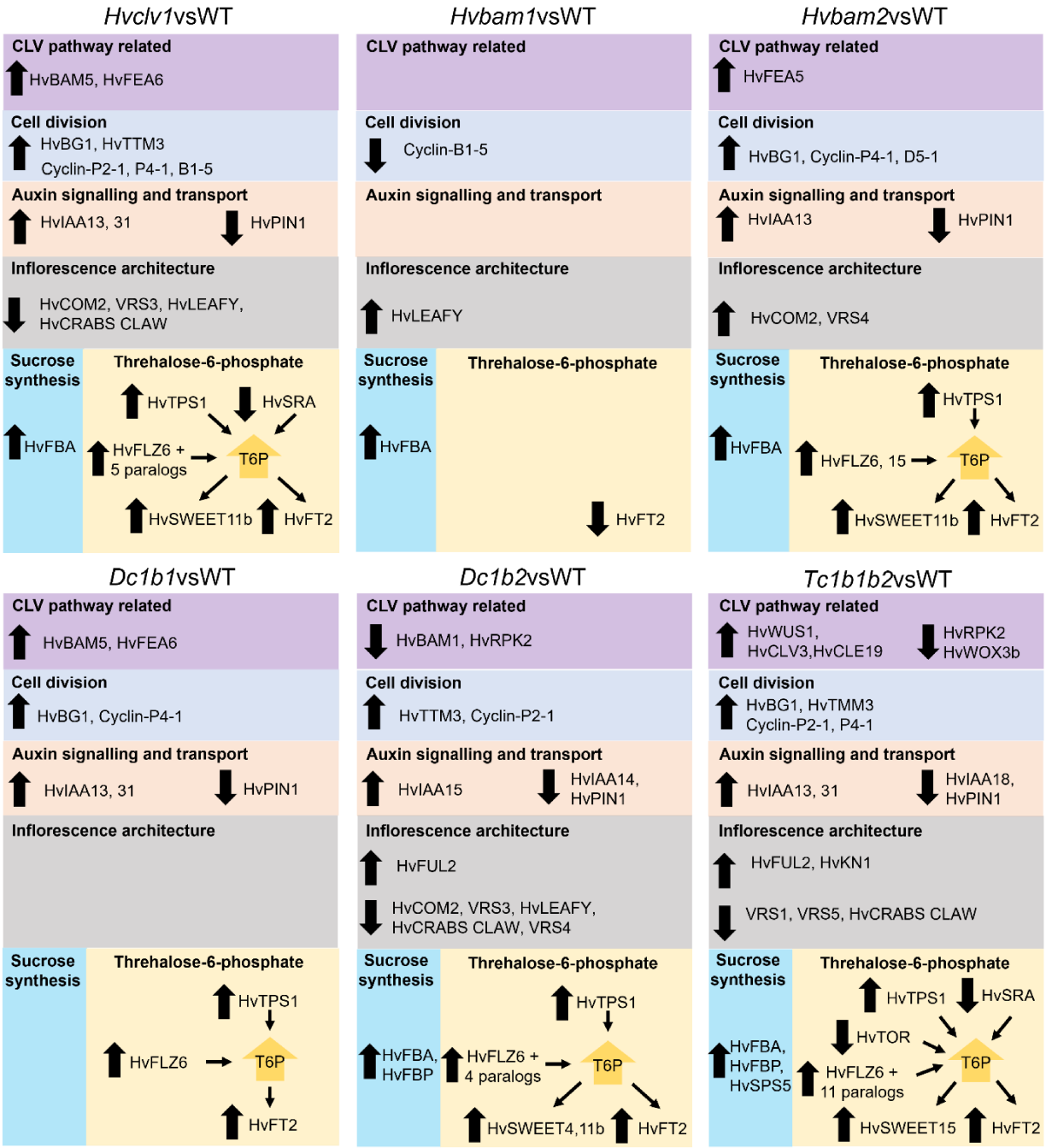

Fig.4: Schematic summary of bulk RNA sequencing results in all mutant combinations

Results from bulk RNA sequencing of WT and mutant inflorescences at W 3.5. Black arrows pointing upward indicate upregulated genes compared to WT, while arrows pointing downward indicate downregulated genes compared to WT. Areas of different colours group genes with a generally similar function. CLAVATA pathway-related genes (**purple areas**), genes involved in cell division (**blue areas**), auxin signalling (**orange areas**), inflorescence architecture (**grey areas**), T6P signalling (**yellow areas**) and sucrose synthesis (**cyan areas**).

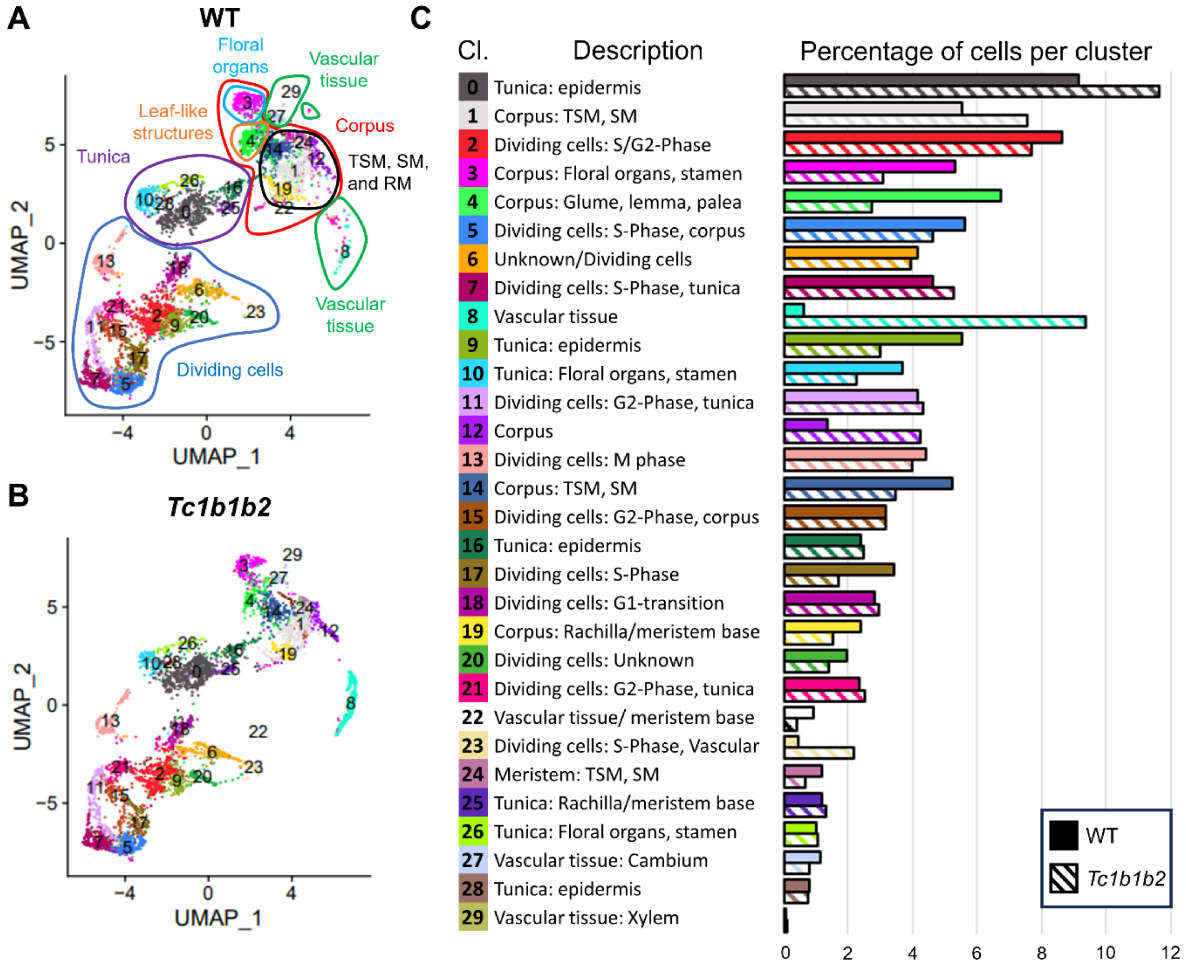

Fig.5: Integrated scRNA-seq clusters analysis in WT and *Tc1b1b2*

(A,B) Featureplots illustrating the distribution and composition of cell clusters from integrated scRNA-seq results in WT and *Tc1b1b2* inflorescences at W3.5. A general cluster description is displayed for reference by coloured shapes grouping cell clusters that match each description. Cluster descriptions in (A) can be translated into (B). **(C)** Description of each cluster based on the expression of marker genes and percentage of cells per cluster in WT and *Tc1b1b2*, based on the total number of cells of each sample (6,238 cells for WT and 6,960 cells for *Tc1b1b2*). The calculation of statistical differences between samples was not possible since only one scRNA-seq replicate was analysed.

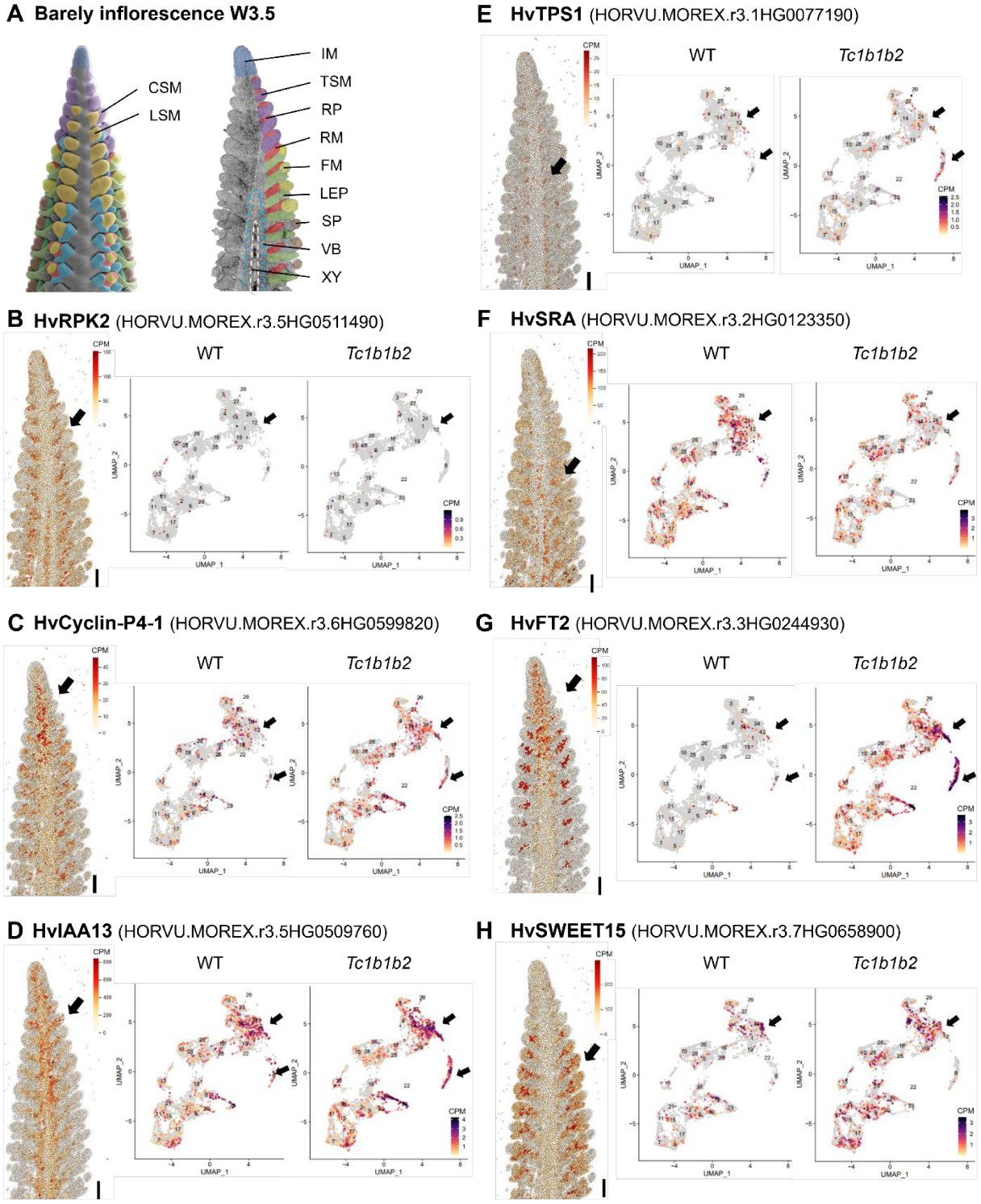

Fig.6: Validation and spatial expression of differentially regulated genes in *Tc1b1b2* compared to WT

(A) SEM picture and longitudinal section of barley inflorescence at W3.5. Colour code: inflorescence meristem (IM) in blue, triple spiekelet meristem (TSM) and central spikelet meristem (CSM) in purple, lateral spikelet meristem (LSM) in orange, glume primordia (GP) in cyan, rachilla primordium (RP) and rachilla meristem (RM) in red, floret meristem (FM) in yellow, lemma primordium (LEP) in light green, stamen primordium (SP) in brown, vascular bundles (VB) cyan segmented line, and xylem (XY) white segmented line. **(B-H)** On the left pictures of the predicted expression pattern by Barvista platform in barley inflorescence at W3.5 *cv.*Golden Promise. On the right, a comparison between Featureplots illustrating specific gene expression in WT and *Tc1b1b2* from integrated scRNA-seq results. Heatmaps indicate the normalized counts per million (CPM). Scale bars = 100 µm.

10. Extended Data Figures

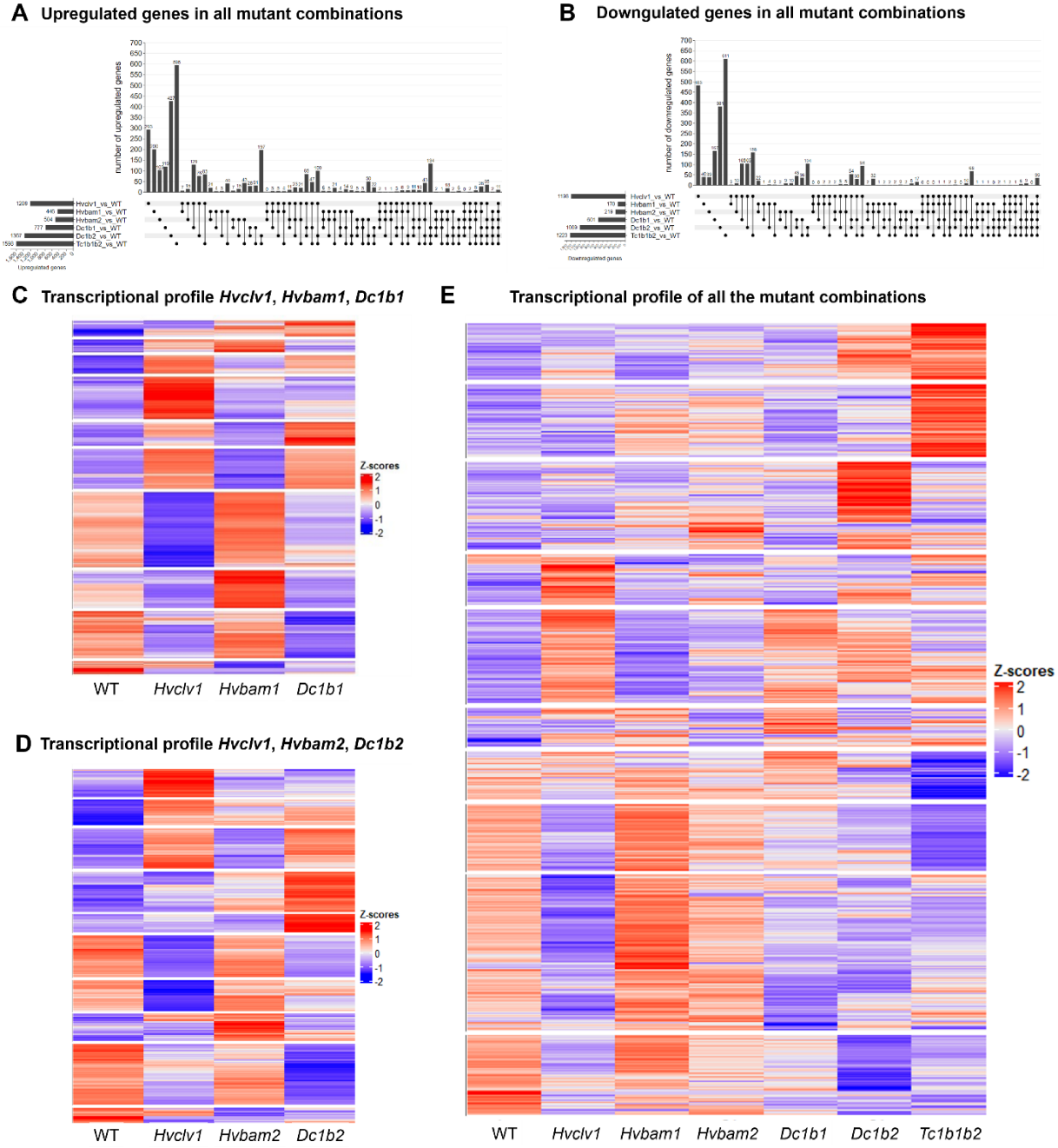

ExtDataFig.1: Number of differentially expressed genes compared to WT and transcriptional profile of different mutant combinations

(A,B) Plots displaying the number of differentially expressed genes in all the mutant combinations and the number of commonly regulated genes for each genotype comparison. Upregulated genes compared to WT in (A) and downregulated genes compared to WT in (B). **(C-E)** Heatmaps illustrate the z-score of median transcripts per million (TPM) values for each differently expressed gene (DEG) in the considered mutant combinations. DEGs with a similar expression trend between genotypes were clustered on the y-axis.

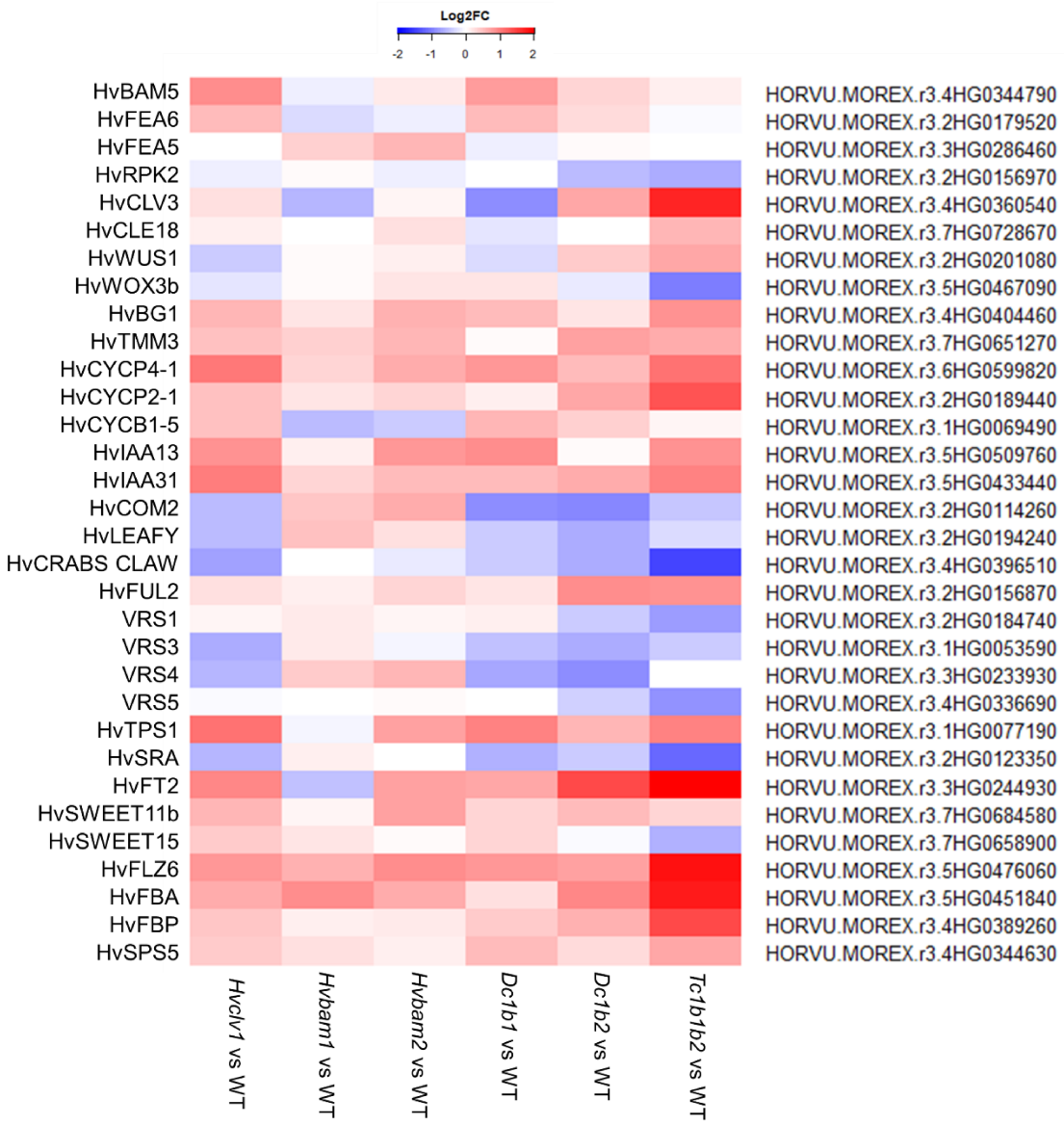

ExtDataFig.2: Expression of the mentioned differentially regulated genes in all the mutant combinations compared to WT

Heatmap displaying Log2FC values of genes mentioned in Fig.5 in all the mutant combinations vs WT. Gene name on the left and the respective MorexV3 identifier on the right. Colours indicate Log2FC values from -2 to 0 (scale of blues) and from 0 to 2 (scale of reds).

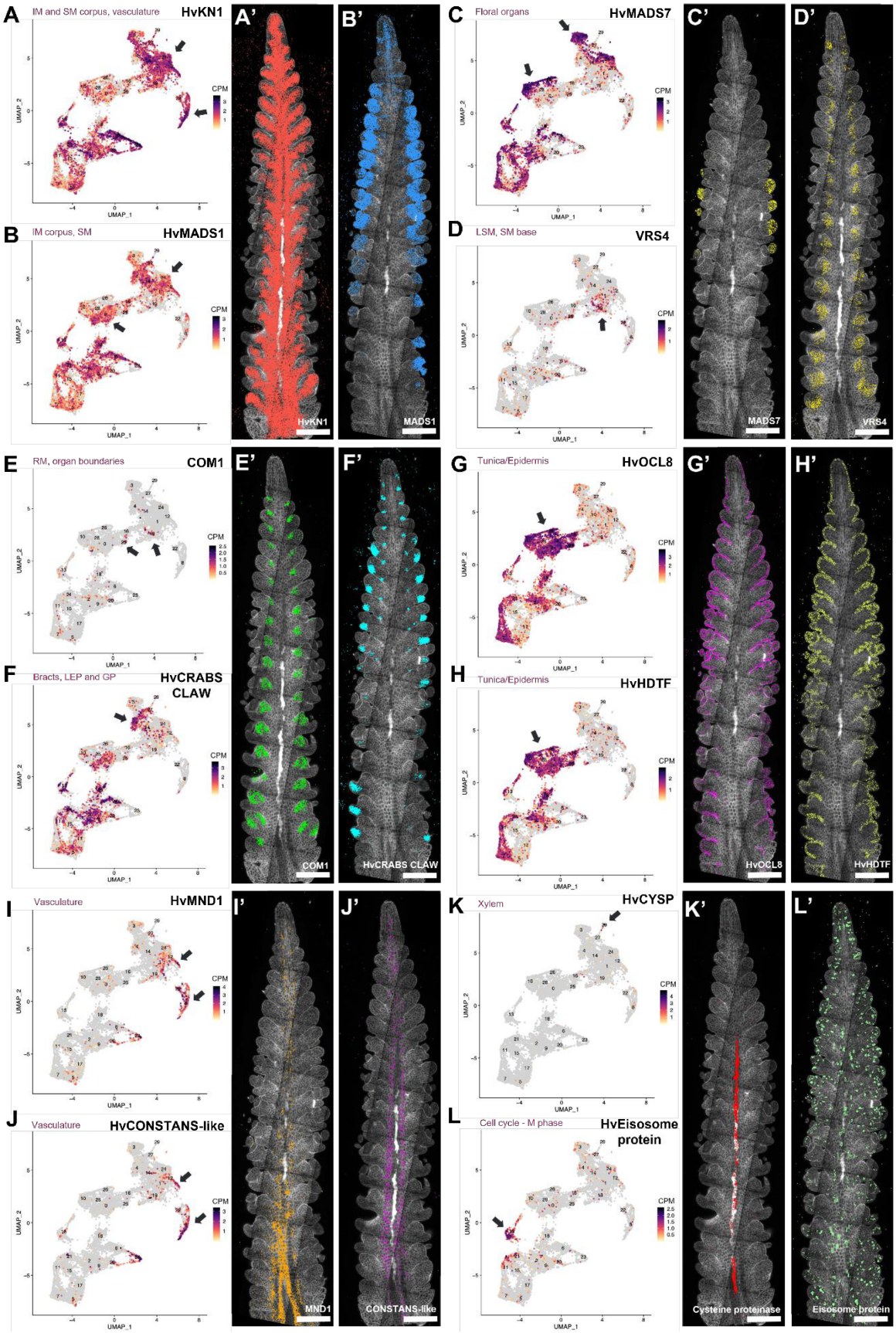

ExtDataFig.3: Marker genes describing the scRNA-seq clusters

(A-L') Featureplots illustrating the expression of the selected marker genes from the integrated scRNA-seq results of three WT replicates, and their respective expression patterns form smRNAfish on barley *cv*. Golden Promise inflorescences at W3.5 Heatmaps indicate the normalized counts per million (CPM). Scale bars = 200 µm.

11. Supplementary information

Suppl.Info1: *Hvclv1, Hvbam1, Hvbam2* mutant combinations

All mutant are composed of combinations of mutations in HvCLV1, HvBAM1 and HvBAM2 as listed below. *Hvclv1-1 allele* carries a 1bp insertion after 70bp that caused a shift in the reading frame and an early stop codon after 476 amino acids (aa), generating a misfolded protein which only shares the first 23aa with the WT sequence (1016aa). *Hvbam1* carries a 1bp insertion 620bp after the coding start that caused a shift in the reading frame and an early stop codon after 286 aa, generating a misfolded protein which shares the first 206aa with the WT sequence (1031aa). *Hvbam2* carries a 2bp deletion 663bp after the coding start that caused a shift in the reading frame and an early stop codon after 319 aa, generating a misfolded protein which shares the first 221aa with the WT sequence (1021aa).

<u>Alignment: sgRNA target sequence (blue), insertion (green), deletion (red)</u>

```
HvCLV1          ATGCCGCCACCTCACCTGCTCACCATCCTCCTACCTCTCCTCCTCCTCCCGGCCCCT
Hvclv1-1        ATGCCGCCACCTCACCTGCTCACCATCCTCCTACCTCTCCTCCTCCTCCCGGCCCCT
                ************************************************************

HvCLV1          TCCTCCGGCT-CCCCGGACCGCGACATCTACGCGCTCGCCAAGATCAAGGCCGCCCT…
Hvclv1-1        TCCTCCGGCTTCCCCGGACCGCGACATCTACGCGCTCGCCAAGATCAAGGCCGCCCT…
                ********** *********************************************

--------------------------------------------------------------------------------

HvBAM1          ATGCGTCTCCCCCTCCTCCTCCTCGTCCTCCTCGCCGGCATCTCCGCCGGCGGCGCGGCC
Hvbam1          ATGCGTCTCCCCCTCCTCCTCCTCGTCCTCCTCGCCGGCATCTCCGCCGGCGGCGCGGCC
                ************************************************************

HvBAM1          GACGGCGACGCGGACGCGCTGCTCGCGGCCAAGGCGGCGCTGTCGGACCCCACGGGCGCG
Hvbam1          GACGGCGACGCGGACGCGCTGCTCGCGGCCAAGGCGGCGCTGTCGGACCCCACGGGCGCG
                ************************************************************

HvBAM1          CTCGCGTCCTGGGAGGTACCGGCGGCGGCGAGCAACGGGACGGGGTACGCGCACTGCGCG
Hvbam1          CTCGCGTCCTGGGAGGTACCGGCGGCGGCGAGCAACGGGACGGGGTACGCGCACTGCGCG
                ************************************************************

HvBAM1          TGGGCGGGCGTGTCGTGCGGCGCGCGCGGGGCCGTCGCGGGGCTGGCCCTCGGCGGGCTC
Hvbam1          TGGGCGGGCGTGTCGTGCGGCGCGCGCGGGGCCGTCGCGGGGCTGGCCCTCGGCGGGCTC
                ************************************************************

HvBAM1          AACCTCTCCGGCGCGCTGCCGCCGGCGCTGTCCCGCCTGCGCGGCCTCCTCCGCCTCGAC
Hvbam1          AACCTCTCCGGCGCGCTGCCGCCGGCGCTGTCCCGCCTGCGCGGCCTCCTCCGCCTCGAC
                ************************************************************

HvBAM1          GTCGGCGCCAACGCGCTCTCGGGCCCCGTCCCGGCCGCGCTCGGCCACCTCCGCTTCCTC
Hvbam1          GTCGGCGCCAACGCGCTCTCGGGCCCCGTCCCGGCCGCGCTCGGCCACCTCCGCTTCCTC
                ************************************************************

HvBAM1          ACCCACCTCAACCTCTCCAACAACGCCTTCAACGGCTCCCTCCCGCCGGCCCTCGCGCGC
Hvbam1          ACCCACCTCAACCTCTCCAACAACGCCTTCAACGGCTCCCTCCCGCCGGCCCTCGCGCGC
                ************************************************************

HvBAM1          CTGCGCGGCCTCCGCGTGCTCGACCTCTACAACAACAACCTCACCAGCCCGCTCCCGATC
Hvbam1          CTGCGCGGCCTCCGCGTGCTCGACCTCTACAACAACAACCTCACCAGCCCGCTCCCGATC
                ************************************************************


HvBAM1          GAGGTCGCGCAGATGCCGATGCTCCGCCACCTCCACCTCGGCGGCAACTTCTTCTCCGGC
Hvbam1          GAGGTCGCGCAGATGCCGATGCTCCGCCACCTCCACCTCGGCGGCAACTTCTTCTCCGGC
                ************************************************************
```

```
HvBAM1          GAGATTCCCCCCGAGTACGGCCGCTGGACGCGGCTGCAGTACCTCGCGCTCTCCGGCAAC
Hvbam1          GAGATTCCCCCCGAGTACGGCCGCTGGACGCGGCTGCAGTACCTCGCGCTCTCCGGCAAC
                ************************************************************

HvBAM1          GAGCTGTCTGGCAAGATACC-GCCGGAGCTCGGGAACCTCACCAGCCTCAGGGAGCTCT…
Hvbam1          GAGCTGTCTGGCAAGATACCAGCCGGAGCTCGGGAACCTCACCAGCCTCAGGGAGCTCT…
                ******************** *************************************

-------------------------------------------------------------------------------

HvBAM2          ATGCGCCACCACCACCTCCCCCTCTTCGTCCTGCTCGCCGCGCTCGCCGTCAGGCAGACG
Hvbam2          ATGCGCCACCACCACCTCCCCCTCTTCGTCCTGCTCGCCGCGCTCGCCGTCAGGCAGACG
                ************************************************************

HvBAM2          GCCGGCGGCGACGCGGACGCGCTGCTTGCGGCCAAGGCCGTGCTCGATGACCCGACCGGC
Hvbam2          GCCGGCGGCGACGCGGACGCGCTGCTTGCGGCCAAGGCCGTGCTCGATGACCCGACCGGC
                ************************************************************

HvBAM2          TCGCTCGCGTCGTGGTCGAACGCCAGCACCGGCCCCTGCGCGTGGTCCGGCGTGTCCTGC
Hvbam2          TCGCTCGCGTCGTGGTCGAACGCCAGCACCGGCCCCTGCGCGTGGTCCGGCGTGTCCTGC
                ************************************************************

HvBAM2          GACGGGCGCTCCGGCGCGGTCGTCGGCGTCGACCTCTCCGGGCGCAACCTCTCTGGTGCC
Hvbam2          GACGGGCGCTCCGGCGCGGTCGTCGGCGTCGACCTCTCCGGGCGCAACCTCTCTGGTGCC
                ************************************************************

HvBAM2          GTCCCACGCGCCTTCTCCCGGCTACCCTACCTCGCGCGTCTCAACCTCGCCGCCAACTCG
Hvbam2          GTCCCACGCGCCTTCTCCCGGCTACCCTACCTCGCGCGTCTCAACCTCGCCGCCAACTCG
                ************************************************************

HvBAM2          CTCTCCGGTCCCATCCCGCCGTCTCTCTCCCGGCTCGGGCTCCTCACCTACCTCAACCTC
Hvbam2          CTCTCCGGTCCCATCCCGCCGTCTCTCTCCCGGCTCGGGCTCCTCACCTACCTCAACCTC
                ************************************************************

HvBAM2          TCCAGCAACCTGCTCAACGGCTCCTTCCCGCCGCCGCTCGCTCGGCTCCGCGCGCTCCGG
Hvbam2          TCCAGCAACCTGCTCAACGGCTCCTTCCCGCCGCCGCTCGCTCGGCTCCGCGCGCTCCGG
                ************************************************************

HvBAM2          GTTCTTGATTTGTACAACAACAACTTCACCGGCTCGCTCCCGCTCGAGGTCGTCGGGATG
Hvbam2          GTTCTTGATTTGTACAACAACAACTTCACCGGCTCGCTCCCGCTCGAGGTCGTCGGGATG
                ************************************************************

HvBAM2          GCGCAGCTCCGGCACCTCCACCTTGGAGGGAACTTCTTCTCCGGGGAGATTCCGCCGGAG
Hvbam2          GCGCAGCTCCGGCACCTCCACCTTGGAGGGAACTTCTTCTCCGGGGAGATTCCGCCGGAG
                ************************************************************

HvBAM2          TACGGCCGGTGGGGGAGGCTGCAGTATCTCGCCGTCTCCGGAAACGAGCTGTCCGGGAAG
Hvbam2          TACGGCCGGTGGGGGAGGCTGCAGTATCTCGCCGTCTCCGGAAACGAGCTGTCCGGGAAG
                ************************************************************

HvBAM2          ATACCCCCGGAATTGGGGAACCTGACGAGCCTCAGACAGCTCTACATAGGCTACTACAAT
Hvbam2          ATACCCCCGGAATTGGGGAACCTGACGAGCCTCAGACAGCTCTACATAGGCTACTACAAT
                ************************************************************

HvBAM2          AACTACTCCGGGGGGATACCGGCAGAGCTGGGGAACATGACGGAGCTTGTGCGGCTCGA…
Hvbam2          AAC--CTCCGGGGGGATACCGGCAGAGCTGGGGAACATGACGGAGCTTGTGCGGCTCGA…
                ***  ***************************************************
```

HvCLV1 WT protein sequence

MPPPHLLTILLPLLLLLPAPSSGSPDRDIYALAKIKAALVPTPASSPTPPLADWDPAATSPAHCAFTG
VTCDAATSRVVAINLTALPLHAGTLPPELALLDSLTNLTIAACSLPGRVPAGLPSLPSLRHLNLSNNN
LSGPFPAGDGQTTLYFPSIEVLDCYNNNLSGPLPPFGAAHKAALRYLHLGGNYFSGPIPVAYGDVASL
EYLGLNGNALSGRIPPDLARLGRLRSLYVGYFNQYDGGVPPEFGGLRSLVLLDMSSCNLTGPIPPELG
KLKNLDTLFLLWNRLSGEIPPELGELQSLQLLDLSVNDLAGEIPATLAKLTNLRLLNLFRNHLRGGIP
GFVADLPDLEVLQLWENNLTGSLPPGLGRNGRLRNLDVTTNHLTGTVPPDLCAGGRLEMLVLMDNAFF
GPIPESLGACKTLVRVRLSKNFLSGAVPAGLFDLPQANMLELTDNLLTGGLPDVIGGGKIGMLLLGNN
GIGGRIPPAIGNLPALQTLSLESNNFTGELPPEIGRLRNLSRLNVSGNHLTGAIPEELTRCSSLAAVD
VSRNRLTGVIPESITSLKILCTLNVSRNALSGELPTEMSNMTSLTTLDVSYNALTGDVPMQGQFLVFN
ESSFVGNPGLCGGPLTGSSNDDACSSSSNHGGGGVLSLRRWDSKKMLVCLAAVFVSLVAAFLGGRKGC
EAWREAARRRSGAWKMTVFQQRPGFSADDVVECLQEDNIIGKGGAGIVYHGVTRGGGAELAIKRLVGR
GVGGDRGFSAEVGTLGRIRHRNIVRLLGFVSNRETNLLLYEYMPNGSLGEMLHGGKGGHLGWDARARV
ALEAARGLCYLHHDCAPRIIHRDVKSNNILLDSAFEAHVADFGLAKFLGGAAGASECMSAIAGSYGYI
APEYAYTLRVDEKSDVYSFGVVLLELITGRRPVGGFGDGVDIVHWVRKATAELPDTAAAVLAVADCRL
SPEPVPLLVGLYDVAMACVEEASTDRPTMREVVHMLSQPALVAPTAVVDENTARPDDDLILSF*

Hvclv1-1 protein sequence

MPPPHLLTILLPLLLLLPAPSSGFPGPRHLRARQDQGRPRAHPRILPDAAARRLGPGGDIPSPLRIHR
RHMRRRHLPRRRHQPHRPPAPRRHAAPGARPPRLPNQPHHRRLLPPRPRPRGPPVPAIPPPPQPLQQQ
PLRPLPRRRRTDNVVLPVHRGPRLLQQQPLRPAPALRRRAQGRAPLPPPRRELLLRPHPGGLRRRRQP
RVPRPQRQRALRQDPAGPGPAGPAPEPLRRLLQPVRRRRAARVRRAAQPRAARHEQLQPHRPHPARAR
QAQEPRHALPPLEPIVWRDSARAGGAPEPPVAGPVRQRPRRRDTGDPGQAHEPQAAQPVPEPPPRRDT
RVRRRPAGPRGAAALGEQPHRQPPAGTRAQRPAQEPRRHHQPPHRHRAAGPLRGREARDARAHGQRLL
RPHPGVAGRVQDAGARPPQQELPQRRRAGRALRPAAGQHARAHRQPAHGRPPRRDRRRQDRHAAAGE*

HvBAM1 WT protein sequence

MRLPLLLLVLLAGISAGGAADGDADALLAAKAALSDPTGALASWEVPAAASNGTGYAHCAWAGVSCGA
RGAVAGLALGGLNLSGALPPALSRLRGLLRLDVGANALSGPVPAALGHLRFLTHLNLSNNAFNGSLPP
ALARLRGLRVLDLYNNNLTSPLPIEVAQMPMLRHLHLGGNFFSGEIPPEYGRWTRLQYLALSGNELSG
KIPPELGNLTSLRELYIGYYNAYSGGVPPELGNLTDLVRLDAANCGLSGKIPPELGRLQKLDTLFLQV
NGLTGAIPSDLGSLKSLSSLDLSNNALAGEIPPSFSQLKNMTLLNLFRNKLRGDIPDFVGDLPSLEVL
QLWENNFTGSVPRRLGGNNRLQLVDLSSNRLTGTLPPDLCAGGKLHTLIALGNSLFGAIPDSLGQCKS
LSRIRLGENYLNGSIPKGLFELQKLTQVELQDNLLTGDFPAVVGAAAPNLGEINLSNNQLTGVLPASI
GNFSGVQKLLLDRNSFSGALPAEVGRLQQLSKADLSGNAIEGGVPPEVGKCRLLTYLDLSRNNLSGKI
PPAISGMRILNYLNLSRNHLDGEIPPSISTMQSLTAVDFSYNNLSGLVPGTGQFSYFNATSFVGNPSL
CGPYLGPCRPGIADGGHPAKGHGGLSNTIKLLIVLGLLLCSIIFAAAAILKARSLKKASDARMWKLTA
FQRLDFTCDDVLDSLKEENIIGKGGAGTVYKGSMPNGDHVAVKRLSAMVRGSSHDHGFSAEIQTLGRI
RHRHIVRLLGFCSNNETNLLVYEYMPNGSLGELLHGKKGEHLHWDARYKIAIEAAKGLCYLHHDCSPL
ILHRDVKSNNILLDSDFEAHVADFGLAKFLQDTGASECMSAIAGSYGYIAPEYAYTLKVDEKSDVYSF
GVVLLELVTGRKPVGEFGDGVDIVQWVKMMTGPSKEQVMKILDPRLSTVPVHEVMHVFYVALLCTEEH
SVQRPTMREVVQILSELPKPAASQGDGEEELPLSGDGPESNPPAPTSSSTEAPTGNAKDHQQQHTSSE
SSPPPDLISI*

Hvbam1 protein sequence

MRLPLLLLVLLAGISAGGAADGDADALLAAKAALSDPTGALASWEVPAAASNGTGYAHCAWAGVSCGA
RGAVAGLALGGLNLSGALPPALSRLRGLLRLDVGANALSGPVPAALGHLRFLTHLNLSNNAFNGSLPP
ALARLRGLRVLDLYNNNLTSPLPIEVAQMPMLRHLHLGGNFFSGEIPPEYGRWTRLQYLALSGNELSG
KIHAGAREPHQPQGALHWLLQRLLRWGPAGARKPHRPRAPRRRQLRPVREDSSGARQAAETRHPLPAG
ERPHRGHTVGPGQP*

HvBAM2 WT protein sequence

```
MRHHHLPLFVLLAALAVRQTAGGDADALLAAKAVLDDPTGSLASWSNASTGPCAWSGVSCDGRSGAVV
GVDLSGRNLSGAVPRAFSRLPYLARLNLAANSLSGPIPPSLSRLGLLTYLNLSSNLLNGSFPPPLARL
RALRVLDLYNNNFTGSLPLEVVGMAQLRHLHLGGNFFSGEIPPEYGRWGRLQYLAVSGNELSGKIPPE
LGNLTSLRQLYIGYYNNYSGGIPAELGNMTELVRLDAANCGLSGEIPPELGNLAKLDTLFLQVNGLTG
GIPPVLGRLGSLSSLDLSNNALSGEIPATFVALKNLTLFNLFRNRLRGDIPQFVGDLPGLEVLQLWEN
NFTGGIPRRLGRNGRFQLLDLSSNRLTGTLPPELCAGGKLETLIALGNSLFGPIPDSLGKCKALTRVR
LGENFLNGSIPEGLFELPNLTQVELQDNLLSGSFPAVVSAGGPNLGGISLSNNQLTGSLPASIGSFSG
LQKLLLDQNAFTGAIPPEIGRLQQLSKADLSGNSFDGGVPSEIGKCRLLTYLDVSQNKLSGDIPPAIS
GMRILNYLNLSRNQLDGEIPVTIAAMQSLTAVDFSYNNLSGLVPVTGQFSYFNATSFVGNPGLCGPYL
GPCRPGGAGTDHGAHTHGGLSSSLKLIIVLVLLAFSIAFAAMAILKARSLKKASEARAWRLTAFQRLE
FTCDDVLDSLKEENMIGKGGAGTVYKGTMPDGDHVAVKRLSTMSRGSSHDHGFSAEIQTLGRIRHRYI
VRLLGFCSNNETNLLVYEYMPNGSLGELLHGKKGGHLHWDTRYKIAVEAAKGLCYLHHDCSPPILHRD
VKSNNILLDSDFEAHVADFGLAKFLQDSGTSECMSAIAGSYGYIAPEYAYTLKVDEKSDVYSFGVVLL
ELITGKKPVGEFGDGVDIVHWIKMTTDSKKEQVIKIMDPRLSTVPVHEVMHVFYVALLCVEEQSVQRP
TMREVVQILSELPKPIAKQGGEQLTGSSDGDEPGLSGPPETVEVATDEANEQQRPSSQSSPPPSLISI
*
```

Hvbam2 protein sequence

```
MRHHHLPLFVLLAALAVRQTAGGDADALLAAKAVLDDPTGSLASWSNASTGPCAWSGVSCDGRSGAVV
GVDLSGRNLSGAVPRAFSRLPYLARLNLAANSLSGPIPPSLSRLGLLTYLNLSSNLLNGSFPPPLARL
RALRVLDLYNNNFTGSLPLEVVGMAQLRHLHLGGNFFSGEIPPEYGRWGRLQYLAVSGNELSGKIPPE
LGNLTSLRQLYIGYYNNLRGDTGRAGEHDGACAARRGQLRPLRRDPTGARESREAGHAVSAGERAHRR
HPAGARSTREPQLARPVEQRALRRDSGHLRGPQEPHSVQPLPKQAQG*
```

Suppl.Table1 – list of primers

Construct		Primer	Primer sequence
p35sHyg-Cas9_Tc1b1b2	sgRNA_ HvCLV1	HvCLV1_sgRNA_Fw	agcaGGCCCCTTCCTCCGGCTCCC
		HvCLV1_sgRNA_Rv	aaacGGGAGCCGGAGGAAGGGGCC
	sgRNA_ HvBAM1	HvBAM1_sgRNA_Fw	agcaGCTGTCTGGCAAGATACCGC
		HvBAM1_sgRNA_Rv	aaacGCGGTATCTTGCCAGACAGC
	sgRNA_ HvBAM2	HvBAM2_sgRNA_Fw	agcaGGCTACTACAATAACTACTC
		HvBAM2_sgRNA_Rv	aaacGAGTAGTTATTGTAGTAGCC
	mutant selection by genotyping	HvCLV1_gene_Fw	CGTGCCACTCACATCACATC
		HvCLV1_gene_Rv	TGGTGAGGTTGGTTAGGGAGT
	mutant selection by genotyping	HvBAM1_gene_Fw	CTCTACAACAACAACCTCACCAG
		HvBAM1_gene_Rv	CTTGAGCTGGGAGAAACTCG
	mutant selection by genotyping	HvBAM2_gene_Fw	GCTCCGGGTTCTTGATTTGT
		HvBAM2_gene_Rv	CCTGTTTCGGAAGAGGTTGA
	Selection of Cas9-free plants	Fl_Cas9_Fw	TTGATGTGGGTTTTACTGATGC
		Fl_Cas9_Rv	CTTGTAGCCTCGGCTGTCTC
		Fl_Hyg_Fw	ATTTCGGCTCCAACAATGTC
		Fl_Hyg_Rv	GCAGGTCACTGGATTTTGGT

List of abbreviations

SAM SHOOT APICAL MERISTEM

IM INFLORESCENCE MERISTEM

TSM TRIPLE SPIKELET MERISTEM

CSM CENTRAL SPIKELET MERISTEM

LSM LATERAL SPIKELET MERISREM

BM BRANCH MERISTEM

RM RACHILLA MERISTEM

FM FLORET MERISTEM

RP RACHILLA PRIMORDIUM

LEP LEMMA PRIMORDIUM

GP GLUME PRIMORDIA

SM SPIKELET MERISTEM

CP CARPEL PRIMURDIUM

SP STAMEN PRIMORDIA

CLV CLAVATA

CLE CLAVATA3/ ENDOSPERM SURROUNDING REGION

BAM BARELY ANY MERISTEM

FCP1 FON2-LIKE CLE PROTEIN1

FON FLORAL ORGAN NUMBER

TD1 THICK TASSEL DWARF1

WUS WUSCHEL

COM COMPOSITUM

RA RAMOSA

LRR-RLK LEUCINE-RICH-REPEAT RECEPTOR LIKE KINASES

BG1 BIG GRAIN1

TTM3 TRIPHOSPHATE TUNNEL METALLOENZYME 3

CDC26 CELL DIVISION CYCLE PROTEIN26

IAA AUXIN/INDOLE-3-ACETIC ACID

T6P THREHALOSE-6-PHOSPATE

FT FLOWERING LOCUS T

SWEET SUGARS WILL EVENTUALLY BE EXPORTED TRANSPORTERS

RPK2 RECEPTOR-LIKE PROTEIN KINASE 2

CYC CYCLIN

PIN PIN-FORMED

TPS1 THREHALOSE-6-PHOSPATE SYNTHASE

VRS SIX-ROWED SPIKE

SRA SISTER OF RAMOSA 3

FLZ FCS-LIKE ZINC FINGER

TOR TARGET OF RAPAMYCIN

FBA FRUCTOSE-BISPHOSPHATE ALDOLASE

FBP FRUCTOSE-1,6-BISPHOSPHATASE

SPS SUCROSE-PHOSPHATE SYNTHASE

W WADDINGTON STAGE

SCRNA-SEQ SINGLE-CELL RNA SEQUENCING

RNA-SEQ RNA SEQUENCING

DEG DIFFERENTIALLY EXPTRESSED GENES

Final Acknowledgements

This thesis not only contains years of work but also represents an important period of my life, shaped by all the people who helped me reach this goal.

First of all, I want to express my immense gratitude to my mentor, guide, and bully, Rüdiger, AKA “the boss". The man who always bet on me, accepted my impulsive character, and smiled in front of my horrendous jokes and random outbursts. The man who taught me the aesthetics of science and almost everything I know about plants.

I owe a huge thanks to all the people in the lab, colleagues, and friends who pushed me over the years to always do my best. Especially the barley group, including Edgar, Jan, Hajer, Leonie, and my buddies Vivien, Meik, Anika, Mehdi, Svenja, and Fadi. Thanks also to all the people I collaborated with, especially Tianyu and Thilanka, who became very good friends of mine. A special thanks goes to Jenia and Karine, the coffee break crew, whose constant presence in moments of need was indescribably important to me, together with Gwen, who always helped and supported me. Thanks to Francesco and Allegra, the Italian friends, who shared so many adventures with me and the happiness and frustration of doing a PhD abroad.

I am immensely grateful to my family, my parents Nilo and Loreta, who always supported me and did everything they could to allow me to follow my passions, and to Amedeo, my brother, to whom I have been bound since birth and always will be.

Last but not least, thank you so much to Margherita, my partner in crime, my rock, and my love, the person who makes my life better day by day.